Lysosomal TRPML1 promotes autophagic flux through increased lysosomal SNAREs recruitment and autophagosome-lysosome fusion

PhD thesis

Abuammar Hussein

Supervisor:

Prof. Gábor Juhász

Laboratory of Lysosomal Degradation Research

Institute of Genetics

HUN-REN Biological Research Centre Szeged

Doctoral School of Biology, Faculty of Science and Informatics

University of Szeged

Szeged 2024

Table of contents

LIST OF ABBREVIATIONS

AD	Alzheimer's disease
ALG-2	apoptosis-linked gene-2 protein
ALS	Amyotrophic Lateral Sclerosis
Ap	apilimod
AP-LY	autophagosome-lysosome
AP-AL	autophagosome-autolysosome
Arl8b	ADP-Ribosylation Factor like Protein 8b
Atg	autophagy-related
CaN	calcineurin
CCV	clathrin-coated vesicle
CMA	chaperone-mediated autophagy
DENV2	dengue-virus, strain 2
DFCP1	Double FYVE-containing protein 1
FIP200	FAK family–interacting protein of 200 kDa
FYCO1	FYVE and coiled-coil domain-containing protein 1
Gal-3	galectin-3
GC-ML1	GCaMP6m-TRPML1
GPN	glycyl-l-phenylalanine 2-naphthylamide
HcRed	far-red fluorescent protein
HOPS	homotypic fusion and vacuole protein sorting

IP3R	Inositol 1,4,5-trisphosphate receptor
JIP4	JNK-interacting protein 4
LAMP1/2A	Lysosomal-associated membrane protein1/2A
L-BMAA	neurotoxin β-N-methylamino-L-alanine
LC3	light chain 3B
LIR	LC3-interacting region
LSDs	lysosomal storage disorders
LTDR	lysotracker Deep Red
Lyso-IP	lysosome immunopurification
M6P	mannose-6-phosphate
M6PR	mannose-6-phosphate receptor
MLIV	mucolipidosis type IV
mTOR	mechanistic target of rapamycin complex 1
OPTN	optineurin
p62/SQSTM1	sequestosome-1
PAS	phagophore assembly site/pre-autophagosomal structure
PD	Parkinson's disease
PE	phosphatidylethanolamine
PEI	polyethylenimine
$PI(3,5)P_2$	Phosphatidylinositol 3,5-bisphosphate
PI4P	phosphatidylinositol 4-phosphate

PI3K	Phosphoinositide 3-kinase
PI3P	phosphatidylinositol 3-phosphate
PI4K2A	phosphatidylinositol 4-kinase type 2 alpha
PI4KIIIB	Phosphatidylinositol 4-kinase IIIβ
PI5P	phosphatidylinositol 5-phosphate
PIKfyve	phosphoinositide kinase, FYVE-Type Zinc Finger Containing
PPARγ	peroxisome proliferator activated receptor γ
Rab7/2	Ras-related protein7/2
SNAP29	synaptotagmin-associated protein 29
SNARE	soluble N-ethylmaleimide-sensitive factor attachment protein receptor
SQSTM1	sequestosome1
STX17	Syntaxin 17
Stx7	Syntaxin 7
TFEB	transcription factor EB
TRPML1/2/3	transient receptor potential mucolipin channel 1/2/3
ULK1	Unc-51-like kinase complex 1
VacA	vacuolating toxin A
VAMP7/8	vesicle-associated membrane protein 7/8
VPS34/41	vacuolar protein sorting 34/41
WIPI1/2/4	WD repeat protein interacting with phosphoinositides1/2/4
ZIKV	zika-virus

1. INTRODUCTION

1.1. The concept of autophagy

In 2016, the Nobel Prize in Physiology or Medicine was awarded to Yoshinori Ohsumi, a cell biologist, for his identification of autophagy-related (Atg) genes playing a crucial role in the main autophagy machinery in yeast[1]. This discovery built upon the work of Christian De Duve, a Belgian cytologist and biochemist who coined the term 'autophagy', from Greek "self-eating". De Duve coined the term autophagy by defining it as the single- and double-membrane vesicles carrying parts of intracellular structures/organelles with various levels of degradation[2]. Over the last 15 years, our understanding of autophagy has tremendously increased in respect to its mechanisms and pathophysiological roles[3,4]. At the same time, pharmaceutical agents that target autophagy began emerging as novel remedies for multiple diseases including neurodegenerative[5], autoimmune[6], infectious[7], and malignant diseases[8,9], as well as aging[10,11] . At a molecular level, autophagy refers to a highly conserved catabolic process by which cellular components (including proteins, lipids, and organelles) are enzymatically degraded by lysosomes. The resultant small molecules serve as a source of cellular energy, or towards recycling of necessary cellular components under nutrient deprivation. While short-lived and typically soluble misfolded proteins are degraded *via* a well-defined proteasomal system, long-lived protein aggregates and damaged organelles are degraded by the autophagic machinery. Initially, the morphology of autophagy was characterised in mammalian and insect models, although majority of molecular studies on autophagy were conducted on yeast model[12–14], and later corroborated in mammalian systems.

There are three well-defined forms of autophagy: macro-autophagy, micro-autophagy, and chaperone-mediated autophagy (CMA). Macroautophagy utilizes the targeting, fusion, and lysosomal degradation of intermediate double-membraned autophagosomes containing cytoplasmic cargo. Conversely, microautophagy involves direct uptake of cytoplasmic cargo by lysosomal membrane invagination. CMA involves the recognition of targeted cytosolic proteins by the cytosolic chaperone heat shock cognate 71 kDa (HSC70) through the KFERQ pentapeptide motif present in cargo proteins. This protein complex is recognized by lysosomal-associated membrane protein 2A (LAMP2A) that forms a channel to mediate lysosomal import of unfolded cargo and degradation of these targeted proteins[15,16]. Among these three forms, macro-autophagy (hereafter 'autophagy') is the best-characterized variant and essential source

for biosynthesis and energy production resulting from the breakdown of large macromolecules and organelles[17].

1.1.1. The morphology of autophagy

Autophagy is distinctly different from micro-autophagy and CMA, as its initiation step occurs away from the degrading organelles, lysosomes. A subset of autophagic vesicles called autophagosomes mediate the induction of this process by capturing and transporting cargo to lysosomes. The *de novo* formation of autophagosomes is a characteristic sign of macro-autophagy that does not exist in other forms of autophagy (micro-autophagy and CMA) where only lysosomal membrane is involved. Upon autophagy induction, autophagosome biogenesis occurs from a specialized cellular locale called 'phagophore assembly site' (PAS) in yeast. On the other hand, mammalian cells form phagophores at multiple subcellular locations within the cytoplasm including near the ER, ER-plasma membrane contacts, and ER-mitochondria contacts; typically, phagophores are associated with ER as a donor membrane, whose subdomains named omegasomes serve as initiation sites for the autophagy process[18].

During the initiation step, the isolated double-membrane structures are called phagophores, which act as sequestering chambers. As phagophores continue their expansion, they require an additional source of membrane lipids. Studies indicate that these membranes primarily come from ER and plasma membrane (PM), and lipid transfer is governed by Atg2- lipid transfer is governed by Atg2-WIPI4 complex 4 (WIPI4) complex[19,20]. As phagophores expand, membranes begin to twist from both ends, forming spherical structures. Membrane curvature is possibly governed by membrane-bound protein as well as lipid composition[21]. Eventually, the ends of the phagophore fuse and surround its cargo, forming double-membrane vesicles called autophagosomes. These autophagosomes form in diverse sizes – typically ranging from 0.4 to 0.9 μm, but also larger sizes in mammals ranging from 0.5 to 1.5 μm[18].

Once a mature autophagosome is formed, the autophagosome must transport its content to lysosomes or vacuoles in mammals and yeast, respectively. Subsequently, the outer membrane of autophagosomes tether and fuse with lysosomal/vacuolar membrane. In yeast, autophagosome-vacuole fusion results in the formation of autophagic bodies that are deposited into the vacuolar lumen[22], while autophagosome-lysosome (AP-LY) fusion leads to the formation of a new hybrid organelle named autolysosome in mammals[23]. As a result, autophagic cargos are exposed to the lysososomal/vacuolar acidic environment and lysosomal/vacuolar resident hydrolases, leading to the breakdown of cargo. The resultant small molecules are released back into the cytoplasm with the help of lysosomal permeases for energy

generation and cellular biosynthetic purposes[24]. In mammals, autophagy often overlaps with the endocytic pathway through fusion of autophagosomes with early/late endosomes to generate amphisomes that also fuse with lysosomes, forming autolysosomes[25].

1.1.2. Molecular mechanism of autophagy

Initiation

Autophagy machinery can be activated by stimuli including nutrient starvation, hypoxia, damaged mitochondria, infection, and oxidative stress[26]. In mammals, the initiation step of autophagy is regulated by the activity of Unc-51-like kinase complex 1 (ULK1). This ULK1 initiation complex is constituted from the mammalian homolog of yeast Atg1, the ULK1/2 kinase, and also accessory proteins Atg13, Atg101, and FAK family–interacting protein of 200 kDa (FIP200)/RB1CC1, which are required for the initiation of autophagosome formation[27–29]. Atg13 directly binds to ULK1/2, while FIP200 serves as a scaffold protein for hierarchically recruiting all the other Atg proteins[30]. At this step, the ULK1-Atg13-FIP200 complex initiates the so-called nucleation site which is a putative site in the cytoplasm and crucial for autophagosome formation (**Figure 1**)[31].

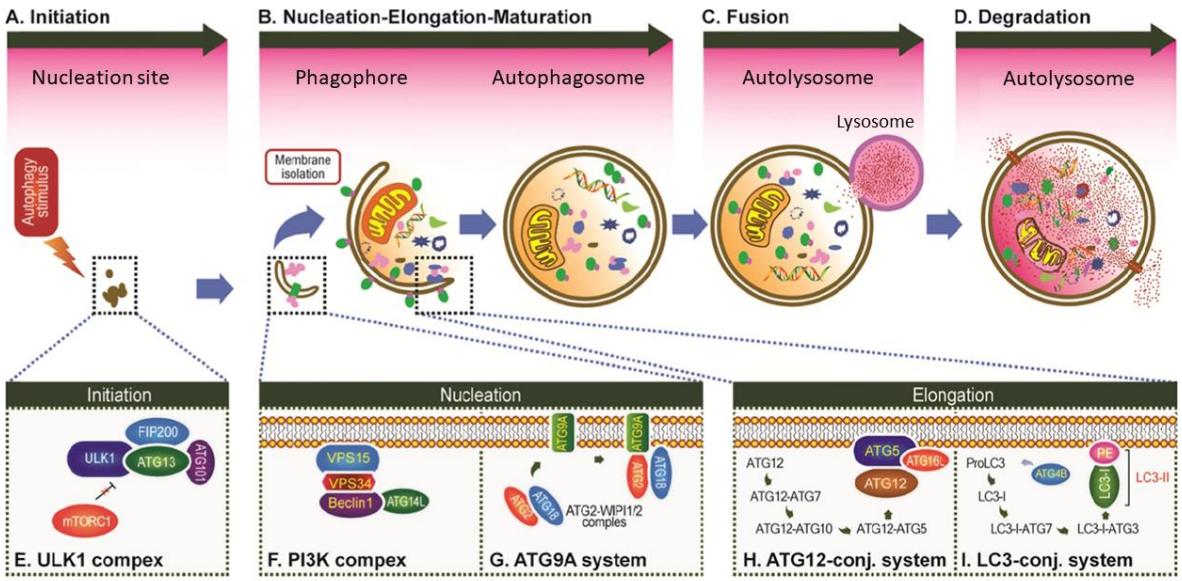

Figure 1: Scheme illustrates stages of autophagy process. a *Initiation, activated ULK1 kinase leads to ULK1 complex formation and recruitment to PAS.* ***b*** *Nucleation, localization of PI3K complex, formed from other ATG proteins and lipids, to phagophore; Elongation, isolation membrane expands and engulfs cytoplasm and organelle; Maturation, closure, and trafficking of autophagosomes.* ***c*** *Fusion, docking of autophagosome and lysosome followed by mixing contents.* ***d*** *Degradation, degradation of material inside autolysosomes.* ***e*** *The ULK1 complex composed of from ULK1, ATG13, FIP200, and ATG101.* ***f*** *The class III PIK complex I composed of Beclin1, VPS34, VPS15, and ATG14L.* ***g*** *The ATG9A system is composed of ATG9A, ATG2, and WIPI1/2.* ***h*** *The*

*ATG12-conjugation system composed of from ATG12, ATG7, ATG10, ATG5, and ATG16L. **i** The LC3-conjugation system composes of ProLC3, ATG4, LC3-I, and LC3-II (LC3-I-PE)*[32].

Nevertheless, the critical interaction of the mechanistic target of rapamycin complex 1 (mTOR), a master regulator of cell growth, to the initiation complex is completely dependent upon nutrient availability. mTOR associates with the ULK1 complex in well-fed cells and dissociates during nutrient-depleted condictions[27]. Once mTORC1 is bound to ULK1, it inhibits ULK1 and Atg13 by direct phosphorylation of these proteins. In contrast, upon nutrient deprivation, mTOR detaches from the ULK1 complex, leading to its dephosphorylation and activation, thereby autophagy initiation[27] (**Figure 2**).

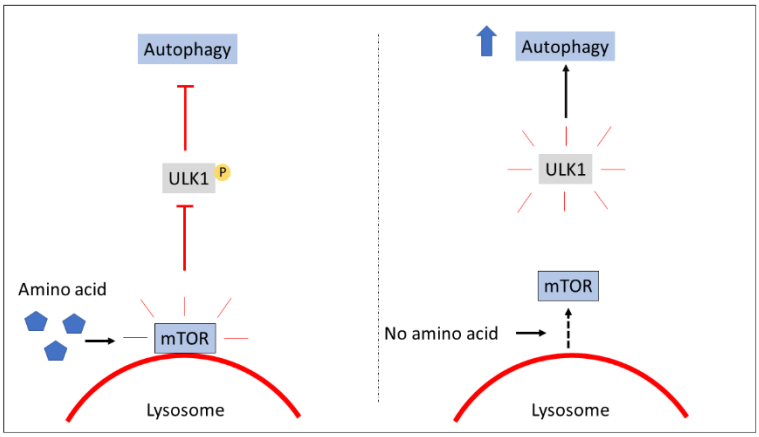

***Figure 2: Proposed model of autophagy regulation by mTOR signaling**. Amino acid activates and translocates mTOR to lysosomes, which in turn inhibits autophagy through ULK1 phosphorylation. In contrary, amino acid depletion inhibits and detaches mTOR from lysosomes, which in turn activates autophagy through downstream ULK1 signaling*[33].

Nucleation, elongation, and maturation

Nucleation starts after ULK1 complex activation under nutrient starvation[34]. This step involves the recruitment of several Atg proteins at the nucleation site for the formation of an isolation membrane or phagophore[35]. A class III PI3K complex is recruited to the phagophore through its member VPS15 that forms a complex with vacuolar protein sorting 34 (VPS34), beclin-1 (BECN1), and autophagy-related 14 L (ATG14L)[34] (**Figure 1**); and is crucial for the generation of the phospholipid PI(3)P needed for autophagy[36,37]. Consequently, the ATG2-WIPI complex is recruited to nucleation site *via* interaction of its transmembrane protein ATG9A[34]. Once Atg9A is phagophore-tethered, a cup-shaped membrane structure appears followed by continuous elongation, engulfing parts of the cytoplasm including organelles[38].

Finally, the ATG12—ATG5, and light chain 3 (LC3) conjugation systems are two ubiquitin-like complexes, mediating the formation of a typical mature bilayer of

autophagosomes[38] (**Figure 1**). These two conjugation systems are a total of eight ATG proteins, including ATG3, ATG4, ATG5, ATG7, ATG8, ATG10, ATG12, and ATG16; and work in a molecular cascade during autophagosome formation[39]. In the LC3 conjugation system, microtubule-associated protein 1A/1B-light chain 3 (MAP1LC3) (hereafter 'LC3'), a ubiquitin-like protein and homologue of yeast Atg8, is first cleaved by cysteine protease Atg4[40]. The exposed C-terminal Gly is activated by the E1-like enzyme Atg7, to form Atg7-LC3 intermediate complex[41]. Afterwards, LC3 is translocated onto an E2-like enzyme Atg3, to form LC3-Atg3 intermediate complex[42]. Finally, LC3 is conjugated to phosphatidylethanolamine (PE) at its Gly residue to generate LC3—PE conjugate, in which Atg12—ATG5 conjugation complex plays a major role[42,43]. LC3-PE conjugate anchors to the isolation membrane and plays an essential role in both autophagosome formation and cargo sequestration during autophagy. Similarly, in Atg12—ATG5 system, C-terminal Gly of Atg12, a ubiquitin-like protein, is activated by Atg7 to form Atg12-Atg7 intermediate complex. Next, Atg12 is translocated to an E2-like enzyme Atg10, to form an Atg10-Atg12 intermediate complex[44]. Finally, C-terminal Gly of Atg12 is conjugated to the lysine side chain of Atg5 to form Atg12—ATG5 complex[45]. Atg12—ATG5 complex associates with Atg16 *via* direct interaction with Atg5 to form Atg12—ATG5-Atg16 complex, E3-like function. This complex localizes to the isolation membrane and facilitates the proper localization of the LC3 conjugation system and its lipidation[46].

The growing phagophores may non-specifically capture cytoplasmic material in response to nutrient starvation, a process known as bulk autophagy. Phagophores usually specifically target cargo such as damaged organelles, protein aggregates, and intracellular pathogens, a process known as selective autophagy [47] . Selective autophagy relies on autophagy receptors that associate with cargo and utilize their LIR motif to bind with LC3 on the inner membrane surface of the phagophore. This process involves the recognition and binding of the cargo to the phagophore, ultimately leading to degradation by autophagy, which requires a large amount of LC3. The current understanding of selective autophagy originated with the discovery of p62/SQSTM1 (Sequestosome-1) as a selective autophagy receptor responsible for targeting ubiquitinated cargo to the autophagy machinery for degradation. Later, an increasing number of autophagy receptors have been identified, such as OPTN (optineurin) and FAM134B [48].

Fusion

Mature autophagosomes must be transported to perinuclear region where they fuse with late endosomes/lysosomes. Autophagosome membranes are suggested to originate from

multiple sites, such as ER, PM, and mitochondria, and therefore, they can be found virtually everywhere in the cytoplasm[49]. Autophagosome migration occurs along microtubules to transport intracellular substances in mammalian cells[50]. Mechanistically, Ras-related protein7 (Rab7), a guanosine triphosphate (GTP)-binding protein, is recruited to autophagosomes to tether these vesicles with microtubules, by specifically binding to dynein and kinesin motor proteins. Autophagosome-localized Rab7 interacts with kinesin *via* its effector FYVE-and coiled-coil domain-containing protein 1 (FYCO1) to enable plus-end directed migration of autophagosomes from the juxtanuclear ER network[51]. On the other hand, minus-end directed migration of autophagosomes is mediated by the interaction between Rab7 and dynein *via* the Rab7 effector RILP (Rab-interacting lysosomal protein) (**Figure 3**)[52].

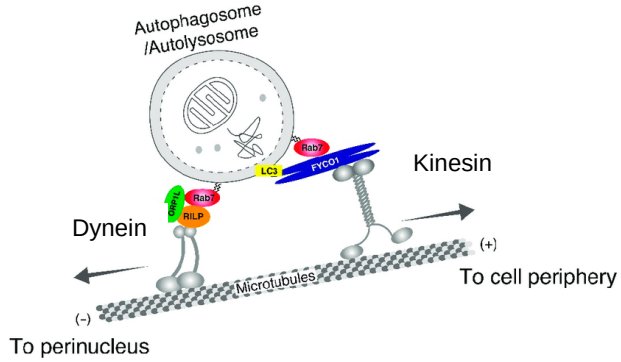

Figure 3: Proposed mechanism of Rab7 in bidirectional movement of autophagosomes along microtubules. *Rab7 connects autophagosomes to microtubules through either FYCO1 and kinesin for plus-end migration (cell periphery) or RILP, and dynein together with Oxysterol binding protein related protein 1L (ORP1L) for minus-end migration (perinucleus)*[53].

Similarly, lysosomes undergo bidirectional transport depending on the environmental cue. For instance, nutrient availability, viral infection, and cellular stress govern the positioning of lysosomes to meet their corresponding functions. Lysosomes are transported towards the perinuclear region during nutrient starvation for fusion with autophagosomes and towards the cell periphery upon re-introduction of growth factors. This bidirectional transport of lysosomes is regulated by ADP-Ribosylation Factor like Protein 8 (Arl8) GTPase which is recruited to lysosomes by BLOC-1 related complex (BORC), lysosomal multi-subunit complex. Arl8 is shown to indirectly bind with motor protein kinesin, driving anterograde transport of lysosome. Arl8 links kinesin with lysosome *via* adaptor protein SKIP (also known as PLEKHM2). Conversely, Arl8 is also shown to indirectly bind with the dynein-dynactin complex, driving retrograde transport of lysosome. Arl8 directly links with adaptor protein RUFY3 which is associated with dynein-dynactin complex *via* dynein activating adaptor JNK-interacting protein 4 (JIP4) (**Figure 4**)[54–56].

Once autophagosomes reach the perinuclear region, they dock and then fuse with lysosomes, forming autolysosomes[49]. During this process, the outer membrane of the

autophagosomal membrane bilayer fuses with the lysosomal membrane. This fusion step involves several factors including soluble N-ethylmaleimide-sensitive factor attachment protein receptor (SNARE) proteins, Rab family proteins, and the HOPS tethering complex.

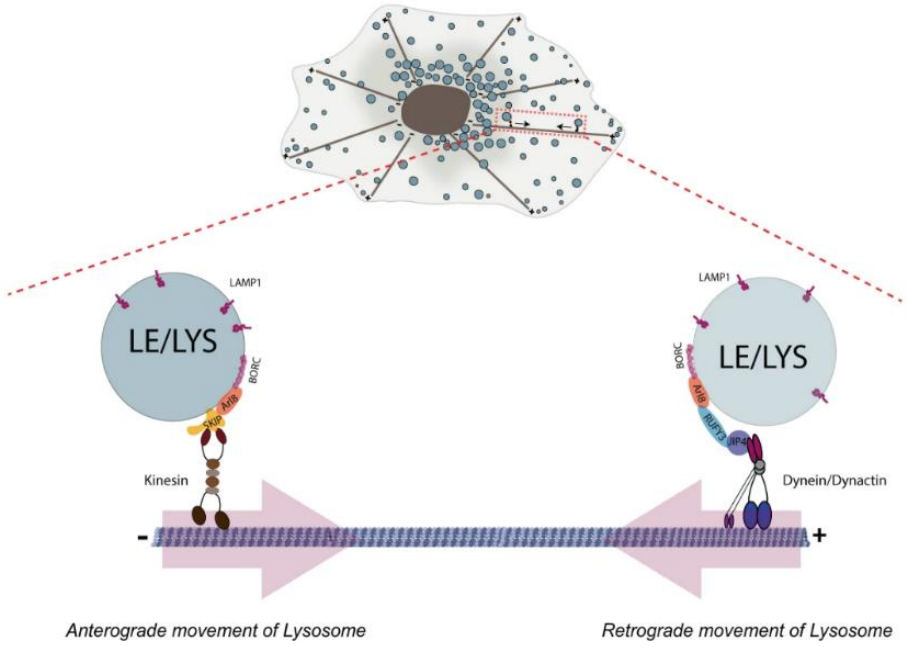

Figure 4: Bidirectional lysosome transport is regulated by Arl8*. Arl8 drives lysosomal transport along microtubules via motor proteins kinesin and dynein. Arl8 binds with kinesin via adaptor protein SKIP (also known as PLEKHM2), promoting anterograde (plus-end) transport of lysosomes. On the other hand, Arl8 binds with adaptor protein RUFY3 which is associated with dynein-dynactin complex through dynein activating adaptor JIP4, promoting retrograde (minus-end) transport of lysosomes*[56].

In the canonical fusion step, Syntaxin 17 (STX17), the prototypical autophagosomal SNARE protein, which is localized to mature autophagosomes, forms a complex with vesicle-associated membrane protein 8 (VAMP8), a lysosomal SNARE together with synaptotagmin-associated protein 29 (SNAP29) from the cytoplasm, thus mediating AP-LY fusion (**Figure 5**) 3)[57]. Furthermore, Rab family proteins and small GTPases regulate eukaryotic membrane trafficking including fusion of lipid bilayer-containing vesicles. Rab7 and another small GTPase Ras-related protein 2 (Rab2) together with the multisubunit tethering complex HOPS (homotypic fusion and vacuole protein sorting) are considered major regulators for AP-LY fusion. During fusion, Rab7 and Rab2 interact with the HOPS subunits vacuolar protein sorting 41 (Vps41) and Vps39 from both vesicular ends. In this way, HOPS tethers both autophagosome and lysosome to promote fusion[58–60].

R-SNARE Ykt6 provides alternative mechanism for AP-LY fusion. *Drosophila* Ykt6 localizes to lysosome and forms prefusion SNARE complex with cytosolic SNAP-29 and

autophagosomal STX17, which then swapped with vesicle-associated membrane protein 7 (VAMP7) to form fusion competent SNARE complex. Mammalian YKT6 localizes to autophagosome and forms complex with cytosolic SNAP-29 and lysosomal Syntaxin 7 (STX7) (**Figure 5**)[61–64].

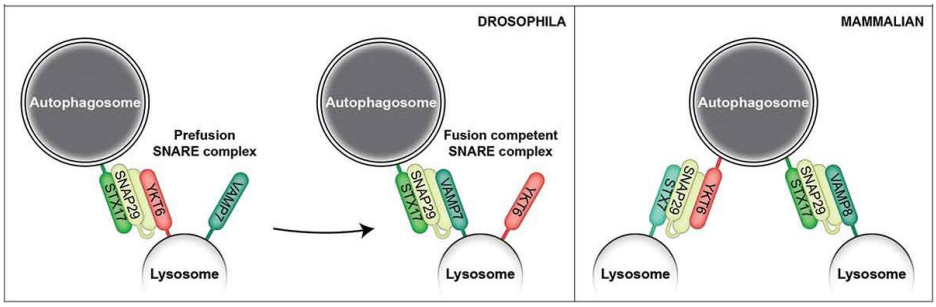

Figure 5: Proposed model of SNAREs function in regulating autophagosome-lysosome fusion*. In Drosophila, lysosomal Ykt6 forms a prefusion SNARE complex with SNAP-29 and STX17, followed by its replacement to VAMP7 to form fusion-competent SNARE complex. In mammalian cells, AP-LY fusion is mediated by the interaction of autophagosomal Ykt6 with cytosolic SNAP29 and lysosomal Stx7 or autophagosomal STX17 with cytosolic SNAP29 and lysosomal VAMP8*[62].

Degradation

The first step of the degradation process is disrupting the inner autophagosomal membrane and its engulfed content, and that is mediated by Atg15 phosopholipase in yeast. The enzyme that does this function in mammals is still unknown[65,66]. The outer membrane of the autolysosome is also exposed to lysosomal enzymes; however, it is spared from degradation due to an unknown mechanism. Some studies speculate that the inner leaflet of the outer autophagosomal membrane lacks the substrate for lipase, while others speculate that the outer autophagosomal membrane inherits membrane-protecting features from lysosomal membrane after fusion[67,68]. Once the inner autophagosomal membrane is disrupted, cytoplasmic contents are directly exposed to lysosomal hydrolases. At least 60 lysosomal hydrolases (phosphatases, nucleases, glycosidases, proteases, peptidases, sulphatases, and lipases) participate in degrading the sequestered cargo, ranging from nucleic acids to engulfed bacteria[69,70]. The majority of these hydrolases require the optimal acidic pH for efficient enzymatic degradation[71,72].

1.1.3. Regulation of autophagy

Autophagy is an essential mechanism for cellular homeostasis and cell survival under stress conditions and known to be involved in the development and pathophysiology of several

organisms including *Drosophila*. Therefore, this process must be finely regulated. Long before the discovery of Atg genes, it was well-known that autophagy is induced in the absence of glucose and amino acid[73,74]. On a metabolic level, the autophagy machinery is regulated through the mTOR pathway and phosphoinositide[75–77].

mTOR

mTOR is a conserved and ubiquitously expressed serine-threonine protein kinase on the lysosome membrane. mTOR responds to the cellular levels of nitrogen and amino acids, besides, it reacts to multiple environmental signals to suppress catabolism and promote cell growth[78,79]. mTOR can be activated by several factors, including depletion of amino acids, growth factors, and reduced cellular energy level. Of note, mTOR is considered as the main negative regulator of autophagy[80]. In nutrient-rich conditions, mTOR is catalytically active and remains localized on lysosomes, phosphorylates ULK1/2 leading to autophagy inhibition. On the other hand, in nutrient-depleted conditions, mTOR is inhibited and detaches from lysosomal membrane which leads to ULK1/2 activation and autophagy induction (**Figure 2**). In mammals, free amino acids are primarily sensed by the vacuolar-type H^+-translocating ATPase (v-ATPase) which is located in the lysosomal membrane. The cytosolic sector V1 of the V1-V0 holoenzyme of the v-ATPase forms a supercomplex with the trimeric Ragulator complex and small GTPases RagA/C[81]. This complex directly translocates mTOR to the lysosomal membrane to be activated by GTPase RHEB in response to amino acids[82,83]. Under amino acid withdrawal or rapamycin treatment (rapamycin is a small molecule mTOR inhibitor), mTOR kinase activity is inhibited and ULK1 is allosterically phosphorylated by AMPK leading to autophagy induction[84]. In addition to ULK1 regulation by mTOR, active mTOR downregulates lysosomal function through phosphorylating transcription factor EB (TFEB). Consequently, this modification prevents TFEB translocation to the nucleus, thereby reducing lysosomal biogenesis and autophagic activity[85].

Phospholipids

Phospholipids contribute to organellar identity and function and therefore they are essential in eukaryotes. The synthesis and turnover of phospholipids are regulated by specific lipid kinases and phosphatases by adding or removing phosphate on positions 3, 4, and 5[77]. Phospholipids are necessary for the regulation of autophagy. Phosphatidylinositol 3-phosphate (PI3P) is primarily required for autophagy initiation. PI3P enriches on ER subdomains called omegasomes and recruits PI3P-binding proteins such as Double FYVE-containing protein 1 (DFCP1), WD-repeat domain phosphoinositide-interacting protein 2 (WIPI2) and ATG16L, therefore promoting phagophore formation. At this step ATG9A positive vesicles along with

phosphatidylinositol 4-kinase IIIβ (PI4KIIIB) distribute from Golgi to autophagosomes, allowing the production of phosphatidylinositol 4-phosphate (PI4P) that is required for autophagosome formation. Upon autophagy induction, phosphatidylinositol 5-phosphate (PI5P) substitutes PI3P in localizing DFCP1 and WIPI2 to the growing phagophore, promoting autophagosome formation. Furthermore, AP-LY fusion is dependent upon the presence of PI4P and PI5P on mature autophagosomes. Finally, phosphatidylinositol 3,5-bisphosphate ($PI(3,5)P_2$) is localized to (endo)lysosomes and implicated in regulating lysosomal function and size. $PI(3,5)P_2$ conversion to PI3P by inositol polyphosphate-5-phosphatase-E (INPPE) was shown to be required for AP-LYS fusion[77,86,87].

1.1.4. Autophagy in health and disease

Given that degradation and reusing of intracellular substances occur by autophagy, this process plays a crucial role in maintaining cellular homeostasis under stress conditions by recycling damaged organelles, protein aggregates, and macromolecules. Nevertheless, autophagy is not limited to starvation adaptation, but its dysregulation is also closely linked to multiple human diseases, such as cancer, neurodegeneration, and aging.

Autophagy in health

Autophagy ensures cellular homeostasis and cell survival under stress conditions in multiple forms: firstly, energy production and anabolism; autophagic degradation generates cellular energy from nutrient stores such as lipids, carbohydrates, and protein, where the resulting metabolites contribute to the anabolic process. For instance, autophagy-derived amino acids are used for protein biosynthesis not only within cells, as these can also be provided to other cells and tissues[88]. Secondly, during development and differentiation, cells rapidly respond to developmental cues by generating metabolites and energy needed for cellular differentiation observed in embryonic central nervous system development in mammals[89,90]. Lastly, during intracellular maintenance, autophagy acts as a quality control pathway in the cell by removing the damaged or unnecessary organelles/molecules, to be replaced by synthesis of new, functional organelles/molecules[91].

Autophagy in human diseases

Cancer

The role of autophagy in cancer is a double-edged sword. Autophagy acts as a tumor suppressor at its initiation step by eliminating harmful cytosolic material that potentially causes cellular damage such as DNA mutation. The deficiency of *BCEN1* gene is associated with breast, ovarian, and prostate tumors, suggesting that autophagy normally suppresses

tumorigenesis[92,93]. This hypothesis is supported by cell-based experiments and animal models which show tumor formation upon genetic inhibition of autophagy[94]. Consistently, pharmacological inhibition of autophagic flux leads to tumorigenesis in various tumor models[95]. On the other hand, it was reported that autophagy contributes to adaptive response of tumors to stressful microenvironments which contributes to therapeutic resistance. The pro-tumorigenic role of autophagy was demonstrated by slow tumor development in Atg5-, ATG14-, or Atg16L1-deficient mice[96]. Vera-Ramirez et al. showed that autophagy is an essential survival mechanism for breast cancer cells, while autophagy inhibition in these cells causes apoptosis[97].

Neurodegenerative diseases

Autophagy is required for proper physiology and homeostasis of neurons in both central and peripheral nervous systems[98,99]. Neurodegenerative diseases are observed in autophagy-deficient mice, and autophagy defects were proposed as an important component of neurodegenerative disease progression in humans. Neurodegenerative diseases known as 'proteinopathies' show accumulation of cellular protein aggregates, including amyloid β (Aβ) in Alzheimer's disease (AD), mutant huntingtin protein in Huntington's disease (HD), and mutant α-synuclein in Parkinson's disease (PD)[100,101]. These protein aggregates are typically degraded by the autophagy-lysosomal as well as ubiquitin-proteasomal pathways, and their degradation failure leads to toxic effects and neurological lesions[102–104]. In parallel, mutations in autophagic receptor genes, such as SQSTM1 (sequestosome1), NBR1 (neighbor of BRCA1 gene 1), and OPTN (optineurin), are closely linked to neurodegenerative diseases[105–107].

Aging

Aging is linked with reduced autophagy in several organisms. Studies showed that aged rats, *C. elegans* have reduced lysosomal degradation relative to younger ones[108,109]. Considering the function of autophagy as a stress response pathway, autophagy promotes longevity and delays aging by reducing tissue damage and promoting tissue repair[110,111]. The conserved degradation process of autophagy leads to cell survival and delayed aging by eliminating cargo that can induce the formation of free radicals, and by mobilizing energy molecules as needed[112]. Autophagy deficiency results in multiple cellular dysfunctions and, therefore, shows a predisposition to age-linked diseases and exacerbated aging. Conversely, physical or pharmaceutical interventions such as caloric restriction or mTOR inhibitor rapamycin enhance autophagy and promote health and longevity[113].

1.2. Lysosomal function during autophagy

1.2.1. Acidification by v-ATPase proton pumping

Lysosomes are the primary catalytic compartments in eukaryotes that breakdown intracellular material sequestered by autophagic vesicles. Proper cargo degradation by resident lysosomal hydrolases requires an acidic environment[114]. This acidification is chiefly regulated by vacuolar H^+-ATPases (v-ATPases) in ATP-dependent manner. Importantly, lysosomal hydrolases efficiently function within a narrow pH range of (4.5-5)[115]. During autophagy, v-ATPase actively pumps protons into lysosomal lumen, generating perilysosomal proton gradients, and reducing luminal pH[115,116].

V-ATPase structure

V-ATPase is a multi-subunit complex associated with yeast vacuole and mammalian lysosomal membranes and consists of two domains: soluble V1 domain and membrane-bound V0 domain[117,118]. The V1 domain consumes ATP and is composed of subunits A, B, C, D, E, F, G, and H; while the V0 domain translocates protons into the lysosomal lumen and is composed of subunits a, c, c', c'', d, and e[119] (**Figure 6**).

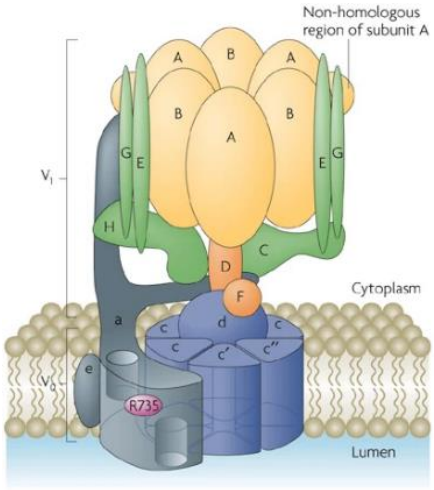

***Figure 6: V-ATPase Structure**. Peripheral V1 domain includes subunits A-H and is responsible for catalyzing ATP. Besides, integral V0 domain includes a, c, c', c'', d, and e; and is responsible for proton pumping across the membrane*[119].

V-ATPase is a rotary apparatus consisting of rotational (rotor) and stationary (stator) subdomains. The stationary subdomain is composed of A3B3 hexamer which contain three catalytic sites for ATP, the peripheral GE subdomains, H, C and a subunit. The rotational subdomains consist of central stalk FD subunits connected with the proteolipid c ring, composed of from c, c' and c'', through d subunit[120,121]. In response to stimuli, ATP hydrolysis by A3B3 catalytic sites leads to their conformational changes and drives rotation of the central

FD stalk as well as c ring. This rotation of the c ring respective to subunit a is an important mechanism for proton translocation[122–124].

V-ATPase regulation

Because intralysosomal lumen must be kept at discrete pH range, lysosomal v-ATPase is tightly regulated. This form of regulation occurs by reversible dissociation of V1 domain from the v-ATPase holocomplex, a process named regulated assembly[125]. Once peripheral V1 and integral V0 domains are associated, it enables a rapid activity of the holocomplex v-ATPase, resulting in proton pumping into lysosomal lumen. In contrast, during dissociation state, the holocomplex is disassembled into its separate components V1 and V0 domains and therefore both the ATP-hydrolytic V1 domain and proton pumping V0 domain are inhibited[119,126].

Regulated assembly is a major mechanism by which v-ATPase is controlled; it is highly conserved in eukaryotes and reacts to multiple nutrient signals, such as glucose and amino acids[127]. In mammals, AMPK and PI3K signaling pathways are implicated in glucose-regulated v-ATPase assembly, while mTOR is solely implicated in amino acid-regulated v-ATPase assembly[128–130]. Both glucose and amino acid starvation promote reversible assembly of v-ATPase on the lysosomal membranes, possibly for energy source during glucose starvation or to enhance protein degradation for amino acid homeostasis[131,132]. On the other hand, high glucose and amino acid concentrations promote V1 disassembly from lysosomal membranes[132–134].

1.2.2. Degradation by lysosomal hydrolases

Lysosome is the final station of the autophagic pathway for the degradation of macromolecules, such as proteins, lipids, polysaccharides, into their small building units of amino acids (AA), free fatty acids (FFA), and monosaccharides, respectively[135,136]. This degradation process requires proteases, lipases, and glycosidases which are resident enzymes in lysosomes[137]. The degradation products are transported away from the lysosomes *via* specific lysosomal transporters[138], or *via* vesicular membrane trafficking such that for energy homeostasis or direct utilisation in biosynthesis[139].

Lysosomes receive their hydrolytic enzymes from Golgi apparatus. The newly synthesized hydrolase is modified at cis-Golgi by adding mannose-6-phosphate (M6P), then it binds to adapter protein (AP) and is recognized by the mannose-6-phosphate receptor (M6PR) to be packaged into a clathrin-coated vesicles (CCVs) which then detach from trans-Golgi and fuse with endosome to deliver the modified hydrolase. Once modified hydrolase is taken up into

endosomes, M6PR is recycled back to the Golgi network[140]. Lysosome maturation from endosomes is a concomitant process, characterized by Rab5-Rab7 switch with progressive decline of luminal pH reaching pH 5[140,141]. This luminal acidification is essential for the detachment of acid hydrolases from the M6PR inside the endosomes (**Figure 7**)[135]. Lysosomal degradation is an adaptive process and regulated by both nutrient status and cellular signaling[142]. Both sequestered intracellular substances *via* autophagy and internalized extracellular substances *via* endocytosis are delivered to lysosomes[136]. Autophagic or endocytic flux promotes lysosomal degradation, while accumulation of catabolites inside lysosomes stops degradation and the autophagy process[143–146].

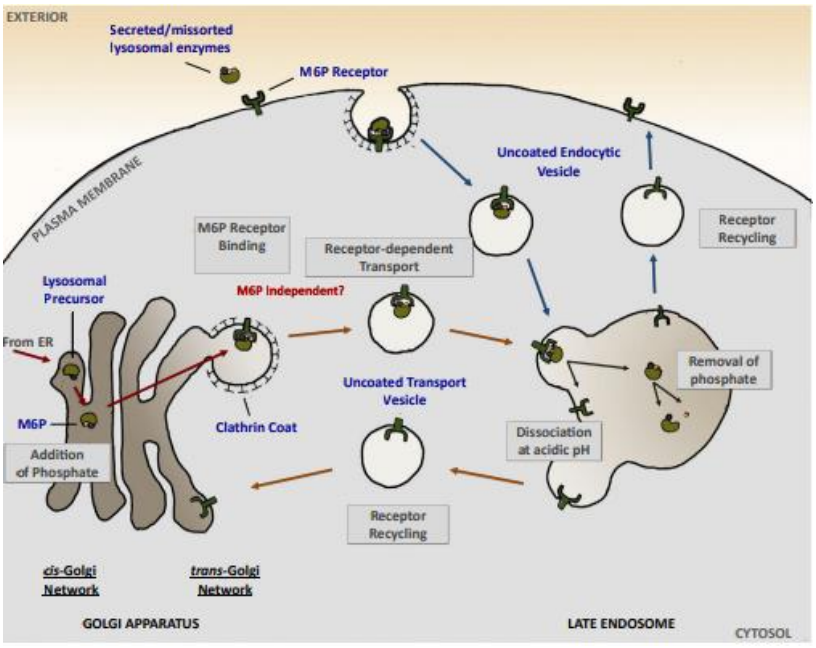

Figure 7: Scheme illustrates sorting of lysosomal enzymes*. In cis-Golgi, ER-derived lysosomal hydrolase precursors are modified by adding M6P. Consequently, at trans-Golgi, lysosomal hydrolases interact with M6P receptors followed by its interacting with adaptor proteins, generating CCVs which then detach from trans-Golgi and mix their contents with late endosomes. Lysosomal hydrolases dissociate and reside inside lysosomes meanwhile receptors are trafficked back to Golgi to be reused. Similarly, secreted or missorted lysosomal enzymes are internalized together with its bound M6P by plasma membrane then delivered to the lysosome* [140].

This adaptation to environmental changes occurs through mTOR signaling regulation. As a result of lysosomal proteolysis, several essential amino acids are transported outside lysosomes *via* specific transporters, such as amino acid transporter solute carrier family 38, member 9 (SLC38A9). Leucine is one among the transported amino acids which was found to be an activator for mTOR signaling through cytosolic Sestrin proteins, thereby terminating lysosomal degradation[147–149].

1.2.3. Regulation of lysosome function

Lysosomes are transcriptionally regulated by the TFEB pathway which is upregulated during autophagy[150]. TFEB is also considered as the master regulator of autophagic and lysosomal function, and its activity is regulated through phosphorylation. TFEB is phosphorylated by mTOR, which leads to cytosolic inactive form of TFEB bound to 14-3-3. In contrast, its dephosphorylated state is mediated by the calcineurin (CaN) phosphatase, which leads to TFEB activation and translocation into the nucleus for transcriptional upregulation of autophagic and lysosomal target genes including v-ATPase subunits, lysosomal membrane-associated proteins (LAMPs), GABARAP family members and lysosomal hydrolases[151–153]. TFEB signaling is critical for autophagy-lysosome pathway. Dysfunction in TFEB activity is implicated in multiple abnormalities, including kidney diseases, neurodegeneration, and alcoholic liver diseases[154–156]. Thus, previous studies have shown that TFEB overexpression or TFEB agonists ameliorate neurodegeneration, including Alzheimer's and PD symptoms, as well as kidney diseases[157–159].

1.3. Calcium and transient receptor potential mucolipin channel 1 (TRPML1)

Ca^{2+} is an intracellular second messenger involved in several cellular functions, including autophagy[160], and therefore its intracellular concentration is tightly controlled by ion channels and transporters embedded into the membrane of intracellular calcium stores, including ER, lysosomes, and mitochondria. Intracellular Ca^{2+} dyshomeostasis is associated with cellular abnormalities seen in diseases, including AD, heart disease and stroke[161,162]. Intracellular Ca^{2+} concentration is estimated to be 100 nM, which is 500-fold lower than in Ca^{2+} stores, such as ER and lysosomes where it is in high micromolar to low millimolar range[163–165], and it changes in response to cellular and environmental signals[163–165].

Elevation in intracellular Ca^{2+} concentration induces autophagy[166]. Transient receptor potential mucolipin channel 3 (TRPML3), a phagophore-localized cation channel, was shown to contribute to autophagy initiation by direct interaction with PI3P, causing Ca^{2+} release from phagophores[167]. Persistent elevation of cytosolic Ca^{2+} due to Sarco/Endoplasmic Reticulum Ca^{2+} Transporting ATPase (SERCA) inhibition blocks autophagic flux by two alternative ways: first, by inhibiting autophagosome formation after the initiation step and before autophagosome closure under starvation conditions[168], and second, by blocking AP-LY fusion[169]. Dysregulated cytosolic Ca^{2+} concentration causes improper lysosomal function and impaired autophagic flux in neurons. Therefore, cytosolic Ca^{2+} signaling must occur in a spatiotemporally regulated

manner for proper autophagic flux[170,171]. Also, lysosomal Ca^{2+} was shown to positively regulate autophagy-lysosome pathway. For instance, increased Ca^{2+} concentration at the vicinity of autophagic vesicles, such as autophagosome, endosome, and lysosome, is required for their fusion and promoting autophagic flux[172–174]. Lysosomal Ca^{2+} release promotes lysosomal processes during fusion with autophagosomes, autophagic degradation, and lysosomal reformation after autophagy[175–177]. These mechanisms are impaired during TRPML1 dysfunction, whose mutations cause mucolipidosis type IV (MLIV), a rare lipid storage disorder which is also neurodegenerative. TRPML1 is the most well-described lysosomal Ca^{2+} channel in context of autophagy[151,178].

1.3.1. Lysosomal Ca^{2+} homeostasis

Lysosomes are known to be the secondary intracellular calcium stores after ER[179]. Intraluminal Ca^{2+} concentration of lysosomes is estimated to be ~ 0.5 mM. This physiological concentration is controlled by diverse lysosomal Ca^{2+} channels including TRPML1, Two-pore channel (TPC), adenosine 5′-triphosphate-gated P2X4 receptor channel (P2X4), and a Ca^{2+}/H^{+} exchanger (CAX) in plants and fungi. Lysosomes receive Ca^{2+} primarily from the ER through inositol 1,4,5-trisphosphate receptors (IP3R) by increasing local Ca^{2+} concentration in the vicinity of the lysosomal membranes at the ER-lysosome membrane contacts. Ca^{2+} ions are then taken up by yet unknown lysosomal Ca^{2+} channels to restore lysosomal function in mammalian and human cells[180]. Indeed, lysosomal Ca^{2+} depletion due to IP3R inhibition or reduction of stored ER Ca^{2+} leads to lysosomal storage disorder-like phenotype, indicating the exclusive role of ER as Ca^{2+} source for lysosome homeostasis[179,180].

1.3.2. TRPML1

TRPML1/mucolipin1 is a transmembrane protein channel located in late endosomal and lysosomal membranes and belongs to the TRP superfamily[181]. In mammals, there are three known members of TRPML channel family–TRPML1, TRPML2, and TRPML3, all of which form tetramers with each subunit composed of six transmembrane domains (TM1-TM6), and mediate Ca^{2+} efflux as well as other cations. TRPML1 is mainly localized on late endosomes and lysosomes and ubiquitously expressed in all cell types. In contrast, TRPML2 is localized on recycling endosomes, while TRPML3 is localized on phagophores and early endosomes, and both TRPML2 and TRPML3 are expressed in specific cell types[182]. Importantly, TRPML1 is the most well-studied channel in this family, whose function has been widely described in autophagy[179].

TRPML1 is a non-selective cation and major Ca^{2+} efflux channel (i.e. it releases Ca^{2+} from lysosomal lumen). It is also permeable to other ions, including H^+, Fe^{2+}, and Zn^{2+}[181]. In mammals, the primary intracellular localization of TRPML1 is late endosomes and lysosomes[183]. TRPML1 was reported as a lysosomal H^+-leak channel whose H^+ leakage function avoids hyperacidification of lysosomes thus maintaining pH homeostasis, and thereby lysosomal function[184]. In addition, Zn^{2+} efflux via TRPML1 has been shown to inhibit autophagy and trigger cell death in different types of cancer, including pancreatic, glioma, breast, and gastric cancer[185]. Nevertheless, over a decade, a multitude of studies have confirmed Ca^{2+} release from TRPML1 and that Ca^{2+} current regulates several pathways during autophagy, such as TFEB activation and autophagosome biogenesis[186–192].

Regulation of TRPML1

TRPML1 regulation by mTOR

TRPML1 actively releases Ca^{2+} to extralysosomal space and that is essential for cell survival during stress conditions like starvation[193]. Long starvation period (4h) induces sustained TRPML1-mediated Ca^{2+} current, which can also be seen upon mTOR-inhibitor torin-1 treatment[176], indicating the possible role of mTOR activity in TRPML1 regulation. Lysosome-localized mTOR inhibits TRPML1 activation by phosphorylation during nutrient-rich conditions, while mTOR detachment from lysosome leads to less TRPML1 phospho-inhibition, causing lysosomal TRPML1 Ca^{2+} efflux during nutrient-depleted conditions. Increased perilysosomal Ca^{2+} gradients activate calmodulin (CaM) signaling and facilitate mTOR reactivation to switch off TRPML1-induced autophagy and restore cell growth upon sustained starvation[194]. The interplay between Ca^{2+} and mTOR activity has been well-studied– inhibition of rapamycin-induced autophagy by cytosolic Ca^{2+} chelation highlights the regulatory effect of cytosolic Ca^{2+} in autophagy mediated by mTOR[195]. Furthermore, the regulatory role of TRPML1-mediated Ca^{2+} in mTOR activity has been demonstrated where lack of TRPML1 Ca^{2+} release due to silencing of *TRPML1* leads to mTOR inhibition. Conversely, TRPML1 overexpression or agonist treatment with ML-SA1 reactivates mTOR in HEK293T cells. Additionally, mTOR activation by TRPML1 Ca^{2+} signaling is likely a CaM-dependent process, supported by the finding that CaM interacts directly with the mTOR signaling pathway[196].

TRPML1 regulation by PI(3,5)P_2

TRPML1 function is regulated by the signaling lipid named PI(3,5)P_2 which is localized primarily on Golgi but transiently synthesized on endolysosomes. PI(3,5)P_2 is synthesized *via* phosphorylation of PI(3)P by the phosphoinositide kinase, FYVE-Type Zinc Finger Containing (PIKfyve) lipid kinase and this PI(3,5)P_2 exists in low abundance with a significant role in endolysosomal homeostasis[197]. PI(3,5)P_2 is known as a specific TRPML1 agonist and the only cellular agonist identified for this channel so far, and its level change is essential for regulating membrane trafficking[198,199] . Moreover, endolysosomal PI(3,5)P_2 synthesis increases during homotypic fusion between endosomes/lysosomes[199.] PI(3,5)P_2 depletion, due to PIKfyve loss-of-function, causes autolysosomal degradation defect in yeast and neurodegeneration phenotypes in mouse model[200,201].

Inhibition of PIKfyve causes an increase in lysosome size and a decrease in lysosome number, consistent with increased lysosome coalescence or/and reduced lysosome reformation[202–206]. PIKfyve inhibition also impairs lysosomal fusion with autophagosome[206]. Notably, other studies demonstrated the role of TRPML1 in regulating lysosome size[191,207]. TRPML1-mediated Ca^{2+} release activates CaM which in turn promotes mTOR activity to induce lysosome fission[207] . TRPML1 suppresses the enlargement of lysosomes caused by vaculin-1 and PIKfyve inhibition[191,207], indicating that PI(3,5)P_2 regulates lysosome size through TRPML1 and mTOR activity.

TRPML1 function in autophagy

TRPML1-mediated Ca^{2+} efflux is found to be a crucial signaling pathway during multiple stages of the autophagy process. TRPML1 induces *de novo* synthesis of autophagic compartments in transcription-independent and dependent mechanisms. First, TRPML1 Ca^{2+} release activates calcium-dependent protein kinase kinase (CaMKKβ) and AMPK pathways, which in turn upregulate ULK1 and VPS34 to initiate phagophore formation[208]. Second, TRPML1 Ca^{2+} release activates Ca^{2+}/CaN pathway, which translocates TFEB to the nucleus to upregulate the biogenesis of autophagy and lysosomal compartments (**Figure 8**) [209,210]. Moreover, it was observed that TRPML1 Ca^{2+} release during amino acid starvation promotes perinuclear localization of lysosomes concomitant with AP-LY fusion. Similarly, pharmacological activation of TRPML1 promotes minus-end directed lysosomal migration towards nucleus where they fuse with autophagosomes, and thus AP-LY fusion is blocked upon inhibition of microtubule function by vinblastine[210]. Ca^{2+} release from TRPML1 is also sensed by the calcium-binding protein apoptosis-linked gene-2 protein (ALG-2), which in turn directly

binds to the dynactin-dynein motor protein complex, promoting lysosomal migration towards the nucleus[175].

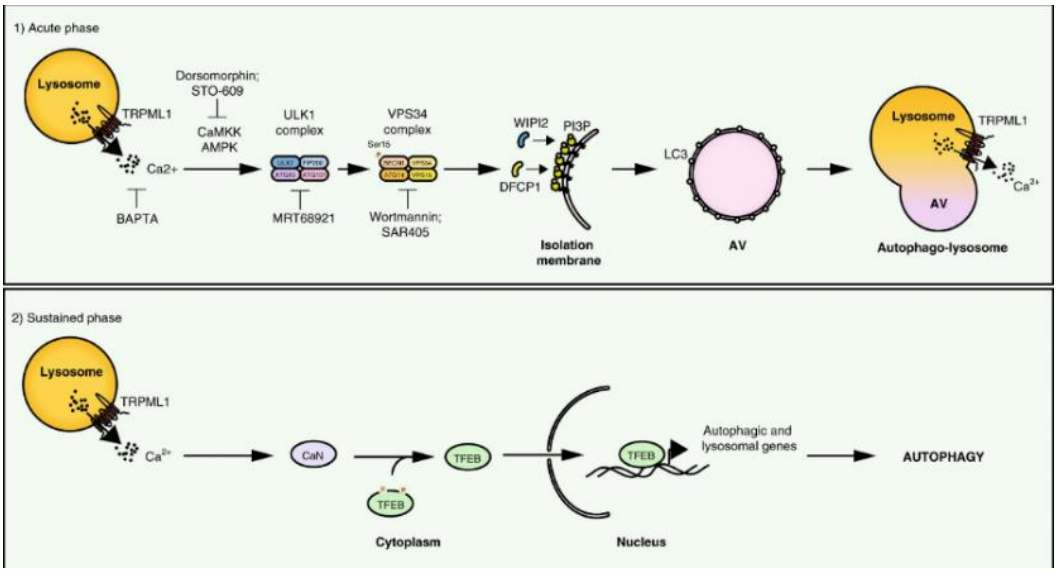

Figure 8: Regulatory function of TRPML1-mediated Ca^{2+} signaling during autophagy*. 1) TRPML1 Ca^{2+} efflux induces autophagosome formation by rapidly activating the Ca^{2+}-CaM-AMPK-ULK1 pathway. 2) Sustained TRPML1 Ca^{2+} efflux transcriptionally upregulates autophagic and lysosomal genes through Ca^{2+}-CaM-TFEB pathway*[211].

Additionally, TRPML1 is also involved in lysosomal tubulation reformation of lysosomes at the end of autophagy (termed 'autophagic-lysosomal reformation' or ALR), both of which are required to generate functional lysosomes[212]. Lysosomes elongate and form tubules as a preceding step for reformation, these two processes are blocked during TRPML1 loss-of function[175]. Lysosome reformation primarily occurs due to rapid lysosomal consumption during prolonged starvation or phagocytosis[144].

Furthermore, several studies reported that pharmacological activation of TRPML1 (for 24h) promotes lysosomal acidification in A549, Huh7, and HEK293T cells, although the mechanism is not completely understood[213]. TRPML1 is also confirmed to play an essential role in lysosomal degradation[214]. Impaired autophagy is observed in a mouse model of Amyotrophic Lateral Sclerosis (ALS) upon exposing motor neurons to neurotoxin neurotoxin β-N-methylamino-L-alanine (L-BMAA). This impaired autophagy is due to compromised autophagic degradation manifested by accumulation of lipidated LC3-II and p62, causing neurotoxicity and cell death. Pharmacological activation of TRPML1 restores the normal degradation of lysosomes in L-BMAA-exposed neurons and reduces cell death[215,216]. Additionally, TRPML1 acts as a sensor for reactive oxygen species (ROS) resulting from damaged mitochondria. TRPML1-induced Ca^{2+} signaling by a selective TRMPL agonist

activates CaN-TFEB pathway to enhance lysosomal biogenesis and autophagy initiation, leading to clearance of damaged mitochondria[217].

TRPML1 in health and disease

TRPML1 dysfunction is associated with neurodegenerative diseases, including AD[218]. For this reason, TRPML1 has been extensively studied regarding its pathological mechanisms and therapeutic potentials. TRPML1 mutations were first identified in 1974 as causative for MLIV. MLIV is a rare neurodegenerative and lysosomal storage disorder with symptoms, including mental retardation, ophthalmological abnormalities and shortened lifespan[219,220]. Cells lacking TRPML1 function exhibit lysosomal Ca^{2+} dyshomeostasis and lysosomal degradation defects, as well as impaired retrograde lipid trafficking[186]. Later, TRPML1 was discovered to be preferentially required for the survival of several cancer types, such as glioblastoma, melanoma, and non-small-cell lung carcinoma[221–223]. A common theme in these studies is the role of TRPML1 in facilitating autophagic activity, thereby cell survival and proliferation of malignant cells. The physiological roles of TRPML1 in diverse cell types were also revealed. For instance, a previous study showed the gradual upregulation of TRPML1 while bone marrow stroma-derived OP9 cells differentiate into mature adipocytes, that was evident in increasing adipocyte marker peroxisome proliferator activated receptor γ (PPARγ)[224]. Expressing siRNA against TRPML1 inhibited adipocyte differentiation and lysosomal exocytosis[224]. TRPML1 is also involved in regulating gastric acid secretion in mice. TRPML1 KO mice develop hypochlorhydria, reduced gastric acid secretion under histamine-induced conditions, leading to increased gastric pH[225].

Remarkably, TRPML1 plays a pivotal role in the pathogenesis of infectious diseases. It was reported that *Helicobacter pylori* employs its vacuolating toxin (VacA) to directly block the activity of TRPML1, enabling it to survive inside a protective vacuole during antibacterial treatment. In the same study, authors found MLIV-like phenotype due to VacA-mediated TRPML1 dysfunction, causing a blockage in AP-LY fusion. They also showed that TRPML1 overexpression or activation by agonists inhibits *H. pylori* vacuole formation, restoring autophagic activity and bactericidal effect in infected cells[226]. The therapeutic potential of the TRPML1 activator, ML-SA1, was not only used against bacteria, but also viruses, such as dengue-virus, strain 2 (DENV2) and zika-virus (ZIKV). ML-SA1 treatment reduced viral titer for both DENV2 and ZIKV in A549, Huh7, and HEK293T cell lines by enchanting lysosomal acidification and protease degradative function[227]. ML-SA1 is also able to reverse uranium

exposure-associated nephrotoxicity in mice renal tubular epithelial cells, which is a hallmark of uranium-exposure associated toxicity in humans[228].

Taken together, the lysosomal ion channel TRPML1 is extensively studied in the context of autophagy-lysosome system. Its function has been implicated in lysosome biogenesis, endosome-lysosome fusion, exocytosis, and lysosomal membrane transport[211,229,230]. On one hand, pharmacological activation of TRPML1 (for 24h) promotes lysosomal acidification and proteolytic function in human cells[213]. On the other hand, multiple studies showed that pharmacological activation of TRPML1 promotes lysosomal cargo degradation[176,213,216,231,232]. Despite the significance of TRPML1 in regulating lysosomal function, little is known about its possible early-onset function, particularly taking into account the fact that ML-SA1-induced TRPML1 Ca^{2+} current persists only for a period of 30 seconds[233].

2. AIM AND OBJECTIVES

To study the role of lysosomal TRPML1 in the regulation of autophagic flux, our objectives were the following:

- To detect TRPML1 activity in response to different drug treatments.

- To investigate the role of TRPML1 Ca^{2+} release in the regulation of autophagosome-lysosome fusion.

- To investigate the role of TRPML1 Ca^{2+} release in the regulation of lysosomal acidification.

- To study the connection between autophagosome-lysosome fusion and lysosome acidification.

3. MATERIALS AND METHODS

3.1.Reagents and antibodies

Reagents: ML-SA1 (Sigma Cat# SML0627), W7 (Sigma Cat# 681629), BAPTA-AM (Sigma Cat# A1076), apilimod (Sigma Cat# SML2974), Lysotracker Red (Thermo Cat# L7528), FITC-Dextran (MW 10,000) (Sigma Cat# FD10S), vinblastine (Sigma Cat# V1377), Magic Red cathepsin B activity assay kit (Bio-Rad Cat# ICT937), Mirus Trans-IT LT1 transfection reagent (Mirus Cat# MIR 2300), OptiMEM (Thermo Cat# 31985070), polyethylenimine linear 25K (Polysciences Cat# 23966), doxycycline (Sigma Cat# D9891), puromycin (Sigma Cat# P8833), concanamycin A (Sigma Cat# C9705), Triton X-114 (Sigma Cat# X114), Intracellular pH calibration buffer kit (Thermo Cat# P35379), protease inhibitor cocktail (Pierce Cat# A32963), Optiprep (Sigma Cat# D1556), HA magnetic agarose beads (Thermo Fisher Scientific Cat# 88837, RRID:AB_2861399), Bicinchoninic acid (BCA) Protein Assay Kit (Pierce Cat# 23227).

Antibodies: pan-cadherin (Sigma-Aldrich Cat# C1821, RRID:AB_476826) (WB: 1:300), HA (Roche Cat# ROAHAHA, RRID:AB_2687407) (WB: 1:1000, IF: 1:200), Syntaxin 7 (Proteintech Cat# 12322-1-AP, RRID:AB_2239979) (WB: 1:1000), VAMP7 (Abcam Cat# ab36195, RRID:AB_2212928) (WB: 1:1000), LAMP1 (DSHB Cat# H4A3, RRID:AB_2296838) (WB: 1:100)?, LAMP1 (DSHB Cat# G1/139/5, RRID:AB_10659721) (WB: 1:50), calnexin (Novus Cat# NB300-518, RRID:AB_10001337) (WB: 1:1000), ATP5a (Abcam Cat# ab14748, RRID:AB_301447), ATP6V1A (Abcam Cat# ab118326, RRID:AB_10899429) (WB: 1:2000), IRDye 800CW goat-anti rabbit (LI-COR Biosciences Cat# 926-32211, RRID:AB_621843), 800CW goat anti-mouse (LI-COR Biosciences Cat# 926-32210, RRID:AB_621842), 680RD goat-anti mouse (LI-COR Biosciences Cat# 926-68070, RRID:AB_10956588), IRDye 800CW Goat anti-Rat IgG (LI-COR Biosciences Cat# 926-32219, RRID:AB_1850025) (all LI-COR antibodies WB: 1:5000), Goat anti-Mouse IgG Alexa Fluor 647 (Thermo Fisher Scientific Cat# A32728, RRID:AB_2633277) (IF: 1:800).

3.2. Cell culture and treatments

This study used HEK293 cells which were purchased from American Type Culture Collection (ATCC) and cultured in sterile conditions with regular checking for mycoplasma contamination. The used culture media consists of high-glucose DMEM, 10% FBS and 50

units/ml of penicillin-streptomycin. Cells were kept at 37°C/5% CO_2 in a humidified incubator. Treatments: ML-SA1 treatment was at 25 μM for 15 minutes and 30 minutes for microscopy and biochemical experiments, respectively; and 50 μM for GCaMP measurements. BAPTA-AM treatment was done at 5 μM for 3 hours and 1.5 hours in complete media for biochemical and microscopy experiments, respectively. Apilimod treatment was done at 1 μM for 1 hour in complete media. W7 treatment was used at 3 μM for 2h in complete media.

Cells were grown in glass-bottom confocal dishes one or two days before transfection. 60-70% confluent cells were transfected using Mirus Trans-IT LT1 reagent or polyethylenimine (PEI). Transit-LT1 reagent was used according to manufacturers' protocol. A 3:1 ratio (using 3 μg PEI mixed with 1 μg DNA per well) was used to prepare lipid:DNA transfection complex in OptiMEM media followed by 30 minutes incubation at room temperature. Lipid:DNA transfection complexes were evenly distributed onto cells and incubated for 24 h. The following plasmids were used:

TRPML1-HA (gift from Craig Montell, Addgene plasmid # 18825; RRID:Addgene_18825), pGP-CMV-GCaMP6m (gift from Douglas Kim & GENIE Project, Addgene plasmid # 40754; RRID:Addgene_40754), pEGFP VAMP7 (gift from Thierry Galli, Addgene plasmid # 42316; RRID:Addgene_42316), pMRXIP GFP-Stx7 (gift from Noboru Mizushima, Addgene plasmid # 45921; RRID:Addgene_45921), EGFP-LC3 (gift from Karla Kirkegaard, Addgene plasmid # 11546; RRID:Addgene_11546), pmRFP-LC3, gift from Tamotsu Yoshimori (Addgene plasmid # 21075; RRID:Addgene_21075), Mucolipin1-pHcRed C1 (gift from Paul Luzio, Addgene plasmid # 62959; RRID:Addgene_62959), Mucolipin1 D471-472K-pHcRed C1 (gift from Paul Luzio, Addgene plasmid # 62961; RRID:Addgene_62961), LAMP1-mGFP (gift from Esteban Dell'Angelica, Addgene plasmid # 34831; RRID:Addgene_34831), pLJM1-Tmem192-mRFP-3xHA (gift from Roberto Zoncu, Addgene plasmid # 134631; RRID:Addgene_134631), GCaMP6m-TRPML1 (this study), pLJC5-Tmem192-3xHA (gift from David Sabatini, Addgene plasmid # 102930; RRID:Addgene_102930), tet-pLKO-puro (gift from Dmitri Wiederschain, Addgene plasmid # 21915; RRID:Addgene_21915), pMDLg/pRRE (gift from Didier Trono, Addgene plasmid # 12251; RRID:Addgene_12251), pRSV-Rev (gift from Didier Trono, Addgene plasmid # 12253; RRID:Addgene_12253), pMD2.G (gift from Didier Trono, Addgene plasmid # 12259; RRID:Addgene_12259).

3.3. Molecular cloning

The human TRPML1 sequence was first amplified with PCR from TRPML1-HA construct using the following primers:

forward: gagtttgtacaaatgatgacagcgaaggcggccgcaattgcccttgccaccatgaca,

reverse: ggtatggctgattatgatctagagtcgcggccgctcaattcaccagcagcgaatgctcc.

Meanwhile, pGP-CMV-GCaMP6m was cleaved with NotI. Gel purification was performed for PCR products and NotI-cleaved backbone and then assembled with NEBuilder HiFi DNA assembly. The following primers were used for sequencing: forward: ctcttcatcgcgctcatcac, reverse: gggatgcttgatggtgtcgt. To build doxycycline-inducible shRNA plasmid, shRNA duplex were generated from Mission (Sigma) shRNA oligos and then inserted between AgeI-EcoRI sites gel-purified tet-pLKO-puro backbone. After plasmid DNA isolation, Clones were confirmed using XhoI diagnostic digest and sequencing. The positive clones were used for lentiviral delivery. The following shRNAs were used:
RAB2A: GCGACACAGGTGTTGGTAAAT (TRCN0000322849),
PI4K2A: CCTCTTCCTGAGAACACTAAC (TRCN0000195396),
VAMP7: GCGAGTTCTCAAGTGTCTTAG (TRCN0000298636).

3.4. RNA extraction and qRT-PCR

Cells were seeded in 60 mm dishes. In the next day, media was changed into doxycycline-containing media and kept for 3-5 days up to 80% confluence. Total RNAs were isolated using Direct-zol RNA Miniprep kit according to manufactures' protocol (Zymo Research). cDNA synthesis of 0.5-1 μg was performed using RevertAid First Strand cDNA Synthesis Kit (Thermo Scientific). Real-time PCR was done in technical replicates using SYBR Green FastMix (Quantabio) in a Rotor-Gene Q qPCR machine (Qiagen). Analysis was done using the $2^{-\Delta\Delta CT}$ method. The following primers were used:
RAB2A: AGAGGTTTCAGCCAGTGCAT and GGATTCTTGCCCTGCCGTAT;
PI4K2A: CGAGGCAATGACAACTGGCTGA and GCCACCTTGATAACAGGCTCCT;
VAMP7: GACCCTGCACTGACCCG and CGGGAACGTTCAAAATCCTCC.

3.5. Lentiviral and shRNA

Lentiviral particles were made by transfection using the following plasmid: transfer plasmids (tet-pLKO-puro, pLJC5-Tmem192-3xHA), pMDLg, pMD2.G and pRSV-Rev. HEK-293T cells were grown in 10 cm dishes up to 50% confluence. Transfection was done using PEI with 3:1 ratio (3 µg PEI for each 1 µg total DNA) for 24 h. Transfection media was substituted with fresh complete media and kept for 48 h. Lentiviral particles were collected and transduced into target cells. A 0.45 µm filter was used to filter lentiviral media which was supplemented with 8 µg/ml polybrene and then added to approximately 50% confluent HEK293 cells in 60 mm dishes. Cells were selected using 2 µg/ml puromycin for 48 hours after transduction time and stable clones were generated by limiting dilution. Stable cell lines were kept in doxycycline-containing media (2 µg/ml) for 72-96 hour to induce shRNA expression. Knockdown was confirmed with western blotting/qRT-PCR.

3.6.Lysosomal pH measurement

Cells were seeded in glass-bottom confocal dishes. 50-60% confluent cells were pulsed with 250 µg/ml FITC Dextran, 10 kD for 16-18 h. The following day, FITC Dextran-containing media was removed, and cells were washed twice with PBS and then chased for 1h in fresh complete media without FITC Dextran. Any needed treatment was performed during the chase period. The existing media was exchanged to live cell imaging solution (140 mM NaCl, 2.5 mM KCl, 1.8 mM $CaCl_2$, 1 mM $MgCl_2$, 20 mM HEPES, pH=7.4, sterile filtered) followed by imaging in a LSM 800 confocal system using a Plan-Apochromat 63x/1.40 Oil DIC M27 objective. Cells were excited with a wavelength of 488 nm and emission was captured in the standard FITC filter. After Images were collected from the experimental sample, media was sequentially replaced with imaging solutions of different pH calibration buffers (pH 7.5>6.5>5.5>4.5, each supplemented with 10 µM valinomycin and 10 µM nigericin). After a 5 min incubation period of each pH calibration buffer, images were captured from the same cells with the same acquisition settings. The cellular boundaries were marked and fluorescence intensities for the experimental sample and pH value from the same cell were recorded using Zeiss Zen Blue software. A standard curve was generated from ≥15 cells using GraphPad Prism v8. Using this curve, pH values were obtained from interpolating experimental data.

3.7.Quantification of TRPML1 Ca^{2+} release

Cells were seeded in glass-bottom confocal dishes one day before transfection. The day after, GCaMP6m-TRPML1 (GC-ML1) plasmid was used to transiently transfect the cells. After 20-24 hour, media was exchanged to low external Ca^{2+} buffer (145 mM NaCl, 5 mM KCl, 3 mM $MgCl_2$, 10 mM glucose, 1 mM EGTA and 20 mM HEPES, pH 7.4; estimated free Ca^{2+} <10 nM) for 15 minutes [233]. A ratiometric GCaMP imaging was performed according to a method used earlier [234]. Images were collected with a Zeiss LSM 800 confocal unit using a Plan-Apochromat 63x /1.40 Oil DIC M27 objective. GCaMP6 imaging was carried out in a temperature-controlled environment. After desirable cells were selected, the low Ca^{2+} buffer was discarded, and imaging was initiated. At 1 min of imaging, 25 µM ML-SA1 dissolved in a low external Ca^{2+} buffer was added to the cells. Cells were illuminated at a Ca^{2+} sensitive wavelength and a Ca^{2+} insensitive wavelength of 488 nm and 405 nm, respectively. Images were collected in a range of 505-565 nm with a time interval of 0.63 s and whole imaging time of 5 minutes. Boundary of the whole cell was marked in Zeiss software and fluorescence intensities from both channels were recorded throughout imaging time for minimum 5 cells in each sample. To estimate the ratiometric GCaMP fluorescence for each timeframe, background fluorescence value was subtracted from Ex. 488 nm and then divided by those obtained from Ex. 405 nm. The fluorescence values were plotted over time in seconded using GraphPad Prism v8.

3.8.Cathepsin B activity assay

HEK-293 cells were seeded on 12 mm coverslips. Upon reaching 70% confluence, cells were exposed to necessary treatments and incubated in Magic red-containing complete media (1:62.5::1 µl Magic red: 62.5 µl complete media) at 37°C for 30 minutes. After washing step with PBS, cells were DNA stained with DAPI solution (1 µg/ml) for 10 minutes. Vectashield was used to mount the cells. Cells were excited with wavelength of 580 nm and images were captured in RFP channel with Zeiss Axioimager M2 equipped with an Apotome 2 module and an ORCA Flash 4.0 LT sCMOS camera (Hamamatsu) using Plan-Apochromat 63x/1.40 oil DIC M27 objective.

3.9. Lysosome immunopurification (Lyso-IP)

Lyso-IP was performed according to previously described protocol [235]. TMEM192-3xHA stably expressing HEK-293 cells were grown in a 10 cm dish up to ~80% confluence. All following steps were performed in ice and cold solutions unless stated otherwise. Cells were washed twice and 633 µl KPBS (136 mM KCl, 10 mM H_2PO_4, pH 7.25) was added. Scraper was used to gently collect the cells. Samples were centrifuged at 1000 g for 2 minutes at 4°C. Cell pellet was resuspended in 633 µl KPBS supplemented with 4% OptiPrep (Sigma) and cocktail protease inhibitors. Cells were lysed with first 35x strokes in 2 ml Kontes glass tissue homogenizer and then 5x passing through 25 G needle. After the centrifugation step (1000xg, 2 minutes, 4°C) was performed, 20-33 µl supernatant was kept as post supernatant sample (PNS) and 600 µl supernatant was incubated with 70 µl pre-washed HA magnetic beads with tube rotator for 20 minutes at 4°C. Lysosome bound beads were washed once with 4% Optiprep-containing KPBS solution followed by two times washing with KPBS. Laemmli buffer was added to beads and the samples were eluted by boiling.

3.10. Immunoblotting

~70-80% confluent cells were 1x PBS washed. Fresh PBS solution was added, and cells were harvested using a scraper. Cell pellet was obtained after the centrifugation step (400 g, 5 minutes, 4°C) and then resuspended in a cold lysis buffer (RIPA buffer + cocktail protease inhibitors) for 30-45 minutes in ice. The lysate was centrifuged at 14000 g for 10 min at 4°C. Supernatant was collected and boiled with Laemmli buffer. Protein measurement was performed with BCA kit and equal protein amount was separated in SDS-PAGE and then blotted to 0.45 µm Polyvinylidene fluoride or polyvinylidene difluoride (PVDF) membranes. Blocking was carried out with 5% milk powder dissolved in TBS or intercept TBS blocking buffer for 1 h. Primary antibody was diluted in 5% milk in TBS+0.1% Tween-20 (TBS-T) or intercept TBS-T buffer which was used to incubate the membrane overnight at 4°C. After 14-16 h, membranes were washed three times with TBS-T for 5 min each and then incubated with secondary antibody (LiCOR) in 5% milk in TBS-T or intercept TBS-T buffer with 0.02% SDS for 1.5 hours at room temperature. Membranes were washed three times with TBS-T for 5 min each and then imaged in a LiCOR Odyssey system.

3.11. Analysis of lysosomal SNARE complexes

The experimental procedure was done according to previous study [236]. Lyso-IP was carried out from cells which were grown in 10 cm dishes as described above. Lysosomal proteins were not eluted in Laemmli sample buffer; instead, beads-bound lysosomes were washed and then incubated in a hypotonic buffer (5 mM Tris-Cl, pH 7.0) supplemented with protease inhibitors. After 10 minutes of incubation in ice, the lysosomal luminal fraction was eluted and then boiled in the Laemmli sample buffer. Beads were again incubated with 1% Triton-X 114 supplemented with 5 mM Tris-Cl and protease inhibitor to elute the total lysosomal membrane fraction. This fraction was spun down at 15000 g for 30 minutes at 4°C. The supernatant was named as a soluble membrane fraction which was mixed with a Laemmli sample buffer. While the pellet was named as an insoluble membrane fraction which was separately boiled in a Laemmli sample buffer. All samples were resolved in SDS-PAGE and tested with immunoblotting against Syntaxin 7.

3.12. Immunostaining

HEK-293 cells were grown on glass coverslips inside a 12-well plate. After necessary treatment is finished, cells were washed once with PBS and then fixed using 4% paraformaldehyde (PFA) diluted in PBS for 15 min with gentle rocking. To remove residual PFA, cells were washed three times with PBS followed by a permeabilization step with 0.2% Triton-X 100 diluted in PBS for 10 minutes. Next, the blocking step was performed with 1% BSA+22.52 mg/ml glycine in PBS-T buffer (0.1% Tween-20 in PBS) for 30 minutes. Primary antibodies were diluted in 1% BSA in PBS-T for overnight incubation. In the following day, cells were washed three times with PBS and incubated in secondary antibodies diluted in 1% BSA in PBS-T for 1.5 h. Cells were washed three times with PBS. DAPI staining was done for 5 min and cells were washed once. Cells were mounted in Vectashield media in glass slides.

3.13. Live imaging and confocal microscopy

HEK-293 cells were seeded in glass coverslips or confocal dishes. Up to 70% confluence, imaging was done on a Zeiss Axio Observer.Z1 equipped with a LSM 800 confocal module using a Plan-Apochromat 63x/1.40 oil DIC M27 objective with appropriate excitation/emission filters. To enhance the signal-to-noise ratio, 2x line averaging option was selected, except for GFP-PI(3,5)P_2. Same imaging settings were applied for all samples or replicates within the

experiment. For time lapse imaging, U2OS cells were seeded in confocal dishes one day before transfection. In the next day, cells were transfected with necessary plasmids. In the following day, cells were first washed with a live cell imaging solution (used in pH measurement) and then treated with ML-SA1 dissolved in the same solution. Cells were placed in temperature and CO_2-controlled chamber (37°C/5%CO_2) during imaging with 1-minute intervals using Olympus IX83P1ZF widefield microscope equipped with an ARCA Fusion BT sCMOS camera (Hamamatsu) using UPLXPO 60X/1.42 oil objective. For better visibility, slight brightness/contract modifications were applied to frames in Fiji.

3.14. Image quantification

Nuclear plane of confocal images was typically selected for imaging, which was used for quantification, except for the Magic Red experiment where widefield fluorescence imaging was applied. Same imaging settings were applied for the same samples within the experiment. Images were subjected to binary thresholding prior to the quantification process of GFP-PI(3,5)P_2 and GFP-Stx7 positive puncta. Colocalization assay was manually performed by counting the number of Syntaxin7/ LAMP1/ TMEM192/ VAMP7 structures coexisting with LC3. Relative values of colocalizing puncta were obtained from the ratio of colocalizing puncta to total number of LC3/LAMP1 puncta (autophagosomes/lysosomes) multiplied by 100 to calculate the percentage values. To measure SNARE accumulation inside lysosomes, pixel scale was converted to micron scale using 'Sed Scale' function in Fiji. SNARE-positive area was marked using the 'Freehand Selections' tools and area values were obtained. Meanwhile, TMEM192 circulating SNARE-positive area was also marked and measured for the same lysosome. SNARE-positive area values (in μm^2) were divided by TMEM192 area values (in μm^2) and then converted to percentage values. The function of 'Plot Profile' was used to plot the profile values for a line selection. Obtained microscopy data were consistent from minimum two independent experiments.

Perinuclear index of lysosomes was measured according to previously used protocol [237]. We first measured the average cellular area of 150-50 μm^2 for HEK-293 cells. The nuclear area was excluded from measurements. 1 µm area was adjusted perinuclear area. LAMP intensities within this area and the rest of the peripheral area were measured in Fiji. C1=total LAMP signal in the cell, Np1=1 micron enlarged periphery around nucleus, N1=nuclear LAMP1 signal, I_{total}=C1-N1, $I_{perinuclear}$=Np1-N1, $I_{peripheral}$=C1-Np1, $I_{<1}$=($I_{perinuclear}$/$I_{peripheral}$)-100,

$I_{>1}=(I_{peripheral}/I_{total})-100$, and perinuclear index=$I_{<1}-I_{>1}$. At least 15 cells were measured for each sample.

3.15. Statistical tests

Obtained datasets were first analysed for normality using the Shapiro-Wilk test. For pairwise analysis, datasets were assessed using unpaired Student's t-test if they passed the normality testing ($p>0.05$); otherwise, Mann-Whitney test was applied. Typically, at least 25 cells were subjected for quantification, except 3-5 cells were used for GCaMP experiment; except N values were stated in the respective figure legend. Statistical testing and plot/graph generation were carried out in GraphPad Prism (RRID:SCR_002789), except profile plots which were generated in Fiji. Error bars indicate standard error of means (SEM)). *$p \leq 0.05$, **$p \leq 0.01$, ***$p \leq 0.001$, ****$p \leq 0.0001$, ns $p> 0.05$.

4. RESULTS

4.1. Acute activation of TRPML1 promotes lysosomal acidification and cathepsin activity

To monitor the activity of TRPML1 during experimental conditions, we developed a Ca^{2+} sensor GCaMP6m-TRPML1 (GC-ML1). GCaMP6m is a genetically encoded Ca^{2+} sensor and is composed of a CaM domain fused to GFP, which fluoresces upon Ca^{2+} binding (**Figure 9A**). Lysosomal localization of this construct was validated using Lysotracker Red (LTR) dye, as a lysosome marker, in 2h-starved HEK293 cells, observed as colocalization between LTR-positive puncta and GC-ML1-positive puncta (**Figure 9B**). We also live imaged our GC-ML1 construct to check its response to its agonist. We found that ML-SA1 rapidly induced TRPML1 Ca^{2+} release, which then dropped to basal level within 20 seconds. BAPTA-AM pre-treated cells (BAPTA-AM is a cell-permeable Ca^{2+} chelator) showed no TRPML1 Ca^{2+} release after ML-SA1 treatment (**Figure 9C**). Several studies have shown the importance of TRPML1 in the degradation of intracellular cargo or neurotoxic aggregates [176,213,216,231,232].

To facilitate cargo degradation, lysosomes must be acidic for optimal activity of lysosomal hydrolases. Therefore, we checked lysosomal pH using LTR. We found that ML-SA1 significantly increased the number of LTR-positive puncta within 15 minutes of treatment, indicating lysosomal acidification. BAPTA pre-treatment abolished this increase in the number of LTR-positive puncta after ML-SA1 treatment (**Figure 9D**). The increase of LTR-positive puncta in ML-SA1-treated cells were statistically significant compared to control (untreated) cells (**Figure 9E**). Moreover, FITC-dextran fluorescence quenching occurred (i.e. luminal acidification) within 10 minutes of ML-SA1 treatment, and no further changes were detected after 20 minutes from the time of ML-SA1 treatment, indicating the relative rapidness of this response. Notably, ML-SA1-induced acidification was abolished in Concanamycin A (ConA, v-ATPase inhibitor) treatment. In this experiment, we used FITC-dextran (acid sensitive endocytic tracer) to provide more quantitative lysosomal pH assessment. Here, BAPTA treatment interfered with endocytic uptake of FITC-dextran presumably because it blocks endocytic trafficking, and therefore we used ConA as a negative control for lysosome acidification instead. These findings indicate that lysosomal acidification follows the short term TRPML1 activation (**Figure 9F**).

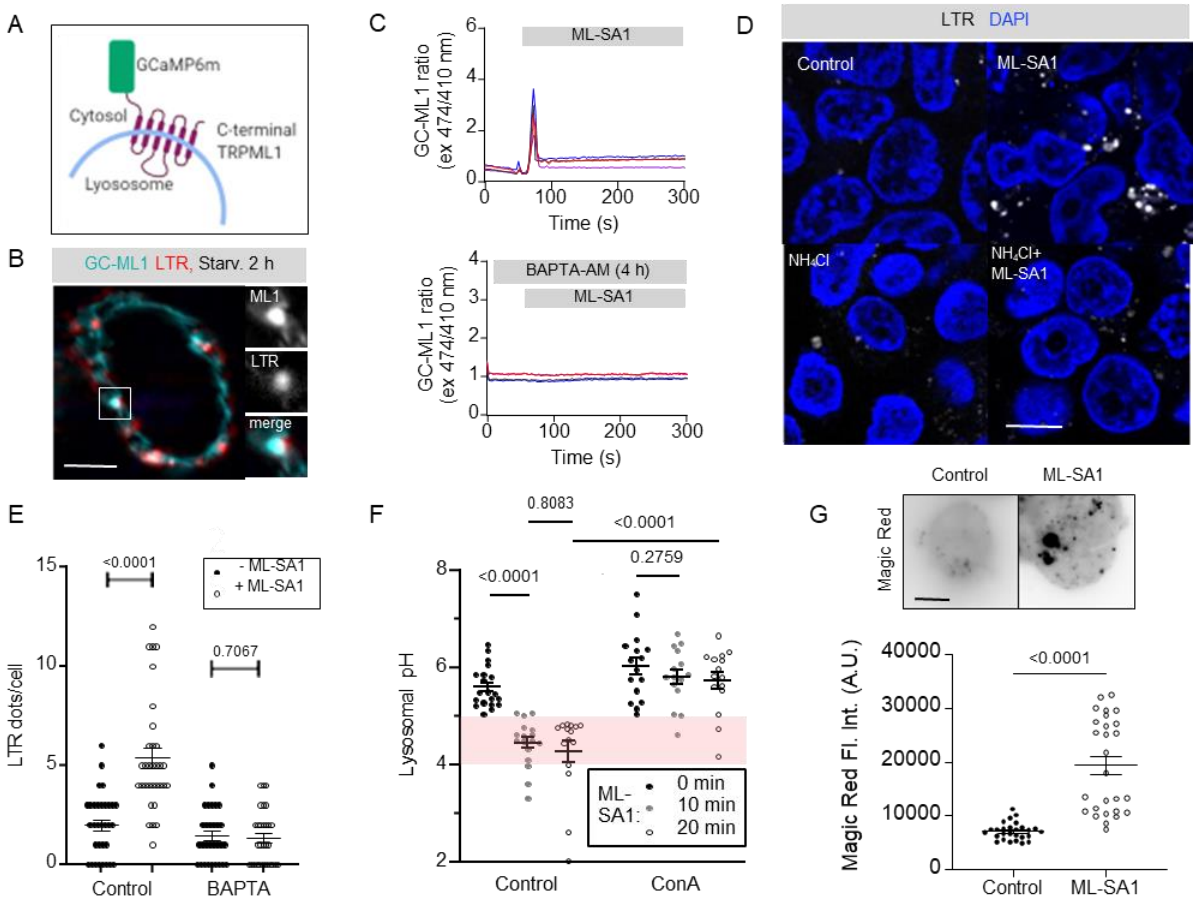

Figure 9: Ca^{2+} efflux from TRPML1 leads to lysosomal activation within 10-20 min.

(A) A diagram illustrating the generated Ca^{2+} sensor GCaMP6m-TRPML1 construct used in this study.

(B) GCaMP6m-TRPML1-positive structures coexisted with acidic Lysotracker Red-positive structures (inset). Bar: 5 µm.

(C) Ca^{2+}efflux from TRPML1 was recorded in HEK-293 cells transiently expressing GC-ML1 construct in either control or BAPTA-AM pre-treated (2 µm, 4 h) and induced by ML-SA1 (25 µM) dissolved in low external Ca^{2+} solution (<10 nM free Ca^{2+}) using ratiometric live imaging (Ca^{2+}dependent wavelength of 474 nm (Ex), Ca^{2+} independent wavelength of 410 nm (Ex)) . N=4 for both control and BAPTA-AM pretreated cells.

(D) HEK293 cells were stained with Lysotracker Red and treated with ML-SA1 (25 µM, 15 min). Acidification response by ML-SA1 was inhibited in BAPTA-AM pre-treated cells. Bar: 10 µm.

(E) Number of Lysotracker Red-positive dots from cells with or without ML-SA1 treatment. N≥30. Statistics: Mann-Whitney test was applied on control samples; Student's t-test was applied on BAPTA samples.

(F) FITC-dextran fluorescence quenching was recorded to measure lysosomal pH after ML-SA1 treatment (10 and 20 min) in either control or ConA (V-ATPase blocker, 100 nM, 1 h) pre-treated cells. Highlighted red background represents the physiological acidic lysosomes (4-5). N≥15 for all samples. p values were calculated from multiple comparisons (mixed effects analysis).

(G) Cathepsin B activity increases after 15 min of ML-SA1 treatment according to the level of its fluorescent substrate Magic Red. Bar: 5 µm. Lower panel: Quantification of whole-cell fluorescence. N=27. Statistics = Mann-Whitney test was applied.

Lysosomal acidification is typically driven by accelerated assembly of v-ATPase holocomplexes (V1-V0 engagement) on lysosomes during starvation-induced autophagy [129,133]. To investigate whether TRPML1 Ca^{2+} efflux promotes v-ATPase assembly towards lysosomal acidification, we checked the status of v-ATPase holocomplex during ML-SA1 treatment. Lysosomes were first immunopurified using lysosome immunopurification (Lyso-IP) after respective treatments. We found that the enrichment of ATP6V1A, a subunit of v-ATPase V1 domain, on lysosomes was slightly increased during ML-SA1 treatment (20 minutes) (**Figure S1A, S1B**). In parallel, we used SidK fluorescent reporter to label v-ATPase V1 domain in live cells. The total SidK puncta numbers slightly increased after ML-SA1 (**Figure S1C, S1D**), and lysosomal acidification could still be observed by greatly increased Lysotracker Deep Red (LTDR)- positive puncta in ML-SA1-treated cells compared to control ones (**Figure S1E**). These two assays indicated that while there is a modest increase in v-ATPase assembly, TRPML1 drives lysosomal acidification mostly through preassembled v-ATPase holocomplexes on the lysosome. We also checked the activity of lysosomal cathepsin using Magic Red, a cathepsin substrate and its fluorescence is directly proportional to cathepsin activity. ML-SA1 treatment strongly promotes cathepsin activity as opposed to control condition (**Figure 9G**). Overall, short-term activation of TRPML1 promotes lysosomal acidification and cathepsin activity.

4.2. Acute activation of TRPML1 promotes local autophagosome-lysosome fusion

A previous study had demonstrated the role of TRPML1 in autophagosomes biogenesis which ultimately fuse with lysosomes [211]. Another study showed the role of TRPML1 in lysosomal migration toward the cellular perinuclear region, a process that proceeds AP-LY fusion upon 2 hours of ML-SA1 treatment [237]. We were curious to check whether fusion occurs within 20 minutes of TRPML1 activation. We found that ML-SA1 significantly increased AP-LY fusion, seen as significantly more colocalization between lysosome marker LAMP1-positive puncta and autophagosome marker LC3B-positive puncta (**Figure 10A**). This increased colocalization between LAMP1- and LC3B- positive puncta due to ML-SA1 was abolished in BAPTA-pretreated cells (**Figure 10A, 10B**). Concomitantly, the number of non-colocalized LC3B-positive puncta (i.e. unfused autophagosomes) reduced upon ML-SA1 treatment, indicating no autophagosomes biogenesis during this period (**Figure 10C**). We checked whether lysosomal migration is affected during this short period of ML-SA1 treatment. LAMP1-mCherry was used to define the lysosomal positioning during different

conditions. We found that lysosomal positioning is unchanged during 15 minutes of ML-SA1 treatment and lysosomes begin clustering around the nucleus from 30 minutes of ML-SA1. This lysosomal clustering mimicked the well-established perinuclear lysosomal clustering during starvation-induced autophagy (**Figure 10D, 10E**), indicating that lysosomal migration is not required for AP-LY fusion induced by short-term activation of TRPML1.

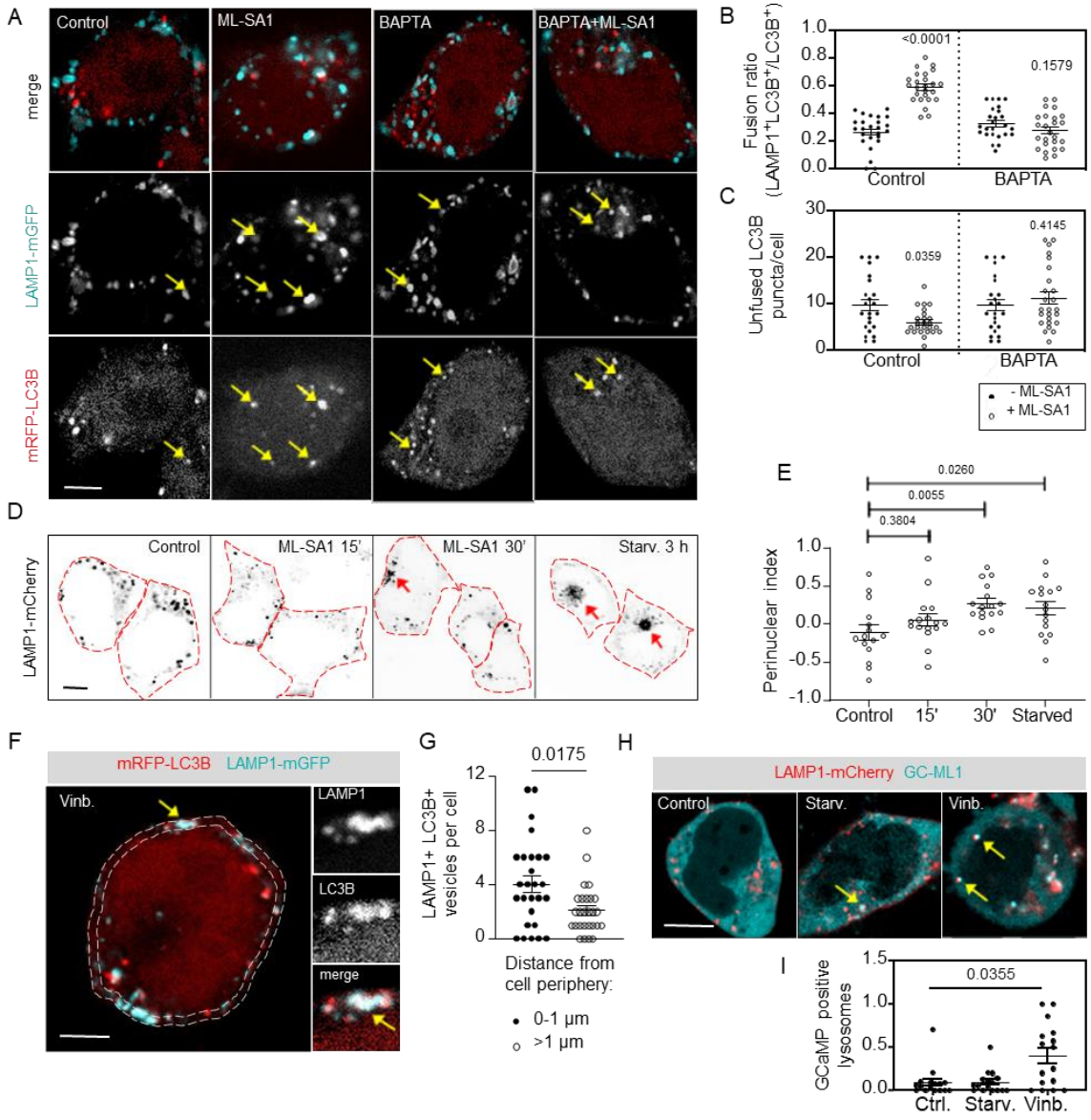

Figure 10: Short-term activation of TRPML1 promotes autophagosome-lysosome fusion independent of lysosome transport.

(A) AP-LY fusion was assessed using LAMP1-mGFP and mRFP-LC3 coexistence after ML-SA1 treatment (25 µm, 15 min) in either control or BAPRA-AM pre-treated cells. Arrows indicate co-existed structures. Bar: 5 µm.

(B) Quantification of fusion ratios by scoring the colocalizing LAMP1 (lysosomes) and LC3- positive structures. N=25. Statistics: Mann-Whitney test was applied on control and ML-SA1 samples; unpaired t-test was applied on BAPTA and BAPTA+ML-SA1.

(C) Quantification of unfused LC3 structures by scoring the non-colocalizing LC3 only structures. N≥23 for all samples. Statistics: Mann-Whitney test was applied.

(D) Lysosome distribution in LAMP1-mch expressing HEK293 cells either control (untreated), ML-SA1 (15 minutes, 30 minutes) treated, or amino acid starved (3 h) cells. Bar: 5 μm. Red arrows indicate lysosome clouds.

(E) Perinuclear index of lysosomes was measured from cells shown in (D) as explained in Methods. N≥15 for all samples. Statistics: One way-ANOVA test was applied and p values were calculated from multiple comparisons.

(F) AP-LY fusion was promoted in vinblastine-treated (20 μm, 2.5 h) cells observed in increased colocalization between LAMP1 and LC3-positive structures. Arrows indicate colocalizing structures. Cell periphery (0-1 μm) is labelled with dotted lines. Bar: 5 μm.

(G) Increased autolysosomes in vinblastine-treated cells at cell periphery. N=27. Statistics: Mann-Whitney test was applied.

(H) Increased GC-ML1-positive lysosomes in vinblastine-treated cells. Arrows indicate colocalizing GC-ML1 and LAMP1-positive structures.

(I) Quantification of colocalizing GC-ML1 and LAMP1-positive structures in control, starved, vinblastine-treated cells. N≥16. Statistics: Kruskal-Wallis test was applied and p values were calculated from multiple comparisons.

To further validate these findings, the microtubule inhibitor vinblastine was used to prevent lysosome migration. Surprisingly, we found that vinblastine treatment caused remarkable colocalization between autophagosomes and lysosomes (**Figure 10F**), observed prominently close to the cell periphery (**Figure 10G**). Moreover, vinblastine-treated cells exhibited a significant colocalization between GC-ML1 with LAMP1-mCherry puncta compared to control (untreated) cells (**Figure 10H and 10I**), further solidifying the connection between TRPML1 activity and AP-LY fusion. We also found a significant increase in TRPML1 cellular agonist PI(3,5)P_2 on lysosomes, observed as more colocalization between LAMP1-mCherry and GFP-PI(3,5)P_2 puncta in vinblastine-treated cells compared to control ones (**Figure S2A and S2B**). This finding explains why there is increased GCaMP activity on vinblastine-treated lysosomes. Moreover, vinblastine treatment increased lysosome size compared to control cells (**Figure S2C**). This again could be due to increased lysosomal PI(3,5)P_2 driving AP-LY fusion through TRPML1 activation, given that PI(3,5)P_2 is locally synthesized during homotypic fusion between lysosomes [199,238]. Additionally, v-ATPase inhibitor Bafilomycin A1 (BafA1) prevented the fusion between autophagosomes and lysosomes in vinblastine-treated cells, as expected (**Figure S2D**). This finding suggests that vinblastine promotes local, non-migratory lysosomal fusion. Altogether, these data indicate that TRPML1 activity promotes AP-LY fusion which is independent of lysosome migration.

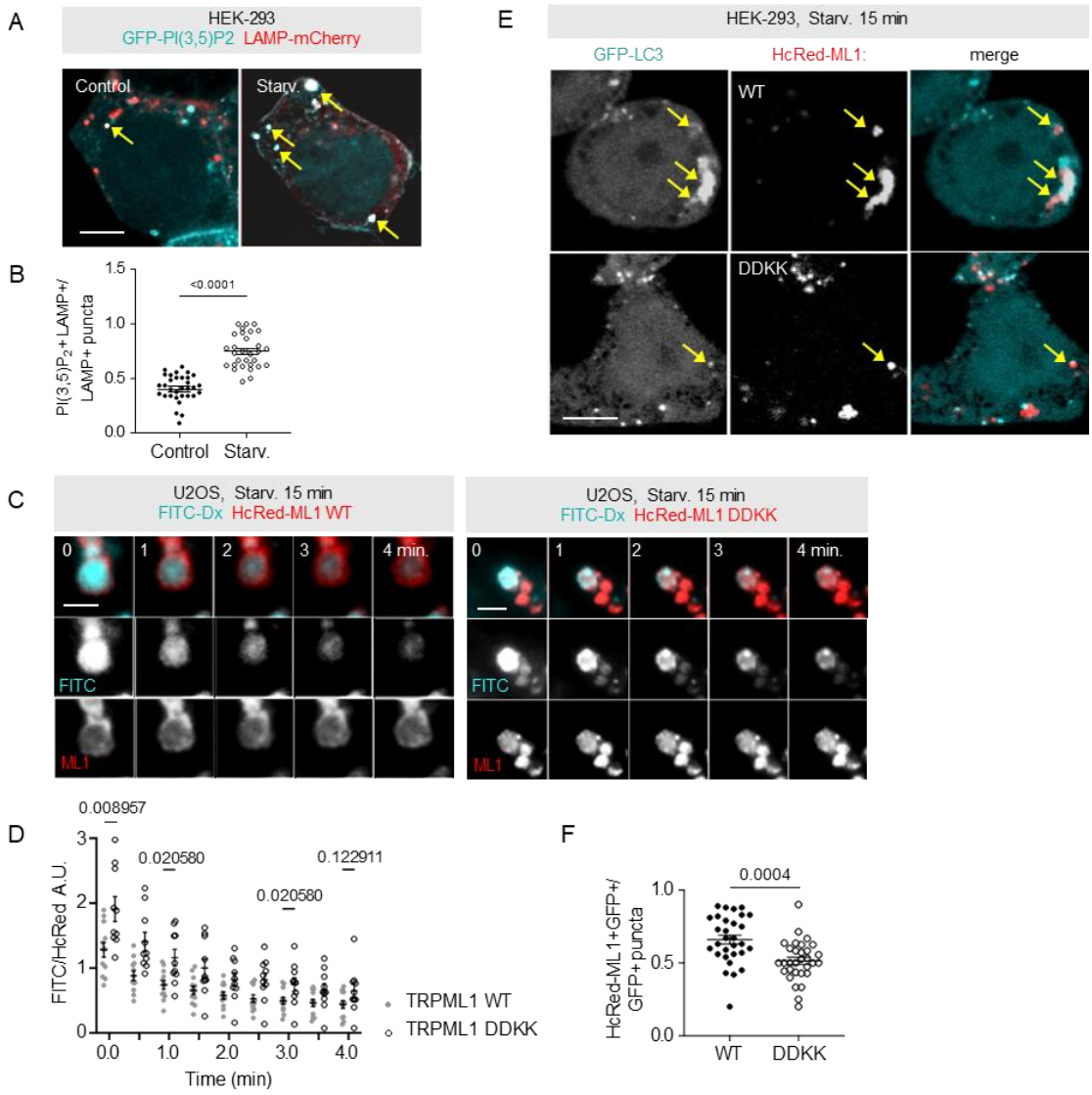

Figure 11: Perturbed lysosomal fusion and acidification responses in mutant TRPML1 during starvation.

(A) Transiently transfected U2OS cells with either wild-type or mutant TRPML1 (D471K/D472K) and both are HcRed-tagged. One day after transfection, cells were pulsed with FITC-Dx-containing complete media and then chased in HBSS. Both TRPML1wt and TRPML1DDKK-transfected cells were Live imaged in HBSS media and more FITC quenching (indicating lysosomal acidification) dynamics was seen in TRPML1wt compared to TRPML1DDKK during indicated time period. Bar: 2 µm (wt) and 5 µm (DDKK).

(B) The intensity of FITC-Dx fluorescence of individual lysosomes was measured at each timepoint and then divided by each respective HcRed fluorescence. N≥10 both samples. Mann-Whitney tests were applied at each timepoint.

(C) Transiently transfected HEK-293 cells with either wild-type or mutant TRPML1 (D471K/D472K) and GFP-LC3 to monitor AP-LY fusion after 30 minutes of starvation period (HBSS). Arrows indicate colocalized structures, which are abundant in TRPML1wt-expressing cells. Bar: 5 µm.

(D) Fusion ratios of colocalizing autophagosomes and lysosomes (LC3 and HcRed) to total autophagosomes (LC3). N=15. statistics=unpaired t test was applied.

4.3. Lysosomal acidification and fusion with autophagosomes are impaired in TRPML1-mutant cells during starvation

Since TRPML1 currents are active during starvation, we wanted to see if lysosomal $PI(3,5)P_2$ is also upregulated. Indeed, 2 hours starvation remarkably increased lysosomal $PI(3,5)P_2$ levels (**Figure 11A, 11B**). Importantly, this increase is not related to an autolysosomal degradation defect like in case of vinblastine. We next aimed to study the physiological role of TRPML1 during autophagy. To this end, we overexpressed wild type HcRed-TRPML1 WT or a pore-forming mutant HcRed-TRPML1 DDKK (D471K/D472K) [239]. The mutant TRPML1 DDKK heterotetramerizes with endogenous TRPML1 and hence its overexpression acts as a dominant negative effect, preventing TRPML1 Ca^{2+} release [240]. To validate the ion conductance in these two constructs, we monitored cytosolic Ca^{2+} in response to ML-SA1. HEK cells were transfected to co-express cyto-GCaMP6m and HcRed-TRPML1 WT or HcRed-TRPML1 DDKK. The cytosolic Ca^{2+} level was markedly attenuated in TRPML1 DDKK- expressing cells, observed as less cyto-GCaMP fluorescent intensity, in response to ML-SA1 compared to TRPML1 WT- expressing cells (**Figure S3A and S3B**).

We next tested lysosomal acidification using FITC-Dx in U2OS expressing TRPML1 WT or TRPML1 DDKK. FITC quenching (i.e. luminal acidification) was clearly faster in TRPML1 WT cells as opposed to TRPML1 DDKK- expressing cells during starvation (**Figure 11C**). Next, FITC fluorescence was measured from individual lysosomes. The FITC fluorescence of individual lysosomes significantly reduced in TRPML1 WT- expressing cells compared to TRPML1 DDKK- expressing ones during starvation (**Figure 11D**). In agreement with that, cells expressing TRPML1 DDKK had significantly less LTDR signal compared to the cells expressing TRPML1 WT at resting state (fed condition) (**Figure S3C and S3D**). Together, both findings highlight the role of TRPML1 in lysosomal acidification during physiological conditions.

Furthermore, we checked AP-LY fusion in cells expressing HcRed-TRPML1 WT or HcRed-TRPML1 DDKK, and HcRed-ML1 was used as a lysosome marker to track their fusion with autophagosomes. We found significantly increased colocalization between HcRed-ML1 and GFP-LC3 in TRPML1 WT-expressing cells compared to DDKK-expressing ones during starvation (**Figure 11E and 11F**), as well as prominent lysosomal clusters at perinuclear region in TRPML1 WT-expressing cells compared to dispersed lysosomes throughout the cytoplasm in DDKK-expressing cells (**Figure 11E**), indicating AP-LY fusion and lysosomal migration

are driven by TRPML1 activity. Altogether, these data demonstrate the role of TRPML1 in regulating lysosomal acidification and AP-LY fusion during starvation.

4.4. Autophagosome-lysosome fusion is required for TRPML1 Ca^{2+} release and lysosomal acidification in response to ML-SA1

To investigate the connection between AP-LY fusion and lysosomal acidification in response to TRPML1 agonist ML-SA1, we generated HEK-293 cells stably expressing Doxycycline (Dox)-inducible (Tet-on) shRNA to knockdown the expression of proteins involved in AP-LY fusion: VAMP7, and phosphatidylinositol 4-kinase type 2 alpha (PI4K2A). VAMP7 is a lysosomal SNARE protein [62]. PI4K2A is a lipid kinase that converts phosphatidylinositol (PI) to PI4P. Importantly, I am a co-author of a recent paper in which we showed that autophagosomal PI4P is a key phospholipid that directly binds to Syntaxin 17 to recruit this autophagosomal SNARE, an autophagosome fusion competence factor[241]. Given an earlier report that PI4P is required to repair lysosomal membrane damage [242], we first wanted to rule out lysosome damage occurrence. This is especially important in case of TRPML1, because membrane damage can lead to leakage of protons and thus disrupting ion homeostasis in the lumen. We studied this during our short ML-SA1 treatment in shRNA expressing cells (shVAMP7 and shPI4K2A) by monitoring galectin-3 (Gal-3) recruitment to lysosome membrane using a GFP-Gal-3 reporter. Gal-3 puncta number was largely unchanged after 15 minutes of ML-SA1 treatment compared to control condition, and significantly elevated when using glycyl-l-phenylalanine 2-naphthylamide (GPN), lysosomal damage inducer (serving as positive control) (**Figure S4A and S4B**). Similarly, shVAMP7- and shPI4K2A- expressing cells (+Dox) did not exhibit any significant differences relative to non-induced cells (−Dox) (**Figure S4E and S4G**), both of which were validated to work on the mRNA and protein expression level (**Figure S4D and S4F**). These results confirm the lysosomal integrity during ML-SA1 treatment in shVAMP7 and shPI4K2A cells. We next validated the knockdowns for their expected phenotypes in blocking AP-LY fusion, using the tandem fluorescent-tagged LC3 (mRFP-EGFP-LC3) reporter – here, GFP fluorescence quenches in the lysosomal acidic environment and thus red only signal indicates AP-LY fusion (i.e. autolysosomes). AP-LY fusion was significantly attenuated in shVAMP7 and shPI4K2A expressing cells during starvation (**Figure 12A and 12D**).

Next, we checked the TRPML1 activity in response to ML-SA1 in these fusion-deficient cells. To address this, we expressed GC-ML1 in shRNA-expressing cells and then

live imaged them starting at one minute before ML-SA1 treatment for a total timeframe of 5 minutes. We found that the GC-ML1 fluorescence response was significantly less in shVAMP7- and shPI4K2A- expressing cells upon ML-SA1 treatment, and similar scenario was observed when measuring maximal whole-cell fluorescence of GC-ML1 (F_{max}-F_0/F_0) (**Figure 12B, 12E, 12C and 12F**), indicating that TRPML1 activity is severely attenuated in fusion-deficient lysosomes. TRPML1 is trafficked to lysosomes *via* the endocytic pathway. To check whether the reduced TRPML1 activity in these knockdowns is due to lysosomal mis-localization of TRPML1, LAMP1-mGFP and HcRed-ML1 WT were co-expressed in shVAMP7-expressing cells. We found that shVAMP7-expressing cells showed normal localization of HcRed-ML1 WT on lysosome during starvation (**Figure 12G**). We next tested the lysosomal acidification of fusion-deficient lysosomes. We found that lysosomal acidification response showed mildly significant reduction in shVAMP7-expressing cells compared to non-induced ones (−Dox) upon ML-SA1 treatment (**Figure 12H**), highlighting the importance of AP-LY fusion for lysosomal acidification. Strikingly, lysosomal cathepsin activity was reduced in shVAMP7-expressing cells compared to non-induced ones (−Dox) in response to starvation and ML-SA1 treatment (**Figure 12I**), indicating that lysosome fusion with autophagosomes is required for lysosomal cathepsin activity. Of note, VAMP7 knockdown was chosen over PI4K2A knockdown to test lysosome activity due to its more specific role in lysosome fusion with autophagosomes. In line with these results, we found that FITC quenching was faster in LC3-positive lysosomes (autolysosomes) compared to LC3 negative lysosomes (naïve lysosomes) during starvation (**Figure 12J and 12K**). Altogether, these data demonstrate the importance of AP-LY fusion for TRPML1 activation, lysosomal acidification and cathepsin activity.

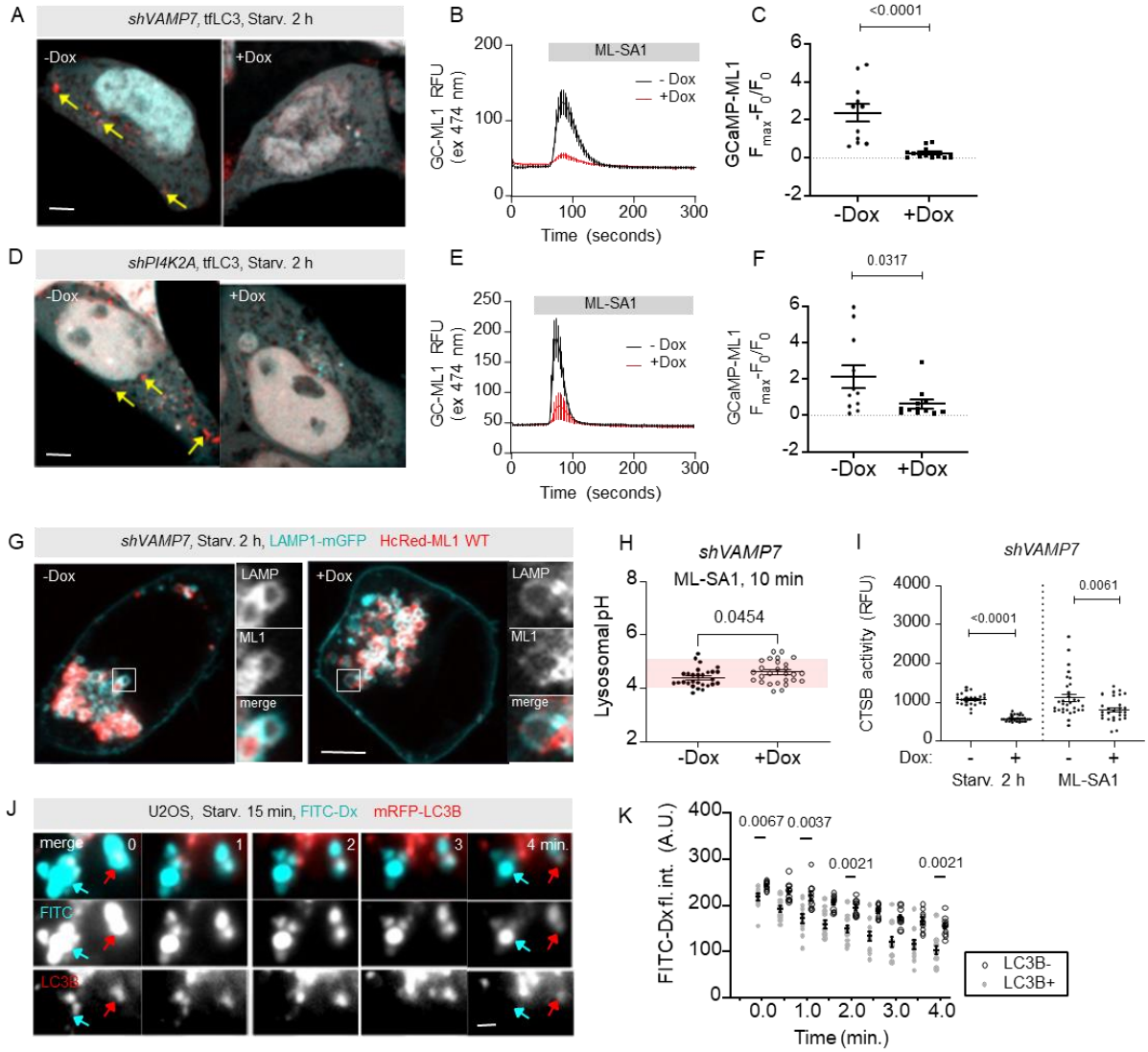

Figure 12: TRPML1-mediated Ca^{2+} release-triggered lysosomal acidification responses need lysosomal fusion.

(A) shVAMP7 expression was induced by incubating stable shVAMP7 expressing cells in 2 µg/ml Dox for 72 hours to knockdown VAMP7. AP-LY fusion was assessed in 2h starved (EBSS) shVAMP7 expressing cells using mFRP-EGFP-LC3B (tfLC3). Arrows indicate single autophagosomes (unfused). See also Figure 11C.

(B) shVAMP7 expressing cells were transiently transfected with GC-ML1. GC-ML1 response to ML-SA1 treatment was significantly reduced. N≥11 for all samples.

(C) Quantification of GC-ML1 response to ML-SA1 treatment in inducible shVAMP7 expressing cells. N≥10 for both samples. Statistics: Mann-Whitney test was applied.

(D) shPI4K2A expression was induced by incubating stable shPI4K2A expressing cells in 2 µg/ml Dox for 72 hours to knockdown PI4K2A. AP-LY fusion was assessed in 2h starved (EBSS) inducible shPI4K2A expressing cells using mFRP-EGFP-LC3B (tfLC3). Arrows indicate single autophagosomes (unfused). See also Figure 11C.

(E) GC-ML1 response to ML-SA1 treatment was significantly reduced in inducible shPI4K2A expressing cells. N=6 for all samples.

(F) Quantification of GC-ML1 response to ML-SA1 treatment in inducible shPI4K2A expressing cells. N≥10 for both samples. Statistics: Mann-Whitney test was applied.

(G) TRPML1 localization on lysosomal membrane was unaffected in shVAMP7-expressing cells (fusion deficient). Inset=localization to lysosomal membrane. Bar:5 µm.

(H) Absolute lysosomal pH was measured based on FITC-Dx quenching shVAMP7 cells during ML-SA1 treatment, demonstrating a statistically significant perturbation of lysosomal pH response. N≥26 for both samples. Statistics: unpaired Student's t-test was applied.

(I) Cathepsin B activity was assessed in either 2h starved (EBSS) or ML-SA1 (25 µM, 20 minutes) treated shVAMP7 cells based on Magic Red staining. Relative Magic Red fluorescence was measured from the whole cell using a similar experimental setup. N≥25 for all samples. Statistics: Mann-Whitney test was applied on both sets of samples (starvation and ML-SA1).

(J) UO2S cells were transiently transfected with mRFP-LC3B and then incubated with FITC-Dx overnight, followed by a short starvation period (15 minutes) in EBSS. Positive structures for both LC3 and FITC represent autolysosomes (red arrow). Positive structures for only FITC represent naive lysosomes (cyan arrow). FITC quenching was directly proportional to lysosomal acidification and more significant in structures that are double positive for LC3 and FITC. Bar: 1 µm.

(K) Quantification of FITC fluorescence that are either LC3B+ or LC3- at each time point. N≥10. Statistics: Holm-Šídák method was applied with multiple t-tests to measure statistical significance.

4.5. TRPML1-mediated Ca^{2+} release promotes the recruitment of Qa-SNARE Stx7 and R-SNARE VAMP7 to lysosomes

Since SNAREs provide direct connection with lysosomal fusogenicity, we aimed to investigate whether the lysosomal SNAREs, including Stx7 and VAMP7, are redistributed during short-term activation of TRPML1. We found a significantly increased colocalization between GFP-Stx7 and TMEM192-mRFP, a lysosome marker, after ML-SA1 treatment compared to control conditions (**Figure 13A and 13C**). In a similar way, we also found significantly increased colocalization between GFP-VAMP7 and TMEM192-mRFP after ML-SA1 treatment compared to control (**Figure 13B and 13D**). These two findings indicate increased lysosomal SNARE localization after TRPML1-mediated Ca^{2+} release and thus promoting lysosomal fusion competence.

We were curious to study the mechanism by which lysosomal fusion competence is promoted by TRPML1 activation. It has been reported that lysosomal SNARE VAMP7 is transported to late endosomes from trans-Golgi network on LAMP carrier vesicles along with LAMP and hVps41, one subunit of HOPS tethering complex. This process is independent of lysosomal hydrolase trafficking mediated by M6PR and CCVs[243]. To study this, we live imaged U2OS cells transiently expressing mCherry-LAMP1 and GFP-VAMP7 during TRPML1 activation. We found an increased association of small vesicles positive for both LAMP1 and VAMP7 to large LAMP1-positive structures starting from 10 minutes of ML-SA1

treatment (**Figure 13E and 13F**). Similarly, we also found an increased association of small vesicles positive for both LAMP1 and Stx7 to large LAMP1-positive structures starting from 10 minutes of ML-SA1 treatment (**Figure S5A**). These findings indicate the increased association of lysosomal SNAREs VAMP7 and Stx7 through LAMP carrier vesicles to lysosomes after TRPML1 activity. Overall, we conclude that TRPML1-mediated Ca^{2+} release promotes the enrichment of lysosomal SNARE VAMP7 and Stx7 *via* LAMP1 SNARE carrier vesicles, enhancing lysosomal fusion competence, and thereby facilitating AP-LY fusion.

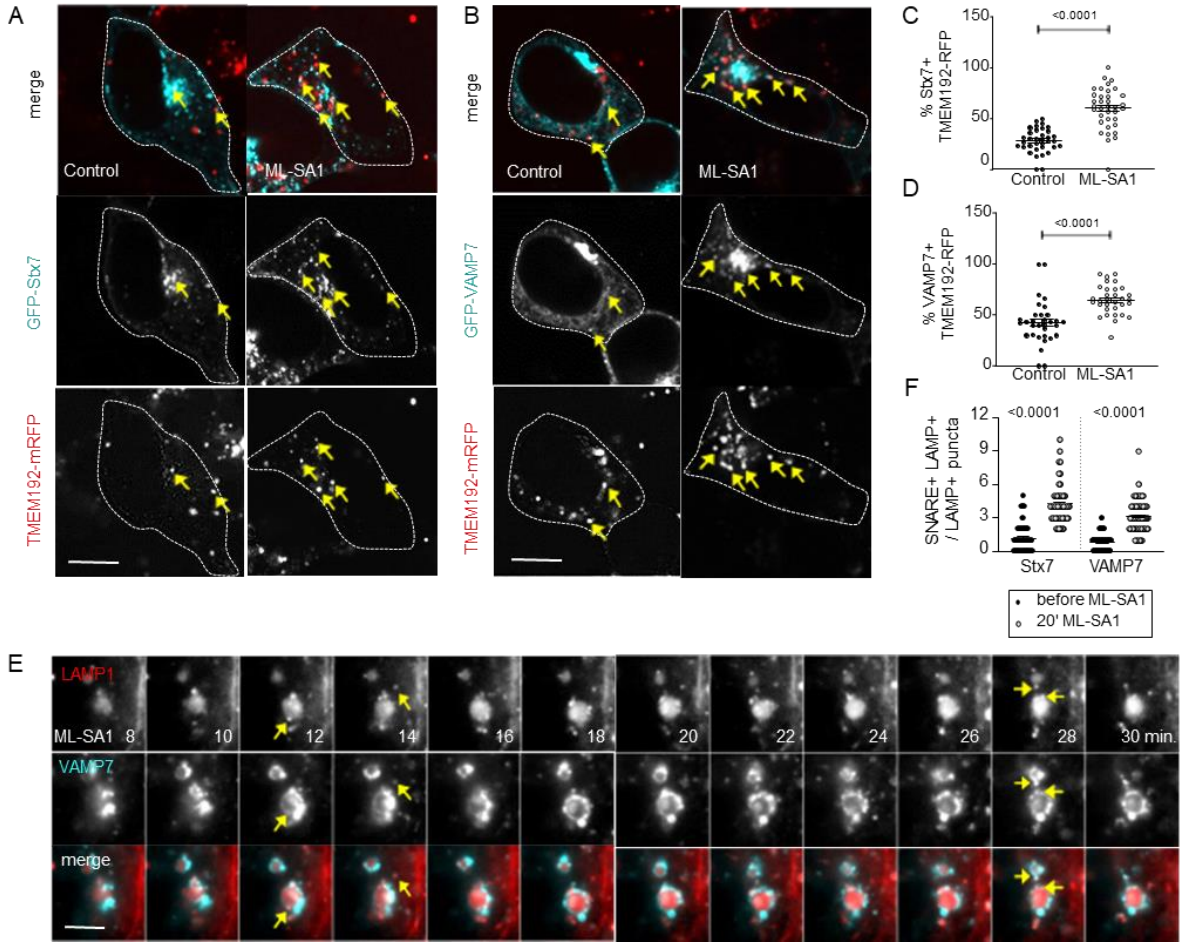

Figure 13: TRPML1-mediated Ca^{2+} release enhances localization of lysosomal Qa-SNARE Stx7 and R-SNARE VAMP7.

(A) Increased lysosomal association of GFP-Stx7 after ML-SA1 treatment. Arrows indicate coexisting structures. Bar: 5 µm.

(B) Stx7-positive structures colocalizing with TMEM192-positive lysosomes were quantified. N=35. Statistics: unpaired Student's t-test was applied.

(C) Increased lysosomal association of GFP-VAMP7 after ML-SA1 treatment. Arrows indicate coexisting structures. Bar: 5 µm.

(D) VAMP7-positive structures colocalizing with TMEM192-positive lysosomes were quantified. N=32. Statistics: Mann-Whitney test was applied.

(E) U2OS cells transfected with mCherry-LAMP1 and GFP-VAMP7, and live imaged following the onset of ML-SA1 treatment. The highlighted periods show Ml-SA1 treatment. Yellow line profiles represent the profile plots to the right. Bar: 5 μm.

(F) Top: profile plot illustrating LAMP1 (red line) and VAMP7(green line)-positive lysosomes at initial stages of ML-SA1 treatment. Middle: small carrier vesicles positive for both GFP-VAMP7 and mCherry-LAMP1 are observed localizing to lysosomes. Bottom: lysosomes are enriched with VAMP7 and LAMP1 at later stages of ML-SA1 treatment.

(G) Quantification of SNARE-positive structures at the margin of large LAMP1-positive structures at 0 and 20 minutes of ML-SA1 treatment. N≥100 for all samples. Statistics: Mann-Whitney test was applied.

4.6. $PI(3,5)P_2$ depletion leads to SNARE sequestration within lysosomes

$PI(3,5)P_2$ is the sole known cellular agonist of TRPML1 and is transiently synthesized by PIKfyve on lysosome membranes. PIKfyve inhibition blocks the synthesis of $PI(3,5)P_2$, leading to lysosome enlargement due to accelerated lysosome coalescence and reduced lysosome fission, as well as defects in AP-LY fusion [205,206]. We first validated the effect of PIKfyve-inhibitor apilimod (Ap) in HEK-293 cells. Ap treatment showed a significant reduction of GFP-$PI(3,5)P_2$ dots after 1 hour treatment (**Figure S5B and S5C**). Next, we checked whether the AP-LY fusion defect in PIKfyve inhibited condition is due to SNARE mislocalization, providing that SNAREs are shown to be abnormally clustered on lysosome membranes in lysosomal storage disorder (LSD) mouse model, which affects cholesterol metabolism [236]. For this purpose, GFP-Stx7 or GFP-VAMP7 and TMEM192-mRFP were co-expressed in HEK-293 cells which then were treated with Ap as above. We found that Stx7- or VAMP7- positive structures appeared in two forms: foci-like on the margin of TMEM192-positive structures or accumulated inside TMEM192-positive structures in Ap-treated cells, compared to perfect membrane colocalization between Stx7-or VAMP7-positive puncta and TMEM192-positive puncta in 1 hour starved cells (**Figure 14C**). In other words, SNAREs showed punctate form on lysosomal membranes or accumulated within lysosomes in $PI(3,5)P_2$-depleted cells (**Figure 14D**).

Next, we wanted to investigate a possible re-activation of TRPML1 in $PI(3,5)P_2$-depleted conditions by overexpression of the wild-type TRPML1. We found that HcRed-ML1 WT lysosomes greatly reduced its luminal Stx7-containing signal as compared to HcRed-ML1 DDKK ones, and restored perfect membrane localization (**Figure 14A and 14B**), indicating that TRPML1 activity rescues the lysosomal sequestration of Stx7 due to $PI(3,5)P_2$ depletion.

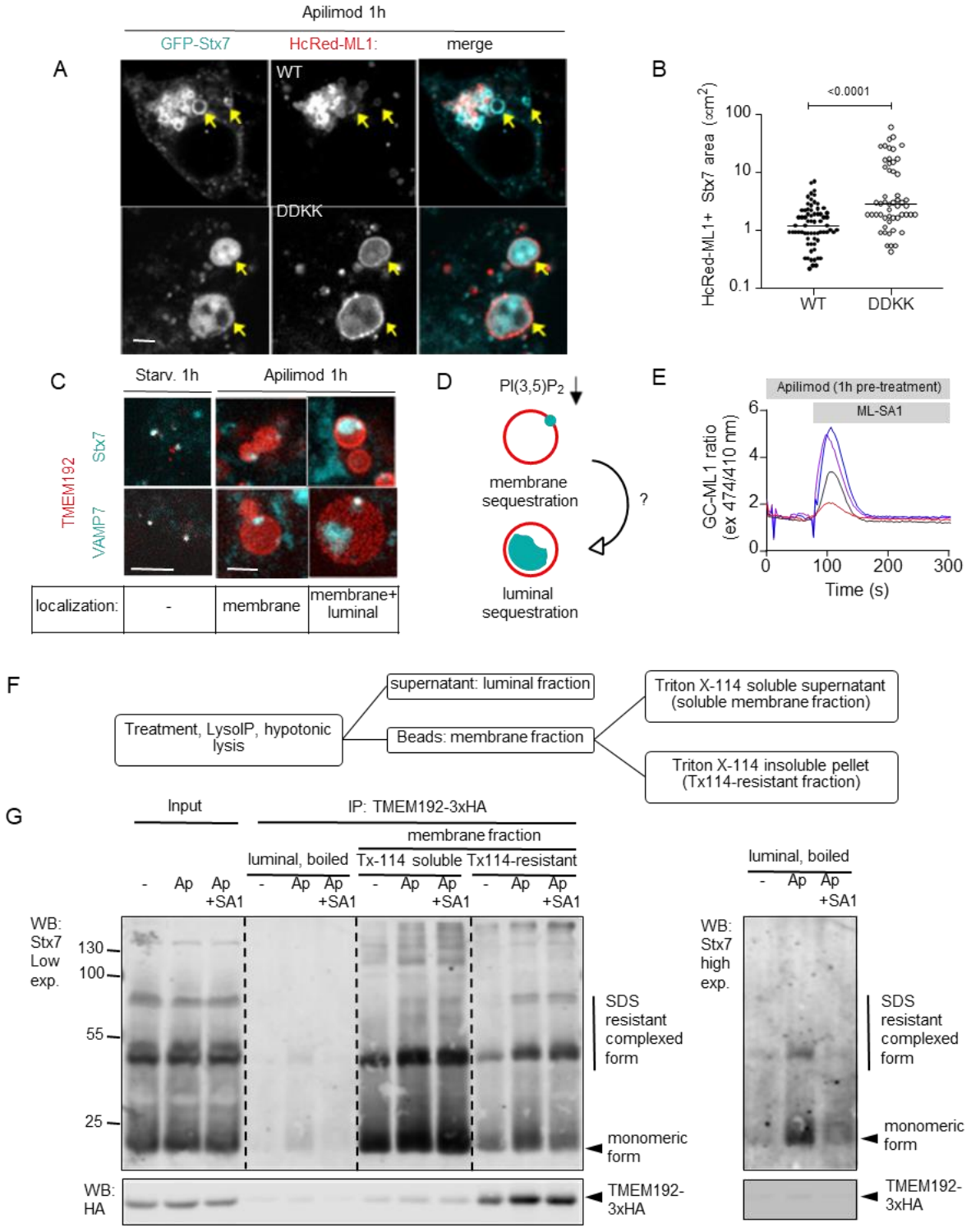

Figure 14: TRPML1 activation rescue aberrant lysosomal SNARE localization and fusion in PI(3,5)P_2-depleted cells.

(A) HEK-293 cells were transiently expressing HcRed-labeled TRPML1^{wt} or TRPML1^{DDKK} and GFP-Stx7 then incubated with Ap (1 µm, 1 h) to block PI(3,5)P_2 synthesis by PIKfyve activity. Arrows point to TRPML1-positive structures (lysosomes) circulating Stx7 signal. Bar: 5 µm.

(B) Quantification shows dramatic increase in the size of Stx7 containing TRPML1-positive structures were observed in TRPML1^{DDKK} cells after Ap treatment, highlighting more Stx7 sequestration. N≥53 for both samples. Statistics: Mann-Whitney test was applied.

(C) Single lysosomes localized by TMEM192-mRFP and colocalized with lysosomal SNAREs Stx7 or VAMP7 in starved (EBSS 1 h) and Ap-treated cells. In PI(3,5)P_2 synthesis blockade, very distinguishable localization of SNAREs can be seen in the form of membrane or luminal sequestration. Bars: 5 µm.

(D) Diagram illustrates typical SNARE distribution in PIKfyve-inhibited cells by Ap, demonstrating foci-like localization on the membrane (top), along with sequestration inside TRPML1-positive structures (bottom) potentially at a later maturation stage.

(E) Ap-treated cells show TRPML1-mediated Ca^{2+} release seen in GC-ML1 signal in response to ML-SA1. N=4.

(F) Strategy of sample preparation for the fractionation of lysosomal proteins after Lyso-IP using TMEM192-3xHA expressing cells into membranes (soluble and resistant to Triton X-114) and luminal fractions.

(G) The level of endogenous Stx7 monomeric and complexed form was increased after Ap treatment in both Triton X-114 resistant luminal fraction (cf. high-exposure blot on the right). Ap and ML-SA1 co-treatment significantly reduced the level of sequestered Stx7 and somewhat reduced the monomeric form of Stx7 in the Triton X-114 resistant membrane fraction (Among these also was membrane protein TMEM192), both point that SNARE recycling from the lysosomes is restored.

4.7. TRPML1-mediated Ca^{2+} release restores lysosomal SNARE mis-localization to correct AP-LY fusion

To confirm TRPML1 response to its agonist ML-SA1 in PI(3,5)P_2 depleted cells, GC-ML1 was expressed in those cells which then were live imaged. We found that PI(3,5)P_2-depleted cells showed heterogeneous and delayed response of TRPML1-mediated Ca^{2+} release compared to control (untreated) ones (**Figure 14E and 9C**). Afterward, we aimed to investigate the possible recovery of lysosomal SNAREs sequestration in PI(3,5)P_2-depleted cells by pharmacologically opening the TRPML1 channel using ML-SA1. We again co-expressed TMEM192-mRFP and GFP-Stx7 or GFP-VAPM7 in HEK-293 cells. We found that ML-SA1 redistributed the localization of Stx7 or VAMP7 signals in TMEM192-positive structures in Ap-pre-treated cells (from foci-like to normally redistributed in lysosomes) (**Figure S5D, S5E, S5F and S5G**). This was in line with our finding where we observed restoration of SNAREs clustering within lysosomes in PI(3,5)P_2 depleted cells due to HcRed-ML1 WT overexpression (**Figure 14A and 14B**).

To validate these results using a biochemical approach, we first immunopurified lysosomes (Lyso-IP) after respective treatments. Lysosomes bound to beads were subjected to a hypotonic solution (5 mM Tris–HCl) to collect the luminal fraction (supernatant), then beads were exposed to Triton X-114 detergent to collect Tx114-soluble membrane fraction (Triton

X-114 soluble supernatant) and resistant membrane fraction (Triton X-114 insoluble pellet) as indicated in the scheme (**Figure 14F**). The following samples were used: Control (untreated), Ap, and Ap+ML-SA1. We found a significant accumulation of monomeric and complexed forms of Stx7 in luminal fraction in Ap-treated cells compared to untreated ones, which prominently reduced after Ap+ML-SA1 co-treatment (**Figure 14G, right panel**). Both monomeric and complexed forms of Stx7 accumulated in the soluble and insoluble membrane fractions in Ap treatment compared to untreated condition, and mildly decreased in the insoluble membrane fraction after Ap+ML-SA1 co-treatment (**Figure 14G**). These results indicate that TRPML1 activity rescues the abnormally sequestered SNAREs in lysosomes due to PI(3,5)P_2-depletion by facilitating the recycling of their monomeric forms. In agreement with this, we found that AP-LY fusion is restored in PI(3,5)P_2-depleted cells after 15 minutes of ML-SA1 treatment (**Figure 15**), Overall, these results indicate that TRPML1 activation redistributes abnormal SNARE clustering and thus rescues AP-LY fusion.

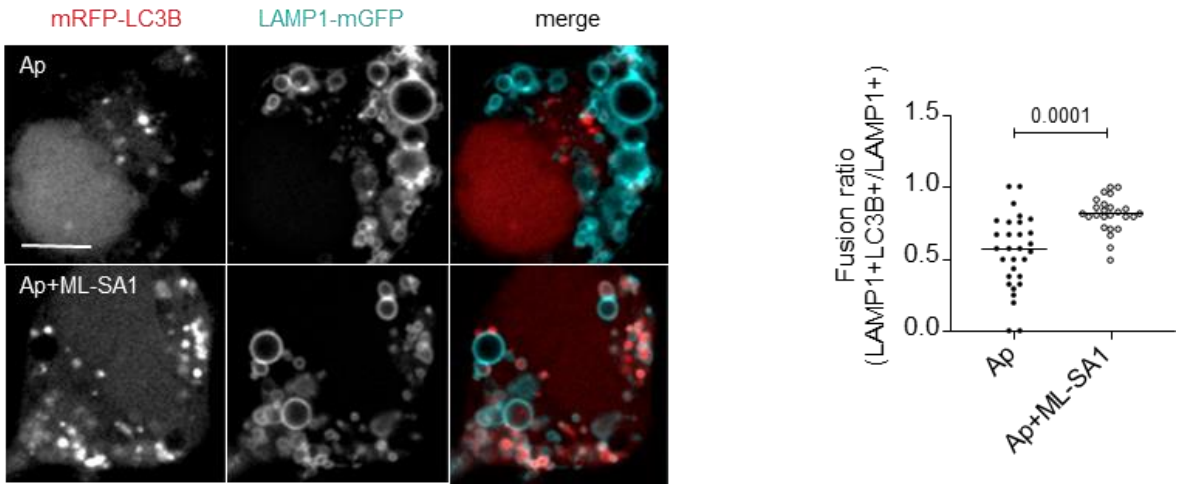

Figure 15: TRPML1 activation rescue lysosomal fusion in PI(3,5)P_2-depleted conditions. *HEK-293 cells expressing mRPF-LC3 and LAMP1-mGFP were treated with Aplilmod (1 µm, 1h), which block AP-LY fusion. Ap and ML-SA1 co-treatment rescued the fusion function of these lysosomes. Bar: 5 µm. Right: quantification of the results illustrates statistically significantly increased fusion events. N≥25 for both samples. Statistics: unpaired t test was applied.*

4.8. Calmodulin is required for Stx7 recycling by TRPML1

To further investigate how TRPML1-mediated Ca^{2+} release can correct the distribution of lysosomal SNAREs, providing that SNARE proteins are recycled to plasma membrane in calmodulin (CaM) dependent manner following endo-lysosomal fusion events [244,245]. Additionally, TRPML1 is shown to correct lysosome size in PIKfyve-inhibited cells by promoting lysosomal fission through CaM [207]. Here, cells co-expressing GFP-Stx7 and

TMEM192-mRFP were treated as indicated below and immunostained for pan-cadherin to mark cell periphery. After Ap treatment, cells were washed and then either untreated or treated with different drugs [ML-SA1, W7 and W7+ML-SA1]. To study CaM involvement in this process, we used CaM inhibitor W7 alone or together with ML-SA1. We found that ML-SA1 increased the number of small dots positive for Stx7 on cell periphery, while it failed to do that in the W7 co-treated cells (**Figure 16**), indicating the SNARE recycling to cell periphery by TRPML1 activity is a calcium- and CaM-dependent process.

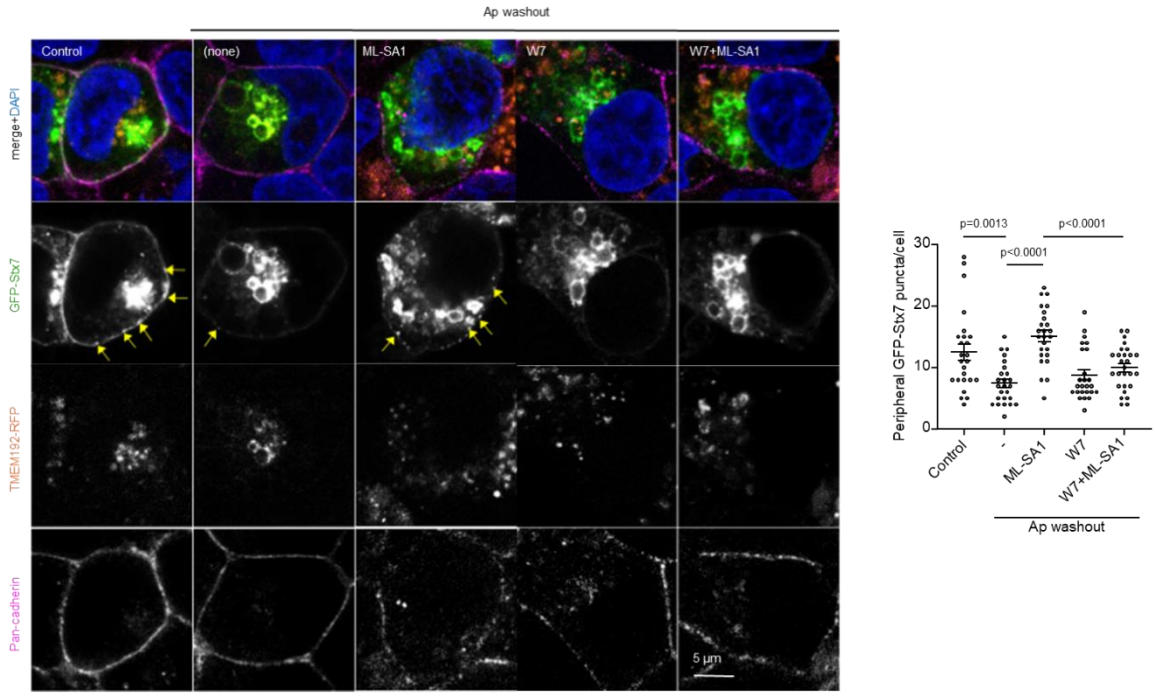

Figure 16: Calmodulin is necessary for recycling of Stx7 from lysosome to plasma membrane.

Stably expressing HEK293 cells for TMEM192-mRFP were transiently transfected with GFP-Stx7 and treated with Ap to block PIKfyve activity, followed by washout in 25 µM ML-SA1, 3 µM W7 (Calmodulin inhibitor) and 25 µM ML-SA1+3 µM W7 containing complete media (20 minutes). Next, cells were fixed with PFA and immunostained for pancadherin (plasma membrane marker). Arrows point to peripheral Stx7 dots that are close to cadherin signal, highlighting post-fusion Stx7 recycling. Left panel: The number of peripheral Stx7 dots per cell during indicated conditions. N≥25 for all samples. Statistics: Student t-test or Mann-Whitney test was applied.

4.9. Increased synthesis of PI(3,5)P_2 on autolysosomes during starvation, leading to TRPM1-mediated Ca^{2+} release

Our previous findings have showed that lysosomal fusion is required for TRPML1 Ca^{2+} efflux in response to TRPML1 agonist. We aimed to investigate the physiological relevance of this finding by detecting PI(3,5)P_2 levels during starvation, as it is the only known cellular agonist for this channel. To achieve this, U2OS cells were transfected with SECFP-STX17TM (blue channel, autophagosome marker), GCaMP6m-TRPML1 (green channel, TRPML1 Ca^{2+}),

and mKate2-ML1N*2 (red channel, $PI(3,5)P_2$ marker), and then incubated with LTDR (lysosome marker) containing HBSS, followed by live imaging. We observed a significant increase in $PI(3,5)P_2$ and GCaMP6m-TRPML1 fluorescence on structures positive for both STX17 and LTDR during the course of starvation (50 minutes). This highlights the increased synthesis of $PI(3,5)P_2$ on autolysosomes during starvation-induced autophagy, leading to TRPML1-Ca^{2+} efflux.

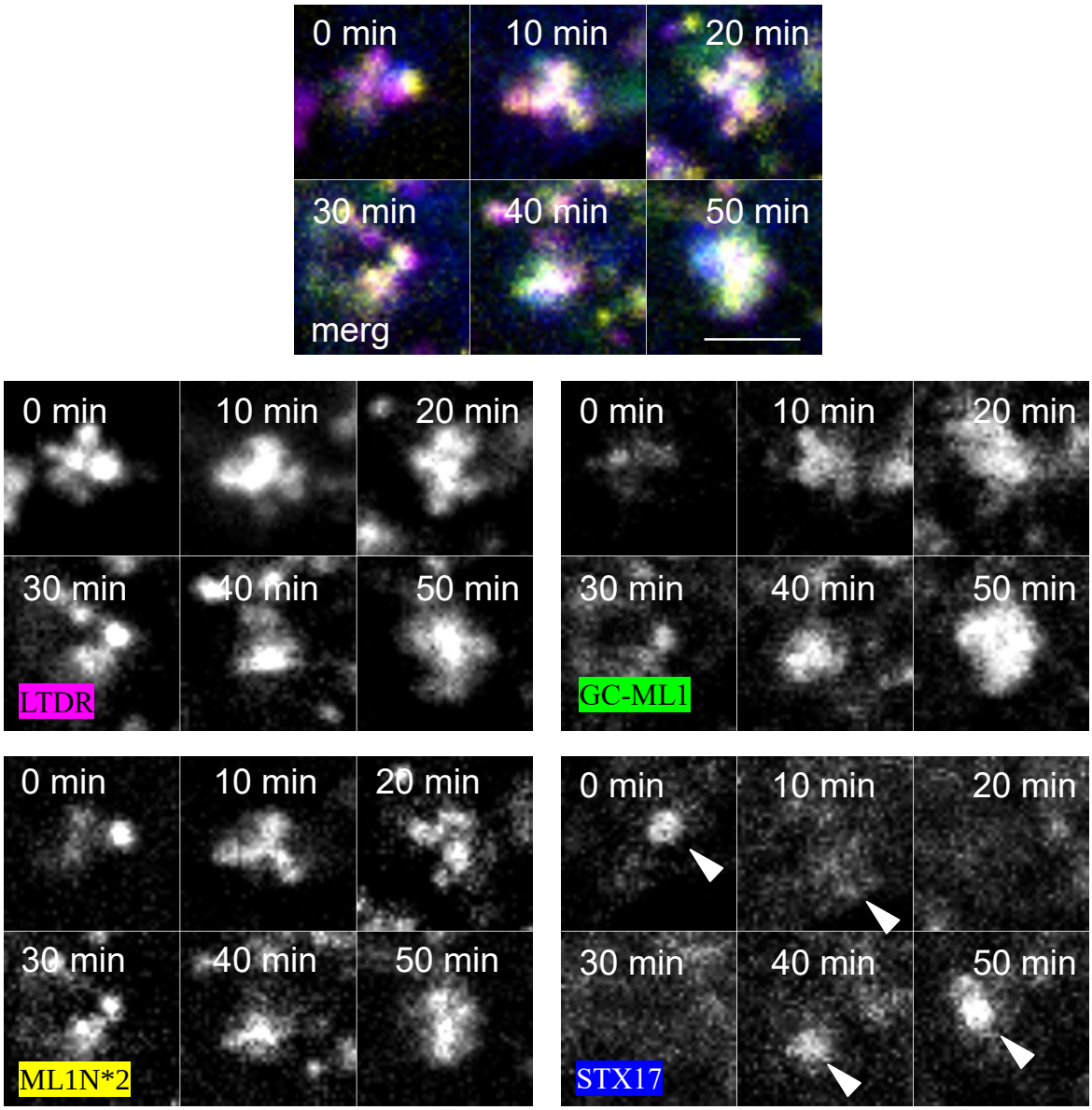

Figure 17: Increased PI(3,5)P_2 synthesis and TRPML1-mediated Ca^{2+} release from autolysosomes during starvation.

*U2OS cells were transfected with SECFP-STX17TM, GCaMP6m-TRPML1 and mKate2-ML1N*2 and incubated in LTDR (50 nM, 15 minutes) -containing HBSS (starvation media). The cells were washed twice and incubated with fresh starvation media (HBSS. Cells were imaged every 2 minutes for 50 minutes. LTDR: lysosome marker. GC-ML1:TRPML1 Ca^{2+}. ML1N*2: PI(3,5)P_2 marker. STX17: autophagosome marker. Bar: 2 µm.*

5. DISCUSSION

Long-term activation of TRPML1 (24 hours) was shown to promote viral removal, such as Dengue- and Zika viruses, by triggering lysosomal acidification [213]. The present work expands on these findings and demonstrates that TRPM1 activation of lysosomes is an early response, observed within 15 minutes of TRPML1 agonist treatment. This finding proposes a dual mode of action of TRPML1 during starvation: i) generation of new autophagosomes through calmodulin signaling [211], and ii) rapid degradation of existing autophagosomes by local fusion/acidification. Moreover, prolonged TRPML1 activation during autophagy is known to activate TFEB, a transcription factor that upregulates the production of proteins for lysosome biogenesis (e.g. LAMP proteins, lysosome transmembrane proteins [TMEM proteins], hydrolases etc.) and therefore add another layer of TRPML1 regulation on top of the two described above [85,229,246]. Lysosomal acidification is typically triggered by the increased assembly of lysosomal v-ATPase holocomplexes, which promotes intralysosomal proton pumping, as seen in response to decreases in free amino acid or glucose levels [133]. Here, TRPM1-induced acidification was concomitant with only a mild increase in lysosomal V1 enrichment, indicating that this prominent acidification was caused by mostly existing pre-assembled v-ATPase holocomplexes.

AP-LY fusion occurs close to the ER network where the majority of the autophagosomes form (from ER-adjacent phagophores). To achieve fusion, lysosomes thus must migrate towards the nucleus along the microtubule track. This is in parallel with anterograde migration of autophagosomes along the microtubule, regulated by the Rab7 effector RILP [53]. During autophagy, Ca^{2+} release from TRPML1 is sensed by Ca^{2+} binding protein ALG-2 which associates with dynactin-dynein motor complex to drive retrograde lysosomal migration, a process seen at 2 hours of starvation or TRPML1 activation. Here, we found that immediate early AP-LY fusion is promoted by short-term activation of TRPML1, and surprisingly retrograde lysosomal migration is dispensable during this process. Notably, the microtubule inhibitor vinblastine increased lysosomal TRPML1 activity, likely due to increased accumulation of lysosomal $PI(3,5)P_2$, concomitant with increased local AP-LY fusion. TRPML1-induced fusion is explained by increased lysosomal SNARE localization, namely Stx7 and VAMP7, enhancing lysosomal fusion competence, a process required for lysosomal fusion with autophagosomes. In agreement with that, we find both AP-LY fusion and lysosomal acidification were affected in mutant TRPML1 during physiological conditions, such as starvation or resting conditions.

Our data highlight the importance of fusing autophagosomes in promoting lysosomal TRPML1 activity. The question remains: How are lysosomes activated upon fusion with oncoming autophagosomes? Given that v-ATPase is the only driver for lysosomal acidification and its assembly is not significantly affected by TRPML1, hence it is possible that Ca^{2+} could directly promote the proteolipid c-ring rotation of the existing v-ATPase holocomplexes. We looked for canonical Ca^{2+} binding sites in V1 (e.g. EF hand and C2 domain) but were unable to find such sites. It is still possible that a non-canonical Ca^{2+} interaction exists: yeast v-ATPase was shown to interact with divalent cations such as copper [247]. It is therefore tempting to suggest that the autophagosomal fusion itself activates the v-ATPase – a recent report suggests that the N-terminal cytosolic domain of several V_0a subunits bind to specific phospholipids such as $PI(3,5)P_2$ and PI4P for their activation [248]. Of note, $PI(3,5)P_2$ is synthesized on the lysosome membrane during autophagy (see above), and while PI4P is primarily abundant in Golgi, it is also synthesized during autophagosome maturation and required for their fusion [241,249].

Lysosomal catalytic function is highly dependent upon SNARE recruitment and AP-LY fusion. Late endosomes receive their membrane proteins, including LAMP1 and VAMP7, from the trans-Golgi network (TGN) on LAMP carrier vesicles [243], while lysosomal hydrolase delivery from TGN occurs *via* CCVs [250]. Here, we identify that both VAMP7 and Stx7 are delivered by LAMP1-positive carrier vesicles as an early response of TRPML1 activation (CV association with lysosomes seen starting at 10 minutes of ML-SA1 treatment), enhancing lysosomal fusion competence, thereby facilitating AP-LY fusion.

$PI(3,5)P_2$ is transiently synthesized on lysosomal membranes by PIKfyve. AP-LY fusion defects were observed in PIKfyve-inhibited cells, concomitant with abnormal SNARE distribution in the enlarged lysosomes. Given that SNAREs are essential for lysosomal membrane fusion, the abnormal sequestration of lysosomal SNAREs is the most probable cause of the observed AP-LY fusion defects, since activation of TRPML1 during PIKfyve-inhibition rescues the fusion defects. Notably, this SNARE sequestration is very similar to the abnormal SNARE clustering on cholesterol-rich membrane microdomains seen in an LSD model [236]. Here, our findings indicate that TRPML1 activity rescues the abnormally lysosomal localized SNARE VAMP7 and Stx7 in PIKfyve-inhibited cells, seen as abrogating luminal SNARE clustering and redistributing them to their normal membrane localization. In agreement with this, TRPML1 corrected the AP-LY fusion defect in PIKfyve-inhibited conditions. Moreover,

following organellar fusion, SNAREs, including Stx7, are shown to be recycled to the plasma membrane through homo- and heterotypic fusion in Ca^{2+}/CaM dependent manner [244,245]. Here, TRPML1-mediated VAMP7 and Stx7 redistribution indeed was observed as recycling of Stx7 to the plasma membrane. Additionally, this process required CaM function, which is not surprising because CaM, downstream of TRPML1 Ca^{2+}, was shown to be required for lysosomal size maintenance in PIKfyve-inhibited cells [207]. A mechanistic summary of TRPML1 early functions towards lysosomal activation is visualized in (**Figure 18**).

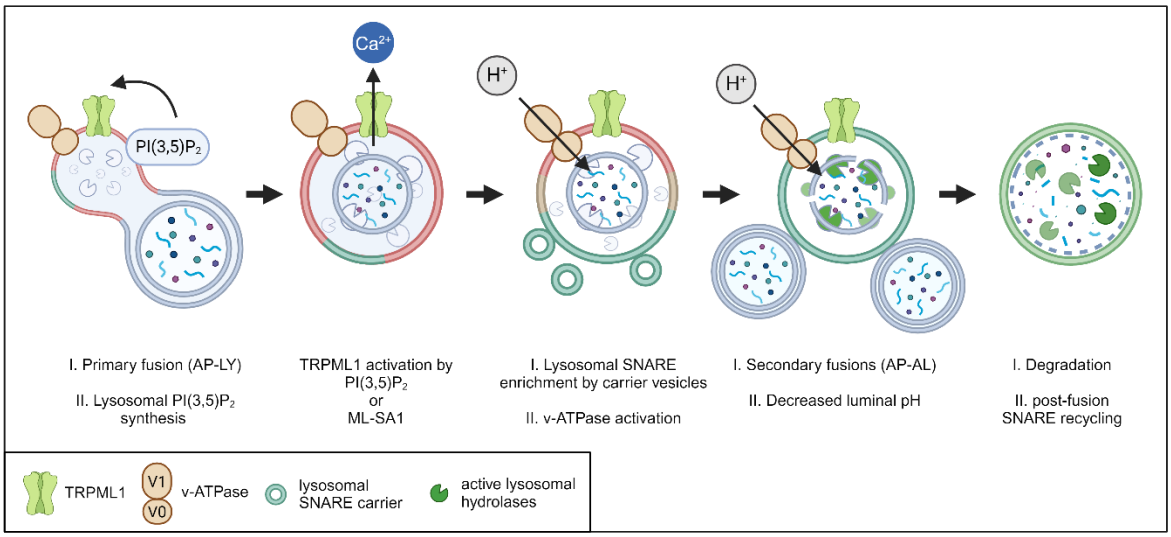

Figure 18: A working model to illustrate an early-onset function of TRPML1*. During autophagy, primary fusions between autophagosomes and naïve lysosomes (AP-LY fusion) is connected to increased lysosomal PI(3,5)P_2. Subsequently, TRPML1 activation by this increasing PI(3,5)P_2 ensues (or by pharmacological agonist activation such as ML-SA1), promoting enrichment of lysosomal SNARE proteins VAMP7 and Syntaxin 7 by LAMP carrier vesicles coupled with v-ATPase-mediated lysosomal acidification. Next, this increased lysosomal fusion competence facilitates further secondary autophagosome-autolysosome (AP-AL) fusion events for the complete degradation of intracellular cargo captured by autophagosomes, followed by post-fusion SNARE recycling to the plasma membrane. PIKfyve inhibition disrupts this process, leading to- i) no TRPML1 activity, ii) abnormal sequestering of lysosomal SNARE proteins.*

Given that v-ATPase is the only source for the acidification lysosomal lumen, our data show that TRPML1 Ca^{2+} release induced lysosomal acidification within a short time frame. This could be achieved either by a possible direct interaction between Ca^{2+} and v-ATPase or activated v-ATPase by phospholipids such as lysosomal PI(3,5)P_2 and autophagosomal PI4P for their as a secondary effect of AP-LY fusion [241,248]. However, connection between Ca^{2+} and v-ATPase still needs further investigation.

Our work along with previous studies demonstrates the physiological role of TRPML1 during starvation [176,193,234]. However, the timing and magnitude of TRPML1 Ca^{2+} current during starvation still needs further investigation.

6. SUMMARY

Autophagy is a cellular degradation pathway that is highly conserved in eukaryotes. Its main pathway is defined as engulfing damaged or unwanted cellular cargo inside vesicles called autophagosomes, delivering them to lysosomes for degradation and recycling. This mechanism is essential for cell survival and homeostasis during stress conditions, including hypoxia, nutrient deprivation, and reactive oxygen species [251]. Autophagy defects lead to diseases, including neurodegenerative disorders, such as AD and Parkinson's disease [252]. The autophagic degradation pathway ensures cellular energy production, degradation of damaged or toxic intracellular material, and reuse of organelles components [253]. For proper autophagic degradation, two critical steps must properly function after autophagosome formation: first, AP-LY fusion to form a hybrid organelle called autolysosome, and second, autolysosomal degradation by lysosomal hydrolases. Defects in those two steps were associated with diseases including Vici syndrome and LSDs causing neurodegeneration [254,255].

Lysosomes are the secondary cellular Ca^{2+} stores after ER. Lysosomal Ca^{2+} content is essential for several cellular functions, including autophagy, exocytosis, and membrane repair [160]. Lysosome membranes contain several ion channels and pumps. Among these channels and pumps, vacuolar-ATPase pump (v-ATPase) and transient receptor potential cation channel, mucolipin subfamily, member 1 (TRPML1), are critical for autophagy [256]. V-ATPase is composed of peripheral V1 and membrane-bound V0 domains, and it promotes luminal acidification by pumping protons into lysosomal lumen in an ATP-dependent manner. TRPML1 is a Ca^{2+} efflux channel that is active during starvation-induced autophagy, promoting autophagic flux through autophagosome formation and lysosome biogenesis [256].

Mucolipidosis type IV, one type of lysosomal storage disorder, is an inherited neurodegenerative disease characterized by delayed development and vision impairment due to lysosomal degradation defect that causes massive accumulation of autophagic vesicles containing undegraded cargo [257]. MLIV is caused by mutations in MCOLN1/TRPML1 gene, which is the cause of lysosomal dysfunction [257]. Since TRPML1 is a lysosomal cation channel that releases Ca^{2+} from the lysosomes upon amino acid depletion [176]. TRPML1 function is implicated in several pathways, including lysosomal biogenesis, lysosome positioning and tubulation, TFEB activation, and exocytosis [211,224,237].

Our study aimed to decipher the role of TRPML1-released Ca^{2+} in regulation of autophagosome (AP)-lysosome (LY) fusion, lysosomal acidification, and the connection between these two processes. The methods used in this study were: i) confocal microscopy, ii)

immunoblotting, iii) qPCR, iv) molecular cloning, v) inducible expression of shRNAs, and vi) Lyso-IP.

Our work finds an early-onset role of TRPML1 during autophagy, which is different from its well-established long-term functions that rely on transcription [213,237]. This early-onset role of TRPML1 was observed after pharmacological TRPML1 activation in the form of rapid lysosomal maturation accompanied by enhanced recruitment of lysosomal SNAREs, ultimately facilitating local AP-LY fusion, autolysosomal degradation, and post-fusion lysosomal SNARE recycling. Here, TRPML1 agonist treatment rapidly increased the perilysosomal Ca^{2+} levels detected as increased GCAMP-TRPML1 fluorescence, which was restored to its basal level within 20 seconds. This perilysosomal Ca^{2+} peak was blocked by intracellular Ca^{2+} chelation. Furthermore, TRPML1 activation greatly reduced intralysosomal pH within 15 minutes, which was also prevented by intracellular Ca^{2+} chelation. Although lysosomal acidification relies on lysosomal v-ATPase activity, assembly of v-ATPase holocomplexes only mildly increased during this period, simply more V1-V0 holocomplex-containing lysosomes became acidic. 15 minutes of TRPML1 agonist activation also clearly enhanced lysosomal cathepsin activity.

Additionally, 15 minutes of TRPML1 activation increased lysosomal fusion with autophagosomes, which was also prevented by intracellular Ca^{2+} chelation. Notably, this short period of TRPML1 activation showed a reduction in the number of unfused autophagosomes, indicating that new autophagosomes did not form during this short-term treatment, in contrast with its reported long-term role on autophagosome formation. This short period of TRPML1 activation did not significantly change lysosomal positioning, again in contrast with its reported long-term role on lysosomal migration. In support of this, microtubule inhibition surprisingly increased basal TRPML1 activity and AP-LY fusion. Microtubule inhibition also increased the accumulation of $PI(3,5)P_2$ on lysosomes concomitant with an enlargement of lysosomes, indicative of undegraded autolysosomes. This increased AP-LY fusion upon microtubule inhibitor treatment was abrogated during BafA1 co-treatment. These findings support an early role of TRPML1 in orchestrating local AP-LY fusion. Consistently, both AP-LY fusion and lysosome acidification were attenuated by expression of pore-forming mutant TRPML1 during starvation and in fed cells. In parallel, the synthesis of TRPML1 agonist $PI(3,5)P_2$ drastically increased in lysosomes of 2 hour starved cells. This likely triggers TRPML1-mediated Ca^{2+} release during starvation, as it is the only known cellular agonist for this channel. As a mechanism behind this increased local fusion, TRPML1 activity showed a marked increase in lysosomal fusion competence by promoting the association of SNAREs Stx7 and VAMP7 to

lysosomes on LAMP carrier vesicles. Crucially, our work shows that lysosomal fusion with autophagosomes is required for maintaining lysosomal Ca^{2+} effluxes and hydrolytic activity. Fusion-impaired lysosomes did not respond to TRPML1 agonist and starvation in the context of TRPML1 Ca^{2+} efflux, intralysosomal acidification, and cathepsin activity. $PI(3,5)P_2$ depletion by inhibiting PIKfyve resulted in abnormal sequestration of lysosomal SNAREs in the lumen. Given that TRPML1 has allosteric binding sites for $PI(3,5)P_2$ and the synthetic agonist ML-SA1, $PI(3,5)P_2$-depleted cells could be rescued by allosteric drug activation that abrogated the abnormal SNARE localization, including luminal sequestration of Stx7, and restored its recycling to the plasma membrane in a Calmodulin-dependent manner. Consequently, agonist activation of TRPML1 for 15 minutes was enough to rescue the AP-LY fusion defect arising from PIKfyve inhibition.

According to our working model, synthesis of lysosomal $PI(3,5)P_2$ is increased on autolysosomes formed after primary fusions between autophagosomes and naïve lysosomes during starvation-induced autophagy. Subsequently, this $PI(3,5)P_2$ (or pharmacological agonist activation by ML-SA1) leads to TRPML1 activation, promoting the enrichment of lysosomal SNARE proteins VAMP7 and Syntaxin 7 that are transported by LAMP carrier vesicles as well as v-ATPase-mediated lysosomal acidification. The resultant autolysosomes become acidic and fusion competent, facilitating more secondary autophagosome-autolysosome (AP-AL) fusion events for the proper degradation of intracellular cargo captured by autophagosomes. These are then followed by post-fusion SNARE recycling to the plasma membrane. PIKfyve inhibition disrupts this process, leading to: i) reduced TRPML1 activity, ii) abnormal sequestering of lysosomal SNARE proteins. Our study complements earlier efforts to understand TRPML1's complex role in regulating autophagy, which showed that it promotes activation of TFEB and biogenesis of autophagy-lysosome pathway genes.

While the role of TRPML1 in facilitating lysosomal cargo degradation has been confirmed by multiple reports [213,216,231,232], ours is the first study to show that TRPML1 promotes early steps: fusion of existing autophagosomes with lysosomes and lysosomal degradation of the first wave of incoming cargo. Our work shows that TRPML1 promotes AP-LY fusion by increased recruitment of lysosomal SNAREs. It is tempting to suggest further investigations on the role of TRPML1 in disease models because TRPML1 could be a potential therapeutic target to correct AP-LY fusion defects observed in autophagic-lysosomal degradation associated diseases such as Vici syndrome and vacuolar myopathy.

7. ÖSSZEFOGLALÓ

Az autofágia olyan sejten belüli lebontási folyamat, amely eukariótákban nagymértékben konzervált. Az autofágia fő útvonala során a sejtekben felhalmozódott káros, vagy nem kívánatos anyagok autofágoszómáknak nevezett vezikulákba csomagolódnak, és végsősoron a lizoszómákba szállítódnak lebontás és újrahasznosítás céljából. Ez a mechanizmus elengedhetetlen a sejtek túléléséhez és homeosztázisához stresszkörülmények, többek között hipoxia, tápanyagmegvonás és reaktív oxigéngyökök keletkezése esetén [251]. Az autofágia hibái betegségekhez vezethetnek, beleértve a neurodegeneratív rendellenességeket, mint például az Alzheimer-kór és a Parkinson-kór [252]. Az autofág lebontási útvonal biztosítja a sejtek energiatermelését, a sérült vagy toxikus intracelluláris anyagok lebontását és a sejtszervecskék összetevőinek újrafelhasználását [253]. A megfelelő autofág lebontáshoz két kritikus lépésnek kell jól működnie az autofagoszóma képződését követően: először az autofágoszóma- lizoszóma fúziónak (amely lehetővé teszi az autolizoszóma nevű hibrid organellum kialakulását), másodszor pedig az autoliszoszóma beltartalmának lebontása a lizoszómális hidrolázok által. E két lépés hibáit olyan betegségekkel hozták összefüggésbe, mint a Vici-szindróma és a neurodegenerációt okozó lizoszomális tárolási zavarok (LSD) [254,255].

A lizoszómák az ER után a sejtek másodlagos Ca^{2+} raktárai. A lizoszomális Ca^{2+} tartalom elengedhetetlenül szükséges számos sejtfunkcióhoz, többek között az autofágiához, az exocitózishoz és a membránjavítási folyamatokhoz [160]. A lizoszómális membránokba számos ioncsatorna és pumpa van beágyazva. E csatornák és pumpák közül kritikus fontossággal bír a vakuoláris-ATPáz pumpa (v-ATPáz), valamint a TRPML1 (transient receptor potential cation channel, mucolipin subfamily, member 1) [256]. A V-ATPáz két részből áll: a perifériás V1 doménből és a membránhoz kötött V0 doménből. Ez a pumpa a luminális savasodást segíti elő azzal, hogy ATP-függő módon protonokat pumpál a lizoszóma lumenébe. A TRPML1 egy $Ca2^{+}$ efflux csatorna, amely az éhezés indukálta autofágia során aktív állapotban van, elősegítve az autofág lebontást (fluxust) az autofagoszóma-képződés és a lizoszóma biogenezis révén [256].

A IV-es típusú mukolipidózis (MLIV) a lizoszomális tárolási betegségek (lysosomal storage disease - LSD) egyik típusa: egy örökletes neurodegeneratív betegség, amelyet a lizoszomális lebontás hibája okoz. Ezen betegség jellemzője a késleltetett fejlődés és látáskárosodás, amely a nem fuzionált autofagoszómák tömeges felhalmozódásával jár, így

felgyülemlenek a lebontásra szánt anyagok [257]. Az MLIV-et az MCOLN1/TRPML1 gén mutációi okozzák, ez vezet lizoszomális működési rendellenességekhez [257]. Mivel a TRPML1 egy lizoszomális kationcsatorna, amely aminosavhiány esetén Ca^{2+}-t szabadít fel a lizoszómákból [176], ezért a lizoszomális Ca^{2+}-felszabadulás hibájának jelentős szerepe van a betegség előrehaladásában. A TRPML1 több folyamatban is szerepet játszik: a lizoszómák biogenezisében, a lizoszómák pozicionálásában és tubulációjában, a TFEB aktiválásában és az exocitózisban [211,224,237].

Kutatásaink célja a TRPML1 által felszabadított Ca^{2+} szerepének megfejtése volt az autofagoszóma (AP)-lizoszóma (LY) fúziójában, a lizoszomális savasodás szabályozásában, valamint e két folyamat közötti kapcsolat feltárása. A vizsgálat során alkalmazott módszerek a következők voltak: i) konfokális mikroszkópia, ii) Western-blot, iii) qPCR, iv) molekuláris klónozás, v) indukálható shRNS expresszáló sejtes rendszer, vi) lizoszóma immunprecipitáció (Lyso-IP).

Dolgozatom a TRPML1 korai szerepéről számol be az autofágia szabályozása során, ami más, mint a már jól ismert hosszabb távú, transzkripciós változásokon alapuló funkciói [213,237]. A TRPML1 e korai szerepét gyors lizoszomális aktiváció formájában figyeltük meg a TRPML1 farmakológiai aktiválása után. Ezt a lizoszomális SNARE-k fokozott rekrutációja követte, ami segíti a lokális AP-LY fúziót, az autolizoszomális degradációt és a fúzió utáni lizoszomális SNARE újrahasznosítást. Megfigyeltük, hogy a sejtek TRPML1 agonista vegyülettel való kezelése gyorsan megnövelte a perilizoszomális Ca^{2+}-szintet a GCAMP-TRPML1 fluoreszcencia növekedése alapján, és ez 20 másodpercen belül visszaállt az alapszintre. A perilizoszomális Ca^{2+} ezen indukált emelkedését intracelluláris Ca^{2+}-kelátorral blokkolni tudtuk. Továbbá, a TRPML1 aktiválása 15 percen belül nagymértékben csökkentette az intralizoszomális pH-t, amit szintén megakadályozott az intracelluláris Ca^{2+} kelátképzés. Annak ellenére, hogy a lizoszomális savasodás a lizoszomális v-ATPáz működésére támaszkodik, mégis a v-ATPáz holokomplexek összeszerelődése csak enyhén nőtt ebben az időszakban. Egyszerűen több V1-V0 holokomplexet tartalmazó lizoszóma lett savas. A TRPML1 15 perces agonista aktiválása szintén egyértelműen fokozta a lizoszomális katepszin enzimaktivitást.

Emellett a TRPML1 15 perces aktiválása növelte a lizoszómák autofagoszómákkal való fúzióját, amit intracelluláris Ca^{2+} kelátképzéssel szintén sikerült megakadályozni. Figyelemre méltó, hogy a TRPML1 rövid aktiválása a nem fuzionált autofagoszómák számának csökkenéséhez vezetett, ami arra utal, hogy új autofagoszómák nem képződtek ezen rövid ideig

tartó kezelés során, ellentétben a TRPML1 autofagoszóma-képződésben betöltött hosszú távú szerepéről szóló jelentésekkel. Figyelemre méltó, hogy a TRPML1 rövid ideig tartó aktiválása nem változtatta meg jelentősen a lizoszómák pozícionálását, ami ismét ellentétben áll a lizoszómák vándorlásában betöltött hosszú távú szerepével. Ezt alátámasztja, hogy a mikrotubulus gátlása meglepő módon növelte a TRPML1 aktivitását, valamint a AP-LY fúziót. A mikrotubulus gátlás a $PI(3,5)P_2$ felhalmozódását is növelte a lizoszómákon, amely együtt járt a lizoszómák megnagyobbodásával, ami a lebontatlan anyagok felhalmozódására utal. A mikrotubulus gátló kezelés hatására megnövekedett AP-LY fúzió a fúziógátló BafA1 együttes alkalmazása során megszűnt. Ezek az eredmények megerősítik a TRPML1 korai szerepét a lokális AP-LY fúzió irányításában. Következetesen mind az AP-LY fúzió, mind a lizoszóma savasodása mérséklődött egy domináns-negatív, pórusképzésre képtelen mutáns TRPML1 expressziója során, amit megfigyeltünk az éhezetetett és táplált sejtek esetében is. Ezzel párhuzamosan a TRPML1 agonista $PI(3,5)P_2$ szintézise drasztikusan megnövekedett a 2 órán át éheztetett sejtek lizoszómáiban. Valószínűleg ez indította el a TRPML1 által mediált Ca^{2+} felszabadulás folyamatát éhezés során, mivel ez az egyetlen ismert celluláris agonistája ennek a csatornának. A TRPML1 a lizoszomális fúziós képességet az Stx7 és a VAMP7 SNARE-eket LAMP fehérjét hordozó vezikulák fokozott lizoszomális transzportja révén segítette. Eredményeink azt mutatják, hogy a lizoszómáknak az autofagoszómákkal való egyesülése szükséges a lizoszomális Ca^{2+} kiáramlásához és a hidrolitikus aktivitás fenntartásához. A fúzióképtelen (SNARE-hiányos) lizoszómák nem reagáltak a TRPML1 agonistára és az éhezésre a TRPML1 Ca^{2+} kiáramlás, az intralizoszomális savasodás és a katepszin aktivitás vonatkozásában. Amikor a PIKfyve kináz gátlásával lecsökkentettük a $PI(3,5)P_2$ mennyiségét, ez a lizoszomális SNARE-k lumenbe történő rendellenes szekvesztrálását eredményezte. Tekintettel arra, hogy a TRPML1 allosztérikus kötőhelyekkel rendelkezik a $PI(3,5)P_2$-re és az ML-SA1 szintetikus agonistára, a $PI(3,5)P_2$-hiányos sejteket allosztérikus drog aktiválással menekíteni tudtuk (ami megakadályozta a SNARE-ek rendellenes lokalizációját), beleértve az Stx7 luminális szekvesztrációját, és Calmodulin-függő módon helyreállította a SNARE-ek plazmamembrán lokalizációját. Ennek következtében a 15 percig tartó TRPML1 agonista aktiválás elég volt ahhoz, hogy menekítse a PIKfyve gátlás által okozott AP-LY fúziós hibát.

Működési modellünk alapján az éhezés indukálta autofágia során a $PI(3,5)P_2$ szintézise megnő az autolizoszómákon, amelyek az autofagoszómák és a korai lizoszómák elsődleges fúziója révén keletkeznek. Ezt követően ez a $PI(3,5)P_2$ (vagy farmakológiai agonista, mint például az ML-SA1) a TRPML1 aktiválásához vezet, elősegítve a VAMP7 és a Syntaxin 7 SNARE-fehérjék lizoszomális feldúsulását, amelyek LAMP-hordozó vezikulák segítségével

szállítódnak oda. Ez v-ATPáz által előidézett lizoszomális savasodással párosul. Az így létrejövő autolizoszómák savassá és fúzió képessé válnak, elősegítve több másodlagos AP-AL fúziós eseményt az autofagoszómák által körülzárt intracelluláris anyag megfelelő lebontása érdekében. A fúzió után történik a SNARE fehérjék újrahasznosítása, vagyis a plazmamembránba felé történő reciklizációjuk. A PIKfyve gátlása megzavarja ezt a folyamatot, ami i) csökkenti a TRPML1 működését, ii) a lizoszomális SNARE-fehérjék rendellenes szekvesztrálásához vezet. Eredményeink kiegészítik a TRPML1 autofágia szabályozásában betöltött komplex szerepének megértésére irányuló korábbi erőfeszítéseket, ahol kimutatták, hogy a TRPML1-nek hosszabb távú aktiváció során fontos szerepe van TFEB aktiválásában, valamint az autofág-lizoszomális útvonal génjeinek biogenezisében.

Annak ellenére, hogy a TRPML1 szerepét a lizoszomális beltartalom lebontásának elősegítésében több korábbi közlemény is bemutatta [213,216,231,232], a mi tanulmányunk elsőként mutatja be, hogy a TRPML1 elősegíti a korai lépéseket: a meglévő autofagoszómák fúzióját a lizoszómákkal és az első hullámban beérkező lebontásra szánt anyag lizoszomális degradációját. Eredményeink arra is rávilágítanak, hogy a TRPML1 elősegíti az AP-LY fúziót azáltal, hogy biztosítja a lizoszomális SNARE-ek fokozott rekrutációját.

Igen hasznos és érdekes lehetne a TRPML1 betegségmodellekben betöltött szerepének további vizsgálata, mivel a TRPML1 potenciális terápiás célpont lehet az AP-LY fúziós hibák kijavítására. Ezeket olyan autofág-lizoszomális lebontással társult betegségekben figyelhetjük meg, mint a Vici-szindróma és a vakuoláris myopátia.

8. ACKNOWLEDGEMENTS

First and foremost, I would like to convey my sincere thanks and deep sense of regard to my supervisor, **Prof. Gabor Juhasz,** for allowing me to work under his supervision during my Ph.D. His excellent guidance and unwavering support have been instrumental in my academic journey. Further, I would also like to express my deepest regards and appreciation to **Dr. Arindam Bhattacharjee** for his precise and insightful responses to my scientific inquiries, which have been incredibly motivating. The skills and experience I acquired from him will undoubtedly be helpful for my future career endeavors. Additionally, I extend my gratitude to **Dr. Hajnalka Laczkó-Dobos** and **Dr. András Jipa** for their immense support and suggestions during my PhD study, **Dr. Gábor V. Horváth** for his assistance, and all group members for their cooperation.

Furthermore, special appreciation for always prompting my studies by **my father** and **my mother** to whom I would gladly dedicate this thesis. I am very grateful for the support provided by my **family, my brothers and my sisters, Muhammed, Mutasem, Nariman, Fayz, Norhan, Wiam, and Haya** wishing me the best of luck. Many thanks to my friends here in Szeged, with special mention to **Dr. Nikita Sharma**, **Waliyullahi Ajibola, Afnan AL Doghmi** for their support and consistent wishes. I am immensely grateful to all my former teachers who inspired me to pursue postgraduate studies, especially **Dr. Nahed Allaham,** whose guidance has been invaluable.

Finally, I would like to acknowledge "Tempus Public Foundation" for funding this research. A part of this research was also supported by the Institute of Genetics, HUN REN Hungarian Research Network, BRC Szeged.

9. REFERENCES

1. Tsukada M, Ohsumi Y. Isolation and characterization of autophagy-defective mutants of Saccharomyces cerevisiae. *FEBS Lett*. 1993;333(1-2). doi:10.1016/0014-5793(93)80398-E
2. Yang Z, Klionsky DJ. Eaten alive: A history of macroautophagy. *Nat Cell Biol*. 2010;12(9). doi:10.1038/ncb0910-814
3. Choi AMK, Ryter SW, Levine B. Autophagy in Human Health and Disease. *New England Journal of Medicine*. 2013;368(7). doi:10.1056/nejmra1205406
4. Noda NN, Inagaki F. Mechanisms of Autophagy. *Annu Rev Biophys*. 2015;44. doi:10.1146/annurev-biophys-060414-034248
5. Menzies FM, Fleming A, Rubinsztein DC. Compromised autophagy and neurodegenerative diseases. *Nat Rev Neurosci*. 2015;16(6). doi:10.1038/nrn3961
6. Zhong Z, Sanchez-Lopez E, Karin M. Autophagy, Inflammation, and Immunity: A Troika Governing Cancer and Its Treatment. *Cell*. 2016;166(2). doi:10.1016/j.cell.2016.05.051
7. Deretic V, Saitoh T, Akira S. Autophagy in infection, inflammation and immunity. *Nat Rev Immunol*. 2013;13(10). doi:10.1038/nri3532
8. Galluzzi L, Pietrocola F, Bravo-San Pedro JM, et al. Autophagy in malignant transformation and cancer progression. *EMBO J*. 2015;34(7). doi:10.15252/embj.201490784
9. Amaravadi R, Kimmelman AC, White E. Recent insights into the function of autophagy in cancer. *Genes Dev*. 2016;30(17). doi:10.1101/gad.287524.116
10. López-Otín C, Galluzzi L, Freije JMP, Madeo F, Kroemer G. Metabolic Control of Longevity. *Cell*. 2016;166(4). doi:10.1016/j.cell.2016.07.031
11. Lapierre LR, Kumsta C, Sandri M, Ballabio A, Hansen M. Transcriptional and epigenetic regulation of autophagy in aging. *Autophagy*. 2015;11(6). doi:10.1080/15548627.2015.1034410
12. Abeliovich H, Klionsky DJ. Autophagy in Yeast: Mechanistic Insights and Physiological Function. *Microbiology and Molecular Biology Reviews*. 2001;65(3). doi:10.1128/mmbr.65.3.463-479.2001
13. Delorme-Axford E, Klionsky DJ. Transcriptional and post-transcriptional regulation of autophagy in the yeast Saccharomyces cerevisiae. *Journal of Biological Chemistry*. 2018;293(15). doi:10.1074/jbc.R117.804641
14. CLARK SL. Cellular differentiation in the kidneys of newborn mice studies with the electron microscope. *J Biophys Biochem Cytol*. 1957;3(3). doi:10.1083/jcb.3.3.349
15. Glick D, Barth S, Macleod KF. Autophagy: Cellular and molecular mechanisms. *Journal of Pathology*. 2010;221(1). doi:10.1002/path.2697
16. Galluzzi L, Baehrecke EH, Ballabio A, et al. Molecular definitions of autophagy and related processes. *EMBO J*. 2017;36(13). doi:10.15252/embj.201796697

17. Cuervo AM. Autophagy: Many paths to the same end. *Mol Cell Biochem*. 2004;263(1). doi:10.1023/B:MCBI.0000041848.57020.57
18. Parzych KR, Klionsky DJ. An overview of autophagy: Morphology, mechanism, and regulation. *Antioxid Redox Signal*. 2014;20(3). doi:10.1089/ars.2013.5371
19. Ravikumar B, Moreau K, Jahreiss L, Puri C, Rubinsztein DC. Plasma membrane contributes to the formation of pre-autophagosomal structures. *Nat Cell Biol*. 2010;12(8). doi:10.1038/ncb2078
20. Hayashi-Nishino M, Fujita N, Noda T, Yamaguchi A, Yoshimori T, Yamamoto A. A subdomain of the endoplasmic reticulum forms a cradle for autophagosome formation. *Nat Cell Biol*. 2009;11(12). doi:10.1038/ncb1991
21. Nguyen N, Shteyn V, Melia TJ. Sensing Membrane Curvature in Macroautophagy. *J Mol Biol*. 2017;429(4). doi:10.1016/j.jmb.2017.01.006
22. Devenish RJ, Klionsky DJ. Autophagy: Mechanism and physiological relevance "brewed" from yeast studies. *Frontiers in Bioscience - Scholar*. 2012;4 S(4). doi:10.2741/s337
23. Yang Z, Klionsky DJ. An overview of the molecular mechanism of autophagy. *Curr Top Microbiol Immunol*. 2009;335(1). doi:10.1007/978-3-642-00302-8_1
24. Yorimitsu T, Klionsky DJ. Autophagy: Molecular machinery for self-eating. *Cell Death Differ*. 2005;12. doi:10.1038/sj.cdd.4401765
25. Tooze J, Hollinshead M, Ludwig T, Howell K, Hoflack B, Kern H. In exocrine pancreas, the basolateral endocytic pathway converges with the autophagic pathway immediately after the early endosome. *Journal of Cell Biology*. 1990;111(2). doi:10.1083/jcb.111.2.329
26. Kroemer G, Mariño G, Levine B. Autophagy and the Integrated Stress Response. *Mol Cell*. 2010;40(2). doi:10.1016/j.molcel.2010.09.023
27. Nao Hosokawa †, Taichi Hara †, Takeshi Kaizuka CK, et al. Nutrient-dependent mTORC1 Association with the ULK1–Atg13–FIP200 Complex Required for Autophagy. *Mol Biol Cell*. 2009;20(m).
28. Hara T, Takamura A, Kishi C, et al. FIP200, a ULK-interacting protein, is required for autophagosome formation in mammalian cells. *Journal of Cell Biology*. 2008;181(3). doi:10.1083/jcb.200712064
29. Ganley IG, Lam DH, Wang J, Ding X, Chen S, Jiang X. ULK1·ATG13·FIP200 complex mediates mTOR signaling and is essential for autophagy. *Journal of Biological Chemistry*. 2009;284(18). doi:10.1074/jbc.M900573200
30. Yamamoto H, Fujioka Y, Suzuki SW, et al. The Intrinsically Disordered Protein Atg13 Mediates Supramolecular Assembly of Autophagy Initiation Complexes. *Dev Cell*. 2016;38(1). doi:10.1016/j.devcel.2016.06.015

31. Kawamata T, Kamada Y, Kabeya Y, Sekito T, Ohsumi Y. Organization of the pre-autophagosomal structure responsible for autophagosome formation. *Mol Biol Cell*. 2008;19(5). doi:10.1091/mbc.E07-10-1048
32. Li X, He S, Ma B. Autophagy and autophagy-related proteins in cancer. *Mol Cancer*. 2020;19(1). doi:10.1186/S12943-020-1138-4
33. Follo C, Vidoni C, Morani F, Ferraresi A, Seca C, Isidoro C. Amino acid response by Halofuginone in Cancer cells triggers autophagy through proteasome degradation of mTOR. *Cell Communication and Signaling*. 2019;17(1). doi:10.1186/s12964-019-0354-2
34. Cheong H, Nair U, Geng J, Klionsky DJ. The Atg1 kinase complex is involved in the regulation of protein recruitment to initiate sequestering vesicle formation for nonspecific autophagy in Saccharomyces cerevisiae. *Mol Biol Cell*. 2008;19(2). doi:10.1091/mbc.E07-08-0826
35. Zhuang X, Chung KP, Jiang L. Origin of the autophagosomal membrane in plants. *Front Plant Sci*. 2016;7(November 2016). doi:10.3389/fpls.2016.01655
36. Burman C, Ktistakis NT. Regulation of autophagy by phosphatidylinositol 3-phosphate. *FEBS Lett*. 2010;584(7). doi:10.1016/j.febslet.2010.01.011
37. Furuya N, Yu J, Byfield M, Pattingre S, Levine B. The evolutionarily conserved domain of Beclin 1 is required for Vps34 binding, autophagy and tumor suppressor function. *Autophagy*. 2005;1(1). doi:10.4161/auto.1.1.1542
38. Suzuki K, Akioka M, Kondo-Kakuta C, Yamamoto H, Ohsumi Y. Fine mapping of autophagy-related proteins during autophagosome formation in Saccharomyces cerevisiae. *J Cell Sci*. 2013;126(11). doi:10.1242/jcs.122960
39. Nakatogawa H, Suzuki K, Kamada Y, Ohsumi Y. Dynamics and diversity in autophagy mechanisms: Lessons from yeast. *Nat Rev Mol Cell Biol*. 2009;10(7). doi:10.1038/nrm2708
40. Kirisako T, Baba M, Ishihara N, et al. Formation process of autophagosome is traced with Apg8/Aut7p in yeast. *Journal of Cell Biology*. 1999;147(2). doi:10.1083/jcb.147.2.435
41. Tanida I, Mizushima N, Kiyooka M, et al. Apg7p/Cvt2p: A novel protein-activating enzyme essential for autophagy. *Mol Biol Cell*. 1999;10(5). doi:10.1091/mbc.10.5.1367
42. Ichimura Y, Kirisako T, Takao T, et al. A ubiquitin-like system mediates protein lipidation. *Nature*. 2000;408(6811). doi:10.1038/35044114
43. Fujioka Y, Noda NN, Fujii K, Yoshimoto K, Ohsumi Y, Inagaki F. In vitro reconstitution of plant Atg8 and Atg12 conjugation systems essential for autophagy. *Journal of Biological Chemistry*. 2008;283(4). doi:10.1074/jbc.M706214200
44. Shintani T, Mizushima N, Ogawa Y, Matsuura A, Noda T, Ohsumi Y. Apg10p, a novel protein-conjugating enzyme essential for autophagy in yeast. *EMBO Journal*. 1999;18(19). doi:10.1093/emboj/18.19.5234

45. Mizushima N, Noda T, Yoshimori T, et al. A protein conjugation system essential for autophagy. *Nature*. 1998;395(6700). doi:10.1038/26506
46. Mizushima N, Noda T, Ohsumi Y. Apg16p is required for the function of the Apg12p-Apg5p conjugate in the yeast autophagy pathway. *EMBO Journal*. 1999;18(14). doi:10.1093/emboj/18.14.3888
47. Johansen T, Lamark T. Selective autophagy mediated by autophagic adapter proteins. *Autophagy*. 2011;7(3). doi:10.4161/auto.7.3.14487
48. Zaffagnini G, Martens S. Mechanisms of Selective Autophagy. Published online 2016. doi:10.1016/j.jmb.2016.02.004
49. Wijdeven RH, Janssen H, Nahidiazar L, et al. Cholesterol and ORP1L-mediated ER contact sites control autophagosome transport and fusion with the endocytic pathway. *Nat Commun*. 2016;7. doi:10.1038/NCOMMS11808
50. Monastyrska I, Rieter E, Klionsky DJ, Reggiori F. Multiple roles of the cytoskeleton in autophagy. *Biol Rev*. 2009;84:431-448. doi:10.1111/j.1469-185X.2009.00082.x
51. Pankiv S, Alemu EA, Brech A, et al. FYCO1 is a Rab7 effector that binds to LC3 and PI3P to mediate microtubule plus end-directed vesicle transport. *J Cell Biol*. 2010;188(2):253-269. doi:10.1083/JCB.200907015
52. Jordens I, Fernandez-Borja M, Marsman M, et al. The Rab7 effector protein RILP controls lysosomal transport by inducing the recruitment of dynein-dynactin motors. *Current Biology*. 2001;11(21). doi:10.1016/S0960-9822(01)00531-0
53. Kuchitsu Y, Fukuda M. Revisiting Rab7 functions in mammalian autophagy: Rab7 knockout studies. *Cells*. 2018;7(11). doi:10.3390/cells7110215
54. Kendrick AA, Christensen JR. Bidirectional lysosome transport: a balancing act between ARL8 effectors. *Nat Commun*. 2022;13(1). doi:10.1038/s41467-022-32965-y
55. Cabukusta B, Neefjes J. Mechanisms of lysosomal positioning and movement. *Traffic*. 2018;19(10). doi:10.1111/tra.12587
56. Kumar G, Chawla P, Dhiman N, et al. RUFY3 links Arl8b and JIP4-Dynein complex to regulate lysosome size and positioning. *Nat Commun*. 2022;13(1). doi:10.1038/s41467-022-29077-y
57. Itakura E, Kishi-Itakura C, Mizushima N. The hairpin-type tail-anchored SNARE syntaxin 17 targets to autophagosomes for fusion with endosomes/lysosomes. *Cell*. 2012;151(6):1256-1269. doi:10.1016/J.CELL.2012.11.001
58. Lőrincz P, Juhász G. Autophagosome-Lysosome Fusion. *J Mol Biol*. 2020;432(8):2462-2482. doi:10.1016/J.JMB.2019.10.028
59. Lürick A, Kümmel D, Ungermann C. Multisubunit tethers in membrane fusion. *Curr Biol*. 2018;28(8):R417-R420. doi:10.1016/J.CUB.2017.12.012

60. Wurmser AE, Sato TK, Emr SD. New component of the vacuolar class C-Vps complex couples nucleotide exchange on the Ypt7 GTPase to SNARE-dependent docking and fusion. *J Cell Biol*. 2000;151(3):551-562. doi:10.1083/JCB.151.3.551
61. Matsui T, Jiang P, Nakano S, Sakamaki Y, Yamamoto H, Mizushima N. Autophagosomal YKT6 is required for fusion with lysosomes independently of syntaxin 17. *Journal of Cell Biology*. 2018;217(8). doi:10.1083/jcb.201712058
62. Bas L, Papinski D, Kraft C. Ykt6 mediates autophagosome-vacuole fusion. *Mol Cell Oncol*. 2018;5(6). doi:10.1080/23723556.2018.1526006
63. Takáts S, Glatz G, Szenci G, et al. Non-canonical role of the SNARE protein Ykt6 in autophagosome-lysosome fusion. *PLoS Genet*. 2018;14(4). doi:10.1371/journal.pgen.1007359
64. Zheng D, Tong M, Zhang S, et al. Human YKT6 forms priming complex with STX17 and SNAP29 to facilitate autophagosome-lysosome fusion. doi:10.1016/j.celrep.2024.113760
65. Epple UD, Suriapranata I, Eskelinen EL, Thumm M. Aut5/Cvt17p, a putative lipase essential for disintegration of autophagic bodies inside the vacuole. *J Bacteriol*. 2001;183(20):5942-5955. doi:10.1128/JB.183.20.5942-5955.2001
66. Teter SA, Eggerton KP, Scott S V, Kim J, Fischer AM, Klionsky DJ. Degradation of Lipid Vesicles in the Yeast Vacuole Requires Function of Cvt17, a Putative Lipase*. Published online 2000. doi:10.1074/jbc.C000739200
67. Takahashi Y, He H, Tang Z, et al. An autophagy assay reveals the ESCRT-III component CHMP2A as a regulator of phagophore closure. *Nat Commun*. 2018;9(1). doi:10.1038/S41467-018-05254-W
68. Ramya V, Rajasekharan R. ATG15 encodes a phospholipase and is transcriptionally regulated by YAP1 in Saccharomyces cerevisiae. *FEBS Lett*. 2016;590(18). doi:10.1002/1873-3468.12369
69. Mizushima N, Levine B, Cuervo AM, Klionsky DJ. Autophagy fights disease through cellular self-digestion. *Nature*. 2008;451(7182):1069-1075. doi:10.1038/NATURE06639
70. Schröder BA, Wrocklage C, Hasilik A, Saftig P. The proteome of lysosomes. *Proteomics*. 2010;10(22):4053-4076. doi:10.1002/PMIC.201000196
71. Yim WWY, Mizushima N. Lysosome biology in autophagy. *Cell Discov*. 2020;6(1). doi:10.1038/S41421-020-0141-7
72. Xiong J, Zhu MX. Regulation of lysosomal ion homeostasis by channels and transporters. *Sci China Life Sci*. 2016;59(8):777-791. doi:10.1007/S11427-016-5090-X
73. Mortimore GE, Schworer CM. Induction of autophagy by amino-acid deprivation in perfused rat liver. *Nature*. 1977;270(5633):174-176. doi:10.1038/270174A0
74. Deter RL, De Duve C. Influence of glucagon, an inducer of cellular autophagy, on some physical properties of rat liver lysosomes. *J Cell Biol*. 1967;33(2):437-449. doi:10.1083/JCB.33.2.437

75. Yin Z, Pascual C, Klionsky DJ. Autophagy: machinery and regulation. *Microb Cell*. 2016;3(12):588-596. doi:10.15698/MIC2016.12.546
76. He C, Klionsky DJ. Regulation mechanisms and signaling pathways of autophagy. *Annu Rev Genet*. 2009;43:67-93. doi:10.1146/ANNUREV-GENET-102808-114910
77. Claude-Taupin A, Morel E. Phosphoinositides: Functions in autophagy-related stress responses. *Biochim Biophys Acta Mol Cell Biol Lipids*. 2021;1866(6). doi:10.1016/j.bbalip.2021.158903
78. Saxton RA, Sabatini DM. mTOR Signaling in Growth, Metabolism, and Disease. *Cell*. 2017;168(6). doi:10.1016/j.cell.2017.02.004
79. Kim J, Guan KL. mTOR as a central hub of nutrient signalling and cell growth. *Nat Cell Biol*. 2019;21(1). doi:10.1038/s41556-018-0205-1
80. Laplante M, Sabatini DM. mTOR signaling in growth control and disease. *Cell*. 2012;149(2):274-293. doi:10.1016/J.CELL.2012.03.017
81. Sancak Y, Bar-Peled L, Zoncu R, Markhard AL, Nada S, Sabatini DM. Ragulator-Rag complex targets mTORC1 to the lysosomal surface and is necessary for its activation by amino acids. *Cell*. 2010;141(2):290-303. doi:10.1016/J.CELL.2010.02.024
82. Abuammar H, Bhattacharjee A, Simon-Vecsei Z, et al. Ion Channels and Pumps in Autophagy: A Reciprocal Relationship. *Cells*. 2021;10(12). doi:10.3390/CELLS10123537
83. Bar-Peled L, Schweitzer LD, Zoncu R, Sabatini DM. Ragulator is a GEF for the rag GTPases that signal amino acid levels to mTORC1. *Cell*. 2012;150(6):1196-1208. doi:10.1016/J.CELL.2012.07.032
84. Wong PM, Feng Y, Wang J, Shi R, Jiang X. Regulation of autophagy by coordinated action of mTORC1 and protein phosphatase 2A. *Nat Commun*. 2015;6. doi:10.1038/NCOMMS9048
85. Settembre C, Di Malta C, Polito VA, et al. TFEB links autophagy to lysosomal biogenesis. *Science*. 2011;332(6036):1429-1433. doi:10.1126/SCIENCE.1204592
86. Hasegawa J, Strunk BS, Weisman LS. PI5P and PI(3,5)P2: Minor, but essential phosphoinositides. *Cell Struct Funct*. 2017;42(1). doi:10.1247/csf.17003
87. Nascimbeni AC, Codogno P, Morel E. Phosphatidylinositol-3-phosphate in the regulation of autophagy membrane dynamics. *FEBS Journal*. 2017;284(9). doi:10.1111/febs.13987
88. Kaur J, Debnath J. Autophagy at the crossroads of catabolism and anabolism. *Nat Rev Mol Cell Biol*. 2015;16(8):461-472. doi:10.1038/NRM4024
89. Kim WR, Sun W. Programmed cell death during postnatal development of the rodent nervous system. *Dev Growth Differ*. 2011;53(2):225-235. doi:10.1111/J.1440-169X.2010.01226.X
90. Kuma A, Hatano M, Matsui M, et al. The role of autophagy during the early neonatal starvation period. *Nature*. 2004;432(7020):1032-1036. doi:10.1038/NATURE03029

91. Deretic V, Kroemer G. Autophagy in metabolism and quality control: opposing, complementary or interlinked functions? *Autophagy*. 2022;18(2):283-292. doi:10.1080/15548627.2021.1933742
92. Choi AMK, Ryter SW, Levine B. Autophagy in human health and disease. *N Engl J Med*. 2013;368(7):651-662. doi:10.1056/NEJMRA1205406
93. Poillet-Perez L, White E. Role of tumor and host autophagy in cancer metabolism. *Genes Dev*. 2019;33(11-12):610-619. doi:10.1101/GAD.325514.119
94. Poillet-Perez L, White E. Role of tumor and host autophagy in cancer metabolism. *Genes Dev*. 2019;33(11-12):610-619. doi:10.1101/GAD.325514.119
95. Galluzzi L, Pietrocola F, Bravo-San Pedro JM, et al. Autophagy in malignant transformation and cancer progression. *EMBO J*. 2015;34(7):856-880. doi:10.15252/EMBJ.201490784
96. DeVorkin L, Pavey N, Carleton G, et al. Autophagy Regulation of Metabolism Is Required for CD8+ T Cell Anti-tumor Immunity. *Cell Rep*. 2019;27(2):502-513.e5. doi:10.1016/J.CELREP.2019.03.037
97. Vera-Ramirez L, Vodnala SK, Nini R, Hunter KW, Green JE. Autophagy promotes the survival of dormant breast cancer cells and metastatic tumour recurrence. *Nat Commun*. 2018;9(1). doi:10.1038/S41467-018-04070-6
98. Mallucci GR, Klenerman D, Rubinsztein DC. Developing Therapies for Neurodegenerative Disorders: Insights from Protein Aggregation and Cellular Stress Responses. *Annu Rev Cell Dev Biol*. 2020;36:165-189. doi:10.1146/ANNUREV-CELLBIO-040320-120625
99. Menzies FM, Fleming A, Caricasole A, et al. Autophagy and Neurodegeneration: Pathogenic Mechanisms and Therapeutic Opportunities. *Neuron*. 2017;93(5):1015-1034. doi:10.1016/J.NEURON.2017.01.022
100. Deng Z, Purtell K, Lachance V, Wold MS, Chen S, Yue Z. Autophagy Receptors and Neurodegenerative Diseases. *Trends Cell Biol*. 2017;27(7):491-504. doi:10.1016/J.TCB.2017.01.001
101. Menzies FM, Fleming A, Caricasole A, et al. Autophagy and Neurodegeneration: Pathogenic Mechanisms and Therapeutic Opportunities. *Neuron*. 2017;93(5):1015-1034. doi:10.1016/J.NEURON.2017.01.022
102. Menzies FM, Fleming A, Caricasole A, et al. Autophagy and Neurodegeneration: Pathogenic Mechanisms and Therapeutic Opportunities. *Neuron*. 2017;93(5):1015-1034. doi:10.1016/J.NEURON.2017.01.022
103. Kim M, Sandford E, Gatica D, et al. Mutation in ATG5 reduces autophagy and leads to ataxia with developmental delay. *Elife*. 2016;5. doi:10.7554/elife.12245
104. Juhász G, Érdi B, Sass M, Neufeld TP. Atg7-dependent autophagy promotes neuronal health, stress tolerance, and longevity but is dispensable for metamorphosis in Drosophila. *Genes Dev*. 2007;21(23). doi:10.1101/gad.1600707

105. Deng Z, Lim J, Wang Q, et al. ALS-FTLD-linked mutations of SQSTM1/p62 disrupt selective autophagy and NFE2L2/NRF2 anti-oxidative stress pathway. *Autophagy*. 2020;16(5):917-931. doi:10.1080/15548627.2019.1644076
106. Odagiri S, Tanji K, Mori F, Kakita A, Takahashi H, Wakabayashi K. Autophagic adapter protein NBR1 is localized in Lewy bodies and glial cytoplasmic inclusions and is involved in aggregate formation in α-synucleinopathy. *Acta Neuropathol*. 2012;124(2):173-186. doi:10.1007/S00401-012-0975-7
107. McCauley ME, Baloh RH. Inflammation in ALS/FTD pathogenesis. *Acta Neuropathol*. 2019;137(5):715-730. doi:10.1007/S00401-018-1933-9
108. Sarkis GJ, Ashcom JD, Hawdon JM, Jacobson LA. Decline in protease activities with age in the nematode Caenorhabditis elegans. *Mech Ageing Dev*. 1988;45(3):191-201. doi:10.1016/0047-6374(88)90001-2
109. Cuervo AM, Dice JF. How do intracellular proteolytic systems change with age? *Front Biosci*. 1998;3. doi:10.2741/A264
110. López-Otín C, Blasco MA, Partridge L, Serrano M, Kroemer G. The hallmarks of aging. *Cell*. 2013;153(6):1194. doi:10.1016/J.CELL.2013.05.039
111. Kenyon CJ. The genetics of ageing. *Nature*. 2010;464(7288):504-512. doi:10.1038/NATURE08980
112. Kaur J, Debnath J. Autophagy at the crossroads of catabolism and anabolism. *Nat Rev Mol Cell Biol*. 2015;16(8):461-472. doi:10.1038/NRM4024
113. Leidal AM, Levine B, Debnath J. Autophagy and the cell biology of age-related disease. *Nat Cell Biol*. 2018;20(12):1338-1348. doi:10.1038/S41556-018-0235-8
114. Mindell JA. Lysosomal acidification mechanisms. *Annu Rev Physiol*. 2012;74:69-86. doi:10.1146/ANNUREV-PHYSIOL-012110-142317
115. Chen R, Jäättelä M, Liu B. Lysosome as a Central Hub for Rewiring PH Homeostasis in Tumors. *Cancers (Basel)*. 2020;12(9):1-12. doi:10.3390/CANCERS12092437
116. Collins MP, Forgac M. Regulation and function of V-ATPases in physiology and disease. *Biochim Biophys Acta Biomembr*. 2020;1862(12). doi:10.1016/J.BBAMEM.2020.183341
117. Sun-Wada GH, Wada Y. Vacuolar-type proton pump ATPases: acidification and pathological relationships. *Histol Histopathol*. 2013;28(7):805-815. doi:10.14670/HH-28.805
118. Cotter K, Stransky L, McGuire C, Forgac M. Recent Insights into the Structure, Regulation, and Function of the V-ATPases. *Trends Biochem Sci*. 2015;40(10):611-622. doi:10.1016/J.TIBS.2015.08.005
119. Forgac M. Vacuolar ATPases: rotary proton pumps in physiology and pathophysiology. *Nat Rev Mol Cell Biol*. 2007;8(11):917-929. doi:10.1038/NRM2272

120. Hirata T, Iwamoto-Kihara A, Sun-Wada GH, Okajima T, Wada Y, Futai M. Subunit rotation of vacuolar-type proton pumping ATPase: relative rotation of the G and C subunits. *J Biol Chem*. 2003;278(26):23714-23719. doi:10.1074/JBC.M302756200
121. Imamura H, Nakano M, Noji H, et al. Evidence for rotation of V1-ATPase. *Proc Natl Acad Sci U S A*. 2003;100(5):2312-2315. doi:10.1073/PNAS.0436796100
122. Hirata T, Iwamoto-Kihara A, Sun-Wada GH, Okajima T, Wada Y, Futai M. Subunit rotation of vacuolar-type proton pumping ATPase: relative rotation of the G and C subunits. *J Biol Chem*. 2003;278(26):23714-23719. doi:10.1074/JBC.M302756200
123. Zhao J, Benlekbir S, Rubinstein JL. Electron cryomicroscopy observation of rotational states in a eukaryotic V-ATPase. *Nature*. 2015;521(7551):241-245. doi:10.1038/NATURE14365
124. Suzuki K, Mizutani K, Maruyama S, et al. Crystal structures of the ATP-binding and ADP-release dwells of the V1 rotary motor. *Nat Commun*. 2016;7:13235. doi:10.1038/NCOMMS13235
125. McGuire C, Cotter K, Stransky L, Forgac M. Regulation of V-ATPase assembly and function of V-ATPases in tumor cell invasiveness. *Biochim Biophys Acta Bioenerg*. 2016;1857(8). doi:10.1016/j.bbabio.2016.02.010
126. M. Kane P. Targeting reversible disassembly as a mechanism of controlling V-ATPase activity. *Curr Protein Pept Sci*. 2012;13(2):117-123. doi:10.2174/138920312800493142
127. Collins MP, Forgac M. Regulation of V-ATPase Assembly in Nutrient Sensing and Function of V-ATPases in Breast Cancer Metastasis. *Front Physiol*. 2018;9(JUL). doi:10.3389/FPHYS.2018.00902
128. Zoncu R, Bar-Peled L, Efeyan A, Wang S, Sancak Y, Sabatini DM. mTORC1 senses lysosomal amino acids through an inside-out mechanism that requires the vacuolar H(+)-ATPase. *Science*. 2011;334(6056):678-683. doi:10.1126/SCIENCE.1207056
129. McGuire CM, Forgac M. Glucose starvation increases V-ATPase assembly and activity in mammalian cells through AMP kinase and phosphatidylinositide 3-kinase/Akt signaling. *J Biol Chem*. 2018;293(23):9113-9123. doi:10.1074/JBC.RA117.001327
130. Palm W, Park Y, Wright K, Pavlova NN, Tuveson DA, Thompson CB. The Utilization of Extracellular Proteins as Nutrients Is Suppressed by mTORC1. *Cell*. 2015;162(2):259-270. doi:10.1016/J.CELL.2015.06.017
131. Stransky LA, Forgac M. Amino Acid Availability Modulates Vacuolar H+-ATPase Assembly. *J Biol Chem*. 2015;290(45):27360-27369. doi:10.1074/JBC.M115.659128
132. McGuire CM, Forgac M. Glucose starvation increases V-ATPase assembly and activity in mammalian cells through AMP kinase and phosphatidylinositide 3-kinase/Akt signaling. *J Biol Chem*. 2018;293(23):9113-9123. doi:10.1074/JBC.RA117.001327
133. Stransky LA, Forgac M. Amino Acid Availability Modulates Vacuolar H+-ATPase Assembly. *J Biol Chem*. 2015;290(45):27360-27369. doi:10.1074/JBC.M115.659128

134. Collins MP, Forgac M. Regulation of V-ATPase Assembly in Nutrient Sensing and Function of V-ATPases in Breast Cancer Metastasis. *Front Physiol*. 2018;9(JUL). doi:10.3389/FPHYS.2018.00902
135. Luzio JP, Pryor PR, Bright NA. Lysosomes: fusion and function. *Nat Rev Mol Cell Biol*. 2007;8(8):622-632. doi:10.1038/NRM2217
136. Huotari J, Helenius A. Endosome maturation. *EMBO J*. 2011;30(17):3481-3500. doi:10.1038/EMBOJ.2011.286
137. Kolter T, Sandhoff K. Principles of lysosomal membrane digestion: stimulation of sphingolipid degradation by sphingolipid activator proteins and anionic lysosomal lipids. *Annu Rev Cell Dev Biol*. 2005;21:81-103. doi:10.1146/ANNUREV.CELLBIO.21.122303.120013
138. Ruivo R, Anne C, Sagné C, Gasnier B. Molecular and cellular basis of lysosomal transmembrane protein dysfunction. *Biochim Biophys Acta*. 2009;1793(4):636-649. doi:10.1016/J.BBAMCR.2008.12.008
139. Saftig P, Klumperman J. Lysosome biogenesis and lysosomal membrane proteins: trafficking meets function. *Nat Rev Mol Cell Biol*. 2009;10(9):623-635. doi:10.1038/NRM2745
140. Hasanagic M, Waheed A, Eissenberg JC. Different Pathways to the Lysosome: Sorting out Alternatives. *Int Rev Cell Mol Biol*. 2015;320:75-101. doi:10.1016/BS.IRCMB.2015.07.008
141. Poteryaev D, Datta S, Ackema K, Zerial M, Spang A. Identification of the switch in early-to-late endosome transition. *Cell*. 2010;141(3). doi:10.1016/j.cell.2010.03.011
142. Settembre C, Fraldi A, Medina DL, Ballabio A. Signals from the lysosome: a control centre for cellular clearance and energy metabolism. *Nat Rev Mol Cell Biol*. 2013;14(5):283-296. doi:10.1038/NRM3565
143. Luzio JP, Pryor PR, Bright NA. Lysosomes: fusion and function. *Nat Rev Mol Cell Biol*. 2007;8(8):622-632. doi:10.1038/NRM2217
144. Yu L, McPhee CK, Zheng L, et al. Termination of autophagy and reformation of lysosomes regulated by mTOR. *Nature*. 2010;465(7300):942-946. doi:10.1038/NATURE09076
145. Rong Y, McPhee C, Denga S, et al. Spinster is required for autophagic lysosome reformation and mTOR reactivation following starvation. *Proc Natl Acad Sci U S A*. 2011;108(19):7826-7831. doi:10.1073/PNAS.1013800108
146. Kolter T, Sandhoff K. Principles of lysosomal membrane digestion: stimulation of sphingolipid degradation by sphingolipid activator proteins and anionic lysosomal lipids. *Annu Rev Cell Dev Biol*. 2005;21:81-103. doi:10.1146/ANNUREV.CELLBIO.21.122303.120013
147. Sun X, Yang Y, Zhong XZ, et al. A negative feedback regulation of MTORC1 activity by the lysosomal Ca2+ channel MCOLN1 (mucolipin 1) using a CALM (calmodulin)-dependent mechanism. *Autophagy*. 2018;14(1):38-52. doi:10.1080/15548627.2017.1389822

148. Wyant GA, Abu-Remaileh M, Wolfson RL, et al. mTORC1 Activator SLC38A9 Is Required to Efflux Essential Amino Acids from Lysosomes and Use Protein as a Nutrient. *Cell*. 2017;171(3):642-654.e12. doi:10.1016/J.CELL.2017.09.046
149. Zoncu R, Bar-Peled L, Efeyan A, Wang S, Sancak Y, Sabatini DM. mTORC1 senses lysosomal amino acids through an inside-out mechanism that requires the vacuolar H(+)-ATPase. *Science*. 2011;334(6056):678-683. doi:10.1126/SCIENCE.1207056
150. Settembre C, Di Malta C, Polito VA, et al. TFEB links autophagy to lysosomal biogenesis. *Science*. 2011;332(6036):1429-1433. doi:10.1126/SCIENCE.1204592
151. Abuammar H, Bhattacharjee A, Simon-Vecsei Z, et al. Ion Channels and Pumps in Autophagy: A Reciprocal Relationship. *Cells*. 2021;10(12). doi:10.3390/CELLS10123537
152. Medina DL, Di Paola S, Peluso I, et al. Lysosomal calcium signalling regulates autophagy through calcineurin and TFEB. *Nat Cell Biol*. 2015;17(3):288-299. doi:10.1038/NCB3114
153. Scotto Rosato A, Montefusco S, Soldati C, et al. TRPML1 links lysosomal calcium to autophagosome biogenesis through the activation of the CaMKKβ/VPS34 pathway. *Nat Commun*. 2019;10(1). doi:10.1038/S41467-019-13572-W
154. Zhang W, Li X, Wang S, Chen Y, Liu H. Regulation of TFEB activity and its potential as a therapeutic target against kidney diseases. *Cell Death Discov*. 2020;6(1). doi:10.1038/S41420-020-0265-4
155. Yang J, Zhang W, Zhang S, et al. Novel Insight into Functions of Transcription Factor EB (TFEB) in Alzheimer's Disease and Parkinson's Disease. *Aging Dis*. 2023;14(3):652-669. doi:10.14336/AD.2022.0927
156. Bala S, Szabo G. TFEB, a master regulator of lysosome biogenesis and autophagy, is a new player in alcoholic liver disease. *Dig Med Res*. 2018;1:16-16. doi:10.21037/DMR.2018.09.03
157. Zhang W, Li X, Wang S, Chen Y, Liu H. Regulation of TFEB activity and its potential as a therapeutic target against kidney diseases. *Cell Death Discov*. 2020;6(1). doi:10.1038/S41420-020-0265-4
158. Yang J, Zhang W, Zhang S, et al. Novel Insight into Functions of Transcription Factor EB (TFEB) in Alzheimer's Disease and Parkinson's Disease. *Aging Dis*. 2023;14(3):652-669. doi:10.14336/AD.2022.0927
159. Gu Z, Cao H, Zuo C, et al. TFEB in Alzheimer's disease: From molecular mechanisms to therapeutic implications. *Neurobiol Dis*. 2022;173. doi:10.1016/J.NBD.2022.105855
160. Medina DL. Lysosomal calcium and autophagy. *Int Rev Cell Mol Biol*. 2021;362:141-170. doi:10.1016/BS.IRCMB.2021.03.002
161. Bojarski L, Herms J, Kuznicki J. Calcium dysregulation in Alzheimer's disease. *Neurochem Int*. 2008;52(4-5):621-633. doi:10.1016/J.NEUINT.2007.10.002
162. Berridge MJ. Calcium signalling remodelling and disease. *Biochem Soc Trans*. 2012;40(2):297-309. doi:10.1042/BST20110766

163. Berridge MJ, Lipp P, Bootman MD. The versatility and universality of calcium signalling. *Nat Rev Mol Cell Biol*. 2000;1(1):11-21. doi:10.1038/35036035
164. Clapham DE. Calcium signaling. *Cell*. 2007;131(6):1047-1058. doi:10.1016/J.CELL.2007.11.028
165. Christensen KA, Myers JT, Swanson JA. pH-dependent regulation of lysosomal calcium in macrophages. *J Cell Sci*. 2002;115(Pt 3):599-607. doi:10.1242/JCS.115.3.599
166. Wang SH, Shih YL, Ko WC, Wei YH, Shih CM. Cadmium-induced autophagy and apoptosis are mediated by a calcium signaling pathway. *Cell Mol Life Sci*. 2008;65(22):3640-3652. doi:10.1007/S00018-008-8383-9
167. Kim SW, Kim MK, Hong S, et al. The intracellular Ca2+ channel TRPML3 is a PI3P effector that regulates autophagosome biogenesis. *Proc Natl Acad Sci U S A*. 2022;119(43). doi:10.1073/PNAS.2200085119/-/DCSUPPLEMENTAL
168. Engedal N, Torgersen ML, Guldvik IJ, et al. Modulation of intracellular calcium homeostasis blocks autophagosome formation. *Autophagy*. 2013;9(10):1475-1490. doi:10.4161/AUTO.25900
169. Mauvezin C, Nagy P, Juhász G, Neufeld TP. Autophagosome-lysosome fusion is independent of V-ATPase-mediated acidification. *Nat Commun*. 2015;6. doi:10.1038/NCOMMS8007
170. Bootman MD, Chehab T, Bultynck G, Parys JB, Rietdorf K. The regulation of autophagy by calcium signals: Do we have a consensus? *Cell Calcium*. 2018;70:32-46. doi:10.1016/J.CECA.2017.08.005
171. Kim Y, Lee Y, Choo M, Yun N, Cho JW, Oh YJ. A surge of cytosolic calcium dysregulates lysosomal function and impairs autophagy flux during cupric chloride-induced neuronal death. *J Biol Chem*. 2024;300(1). doi:10.1016/J.JBC.2023.105479
172. Gordon PB, Holen I, Fosse M, Røtnes JS, Seglen PO. Dependence of hepatocytic autophagy on intracellularly sequestered calcium. *Journal of Biological Chemistry*. 1993;268(35). doi:10.1016/s0021-9258(19)74287-2
173. Lloyd-Evans E, Morgan AJ, He X, et al. Niemann-Pick disease type C1 is a sphingosine storage disease that causes deregulation of lysosomal calcium. *Nat Med*. 2008;14(11):1247-1255. doi:10.1038/NM.1876
174. Pryor PR, Mullock BM, Bright NA, Gray SR, Luzio JP. The role of intraorganellar Ca(2+) in late endosome-lysosome heterotypic fusion and in the reformation of lysosomes from hybrid organelles. *J Cell Biol*. 2000;149(5):1053-1062. doi:10.1083/JCB.149.5.1053
175. Li X, Rydzewski N, Hider A, et al. A molecular mechanism to regulate lysosome motility for lysosome positioning and tubulation. *Nat Cell Biol*. 2016;18(4):404-417. doi:10.1038/NCB3324

176. Wang W, Gao Q, Yang M, et al. Up-regulation of lysosomal TRPML1 channels is essential for lysosomal adaptation to nutrient starvation. *Proc Natl Acad Sci U S A*. 2015;112(11):E1373-E1381. doi:10.1073/PNAS.1419669112
177. Scotto Rosato A, Montefusco S, Soldati C, et al. TRPML1 links lysosomal calcium to autophagosome biogenesis through the activation of the CaMKKβ/VPS34 pathway. *Nat Commun*. 2019;10(1). doi:10.1038/S41467-019-13572-W
178. Medina DL. Lysosomal calcium and autophagy. *Int Rev Cell Mol Biol*. 2021;362:141-170. doi:10.1016/BS.IRCMB.2021.03.002
179. Lloyd-Evans E, Waller-Evans H. Lysosomal Ca2+ Homeostasis and Signaling in Health and Disease. *Cold Spring Harb Perspect Biol*. 2020;12(6):1-20. doi:10.1101/CSHPERSPECT.A035311
180. Garrity AG, Wang W, Collier CMD, Levey SA, Gao Q, Xu H. The endoplasmic reticulum, not the pH gradient, drives calcium refilling of lysosomes. *Elife*. 2016;5(MAY2016). doi:10.7554/eLife.15887
181. Waller-Evans H, Lloyd-Evans E. Regulation of TRPML1 function. *Biochem Soc Trans*. 2015;43(3):442-446. doi:10.1042/BST20140311
182. Cheng X, Shen D, Samie M, Xu H. Mucolipins: Intracellular TRPML1-3 channels. *FEBS Lett*. 2010;584(10):2013-2021. doi:10.1016/J.FEBSLET.2009.12.056
183. Manzoni M, Monti E, Bresciani R, et al. Overexpression of wild-type and mutant mucolipin proteins in mammalian cells: Effects on the late endocytic compartment organization. *FEBS Lett*. 2004;567(2-3):219-224. doi:10.1016/j.febslet.2004.04.080
184. Soyombo AA, Tjon-Kon-Sang S, Rbaibi Y, et al. TRP-ML1 regulates lysosomal pH and acidic lysosomal lipid hydrolytic activity. *J Biol Chem*. 2006;281(11):7294-7301. doi:10.1074/JBC.M508211200
185. Qi J, Xing Y, Liu Y, et al. MCOLN1/TRPML1 finely controls oncogenic autophagy in cancer by mediating zinc influx. *Autophagy*. 2021;17(12):4401-4422. doi:10.1080/15548627.2021.1917132
186. Shen D, Wang X, Li X, et al. Lipid storage disorders block lysosomal trafficking by inhibiting a TRP channel and lysosomal calcium release. *Nat Commun*. 2012;3. doi:10.1038/NCOMMS1735
187. Yamaguchi S, Jha A, Li Q, et al. Transient receptor potential mucolipin 1 (TRPML1) and two-pore channels are functionally independent organellar ion channels. *J Biol Chem*. 2011;286(26):22934-22942. doi:10.1074/JBC.M110.210930
188. Dong XP, Shen D, Wang X, et al. PI(3,5)P(2) controls membrane trafficking by direct activation of mucolipin Ca(2+) release channels in the endolysosome. *Nat Commun*. 2010;1(4). doi:10.1038/NCOMMS1037

189. Schmiege P, Fine M, Blobel G, Li X. Human TRPML1 channel structures in open and closed conformations. *Nature*. 2017;550(7676). doi:10.1038/NATURE24036
190. Chen Q, She J, Zeng W, et al. Structure of mammalian endolysosomal TRPML1 channel in nanodiscs. *Nature*. 2017;550(7676). doi:10.1038/NATURE24035
191. Yang Y, Xu M, Zhu X, Yao J, Shen B, Dong XP. Lysosomal Ca2+ release channel TRPML1 regulates lysosome size by promoting mTORC1 activity. *Eur J Cell Biol*. 2019;98(2-4):116-123. doi:10.1016/J.EJCB.2019.05.001
192. Scotto Rosato A, Montefusco S, Soldati C, et al. TRPML1 links lysosomal calcium to autophagosome biogenesis through the activation of the CaMKKβ/VPS34 pathway. *Nat Commun*. 2019;10(1). doi:10.1038/S41467-019-13572-W
193. Venkatachalam K, Wong CO, Montell C. Feast or famine: role of TRPML in preventing cellular amino acid starvation. *Autophagy*. 2013;9(1):98-100. doi:10.4161/AUTO.22260
194. Sun X, Yang Y, Zhong XZ, et al. A negative feedback regulation of MTORC1 activity by the lysosomal Ca2+ channel MCOLN1 (mucolipin 1) using a CALM (calmodulin)-dependent mechanism. *Autophagy*. 2018;14(1):38-52. doi:10.1080/15548627.2017.1389822
195. Decuypere JP, Kindt D, Luyten T, et al. mTOR-Controlled Autophagy Requires Intracellular Ca(2+) Signaling. *PLoS One*. 2013;8(4). doi:10.1371/JOURNAL.PONE.0061020
196. Li RJ, Xu J, Fu C, et al. Regulation of mTORC1 by lysosomal calcium and calmodulin. *Elife*. 2016;5. doi:10.7554/ELIFE.19360
197. Currinn H, Guscott B, Balklava Z, Rothnie A, Wassmer T. APP controls the formation of PI(3,5)P(2) vesicles through its binding of the PIKfyve complex. *Cell Mol Life Sci*. 2016;73(2):393-408. doi:10.1007/S00018-015-1993-0
198. Dong XP, Shen D, Wang X, et al. PI(3,5)P(2) controls membrane trafficking by direct activation of mucolipin Ca(2+) release channels in the endolysosome. *Nat Commun*. 2010;1(4). doi:10.1038/NCOMMS1037
199. Li X, Wang X, Zhang X, et al. Genetically encoded fluorescent probe to visualize intracellular phosphatidylinositol 3,5-bisphosphate localization and dynamics. *Proc Natl Acad Sci U S A*. 2013;110(52). doi:10.1073/pnas.1311864110
200. Jin N, Lang MJ, Weisman LS. Phosphatidylinositol 3,5-bisphosphate: regulation of cellular events in space and time. *Biochem Soc Trans*. 2016;44(1):177-184. doi:10.1042/BST20150174
201. Zolov SN, Bridges D, Zhang Y, et al. In vivo, Pikfyve generates PI(3,5)P2, which serves as both a signaling lipid and the major precursor for PI5P. *Proc Natl Acad Sci U S A*. 2012;109(43). doi:10.1073/pnas.1203106109
202. Saffi GT, Wang CA, Mangialardi EM, Vacher J, Botelho RJ, Salmena L. Inhibition of lipid kinase PIKfyve reveals a role for phosphatase Inpp4b in the regulation of PI(3)P-mediated lysosome dynamics through VPS34 activity. *Journal of Biological Chemistry*. 2022;298(8). doi:10.1016/j.jbc.2022.102187

203. Wible DJ, Parikh Z, Cho EJ, et al. ARTICLE Unexpected inhibition of the lipid kinase PIKfyve reveals an epistatic role for p38 MAPKs in endolysosomal fission and volume control. doi:10.1038/s41419-024-06423-0
204. Saffi GT, Tang E, Mamand S, et al. Reactive oxygen species prevent lysosome coalescence during PIKfyve inhibition. *PLoS One*. 2021;16(11 November). doi:10.1371/journal.pone.0259313
205. Bissig C, Hurbain I, Raposo G, van Niel G. PIKfyve activity regulates reformation of terminal storage lysosomes from endolysosomes. *Traffic*. 2017;18(11). doi:10.1111/tra.12525
206. Sharma G, Guardia CM, Roy A, et al. A family of PIKFYVE inhibitors with therapeutic potential against autophagy-dependent cancer cells disrupt multiple events in lysosome homeostasis. *Autophagy*. 2019;15(10). doi:10.1080/15548627.2019.1586257
207. Cao Q, Yang Y, Zhong XZ, Dong XP. The lysosomal Ca2+ release channel TRPML1 regulates lysosome size by activating calmodulin. *Journal of Biological Chemistry*. 2017;292(20):8424-8435. doi:10.1074/JBC.M116.772160
208. Scotto Rosato A, Montefusco S, Soldati C, et al. TRPML1 links lysosomal calcium to autophagosome biogenesis through the activation of the CaMKKβ/VPS34 pathway. *Nat Commun*. 2019;10(1). doi:10.1038/S41467-019-13572-W
209. Medina DL, Di Paola S, Peluso I, et al. Lysosomal calcium signalling regulates autophagy through calcineurin and TFEB. *Nat Cell Biol*. 2015;17(3):288-299. doi:10.1038/NCB3114
210. Scotto Rosato A, Montefusco S, Soldati C, et al. TRPML1 links lysosomal calcium to autophagosome biogenesis through the activation of the CaMKKβ/VPS34 pathway. *Nat Commun*. 2019;10(1). doi:10.1038/S41467-019-13572-W
211. Scotto Rosato A, Montefusco S, Soldati C, et al. TRPML1 links lysosomal calcium to autophagosome biogenesis through the activation of the CaMKKβ/VPS34 pathway. *Nat Commun*. 2019;10(1). doi:10.1038/s41467-019-13572-w
212. Chen Y, Yu L. Recent progress in autophagic lysosome reformation. *Traffic*. 2017;18(6). doi:10.1111/tra.12484
213. Xia Z, Wang L, Li S, et al. ML-SA1, a selective TRPML agonist, inhibits DENV2 and ZIKV by promoting lysosomal acidification and protease activity. *Antiviral Res*. 2020;182. doi:10.1016/j.antiviral.2020.104922
214. Venkatachalam K, Long AA, Elsaesser R, Nikolaeva D, Broadie K, Montell C. Motor Deficit in a Drosophila Model of Mucolipidosis Type IV due to Defective Clearance of Apoptotic Cells. *Cell*. 2008;135(5). doi:10.1016/j.cell.2008.09.041
215. Curcio-Morelli C, Charles FA, Micsenyi MC, et al. Macroautophagy is defective in mucolipin-1-deficient mouse neurons. *Neurobiol Dis*. 2010;40(2):370-377. doi:10.1016/J.NBD.2010.06.010

216. Tedeschi V, Petrozziello T, Sisalli MJ, Boscia F, Canzoniero LMT, Secondo A. The activation of Mucolipin TRP channel 1 (TRPML1) protects motor neurons from L-BMAA neurotoxicity by promoting autophagic clearance. *Sci Rep*. 2019;9(1). doi:10.1038/S41598-019-46708-5
217. Zhang X, Cheng X, Yu L, et al. MCOLN1 is a ROS sensor in lysosomes that regulates autophagy. *Nat Commun*. 2016;7. doi:10.1038/NCOMMS12109
218. Zhang L, Fang Y, Cheng X, et al. TRPML1 Participates in the Progression of Alzheimer's Disease by Regulating the PPARγ/AMPK/Mtor Signalling Pathway. *Cell Physiol Biochem*. 2017;43(6):2446-2456. doi:10.1159/000484449
219. Boudewyn LC, Walkley SU. Current concepts in the neuropathogenesis of mucolipidosis type IV. *J Neurochem*. 2019;148(5):669-689. doi:10.1111/JNC.14462
220. Berman ER, Livni N, Shapira E, Merin S, Levij IS. Congenital corneal clouding with abnormal systemic storage bodies: a new variant of mucolipidosis. *J Pediatr*. 1974;84(4):519-526. doi:10.1016/S0022-3476(74)80671-2
221. Yin C, Zhang H, Liu X, et al. Downregulated MCOLN1 Attenuates The Progression Of Non-Small-Cell Lung Cancer By Inhibiting Lysosome-Autophagy. *Cancer Manag Res*. 2019;11:8607-8617. doi:10.2147/CMAR.S216538
222. Kasitinon SY, Eskiocak U, Martin M, et al. TRPML1 Promotes Protein Homeostasis in Melanoma Cells by Negatively Regulating MAPK and mTORC1 Signaling. *Cell Rep*. 2019;28(9):2293-2305.e9. doi:10.1016/J.CELREP.2019.07.086
223. Morelli MB, Amantini C, Tomassoni D, Nabissi M, Arcella A, Santoni G. Transient Receptor Potential Mucolipin-1 Channels in Glioblastoma: Role in Patient's Survival. *Cancers (Basel)*. 2019;11(4). doi:10.3390/CANCERS11040525
224. Kim MS, Muallem S, Kim SH, Kwon KB, Kim MS. Exosomal release through TRPML1-mediated lysosomal exocytosis is required for adipogenesis. *Biochem Biophys Res Commun*. 2019;510(3):409-415. doi:10.1016/J.BBRC.2019.01.115
225. Chandra M, Zhou H, Li Q, Muallem S, Hofmann SL, Soyombo AA. A role for the Ca2+ channel TRPML1 in gastric acid secretion, based on analysis of knockout mice. *Gastroenterology*. 2011;140(3):857-867.e1. doi:10.1053/J.GASTRO.2010.11.040
226. Capurro MI, Greenfield LK, Prashar A, et al. VacA generates a protective intracellular reservoir for Helicobacter pylori that is eliminated by activation of the lysosomal calcium channel TRPML1. *Nat Microbiol*. 2019;4(8):1411-1423. doi:10.1038/S41564-019-0441-6
227. Xia Z, Wang L, Li S, et al. ML-SA1, a selective TRPML agonist, inhibits DENV2 and ZIKV by promoting lysosomal acidification and protease activity. *Antiviral Res*. 2020;182. doi:10.1016/J.ANTIVIRAL.2020.104922
228. Zhong D, Wang R, Zhang H, Wang M, Zhang X, Chen H. Induction of lysosomal exocytosis and biogenesis via TRPML1 activation for the treatment of uranium-induced nephrotoxicity. *Nat Commun*. 2023;14(1). doi:10.1038/s41467-023-39716-7

229. Medina DL, Di Paola S, Peluso I, et al. Lysosomal calcium signalling regulates autophagy through calcineurin and TFEB. *Nat Cell Biol*. 2015;17(3). doi:10.1038/ncb3114
230. LaPlante JM, Sun M, Falardeau J, et al. Lysosomal exocytosis is impaired in mucolipidosis type IV. *Mol Genet Metab*. 2006;89(4). doi:10.1016/j.ymgme.2006.05.016
231. Pollmanns MR, Beer J, Rosignol I, Rodriguez-Muela N, Falkenburger BH, Dinter E. Activated Endolysosomal Cation Channel TRPML1 Facilitates Maturation of α-Synuclein-Containing Autophagosomes. *Front Cell Neurosci*. 2022;16. doi:10.3389/fncel.2022.861202
232. Somogyi A, Kirkham ED, Lloyd-Evans E, et al. The synthetic TRPML1 agonist ML-SA1 rescues Alzheimer-related alterations of the endosomal-autophagic-lysosomal system. *J Cell Sci*. 2023;136(6). doi:10.1242/JCS.259875
233. Shen D, Wang X, Li X, et al. Lipid storage disorders block lysosomal trafficking by inhibiting a TRP channel and lysosomal calcium release. *Nat Commun*. 2012;3. doi:10.1038/ncomms1735
234. Medina DL, Di Paola S, Peluso I, et al. Lysosomal calcium signalling regulates autophagy through calcineurin and TFEB. *Nat Cell Biol*. 2015;17(3). doi:10.1038/ncb3114
235. Davis OB, Shin HR, Lim CY, et al. NPC1-mTORC1 Signaling Couples Cholesterol Sensing to Organelle Homeostasis and Is a Targetable Pathway in Niemann-Pick Type C. *Dev Cell*. 2021;56(3). doi:10.1016/j.devcel.2020.11.016
236. Fraldi A, Annunziata F, Lombardi A, et al. Lysosomal fusion and SNARE function are impaired by cholesterol accumulation in lysosomal storage disorders. *EMBO Journal*. 2010;29(21). doi:10.1038/emboj.2010.237
237. Li X, Rydzewski N, Hider A, et al. A molecular mechanism to regulate lysosome motility for lysosome positioning and tubulation. *Nat Cell Biol*. 2016;18(4). doi:10.1038/ncb3324
238. Vines JH, Maib H, Buckley CM, et al. A PI(3,5)P2 reporter reveals PIKfyve activity and dynamics on macropinosomes and phagosomes. *Journal of Cell Biology*. 2023;222(9). doi:10.1083/jcb.202209077
239. Pryor PR, Reimann F, Gribble FM, Luzio JP. Mucolipin-1 is a lysosomal membrane protein required for intracellular lactosylceramide traffic. *Traffic*. 2006;7(10). doi:10.1111/j.1600-0854.2006.00475.x
240. Zeevi DA, Lev S, Frumkin A, Minke B, Bach G. Heteromultimeric TRPML channel assemblies play a crucial role in the regulation of cell viability models and starvation-induced autophagy. *J Cell Sci*. 2010;123(18). doi:10.1242/jcs.067330
241. Laczkó-Dobos H, Bhattacharjee A, Maddali AK, et al. PtdIns4P is required for the autophagosomal recruitment of STX17 (syntaxin 17) to promote lysosomal fusion. *Autophagy*. Published online 2024. doi:10.1080/15548627.2024.2322493
242. Tan JX, Finkel T. A phosphoinositide signalling pathway mediates rapid lysosomal repair. *Nature*. 2022;609(7928). doi:10.1038/s41586-022-05164-4

243. Pols MS, Van Meel E, Oorschot V, et al. HVps41 and VAMP7 function in direct TGN to late endosome transport of lysosomal membrane proteins. *Nat Commun*. 2013;4. doi:10.1038/ncomms2360
244. Pryor PR, Jackson L, Gray SR, et al. Molecular Basis for the Sorting of the SNARE VAMP7 into Endocytic Clathrin-Coated Vesicles by the ArfGAP Hrb. *Cell*. 2008;134(5). doi:10.1016/j.cell.2008.07.023
245. Mori Y, Takenaka K ichiro, Fukazawa Y, Takamori S. The endosomal Q-SNARE, Syntaxin 7, defines a rapidly replenishing synaptic vesicle recycling pool in hippocampal neurons. *Commun Biol*. 2021;4(1). doi:10.1038/s42003-021-02512-4
246. Settembre C, Zoncu R, Medina DL, et al. A lysosome-to-nucleus signalling mechanism senses and regulates the lysosome via mTOR and TFEB. *EMBO Journal*. 2012;31(5). doi:10.1038/emboj.2012.32
247. Sebők-Nagy K, Blastyák A, Juhász G, Páli T. Reversible binding of divalent cations to Ductin protein assemblies—A putative new regulatory mechanism of membrane traffic processes. *Front Mol Biosci*. 2023;10. doi:10.3389/fmolb.2023.1195010
248. Mitra C, Winkley S, Kane PM. Human V-ATPase a-subunit isoforms bind specifically to distinct phosphoinositide phospholipids. *J Biol Chem*. 2023;(12):105473-105474. doi:10.1016/j.jbc.2023.105473
249. Wang H, Sun HQ, Zhu X, et al. GABARAPs regulate PI4P-dependent autophagosome: Lysosome fusion. *Proc Natl Acad Sci U S A*. 2015;112(22). doi:10.1073/pnas.1507263112
250. Staudt C, Puissant E, Boonen M. Subcellular trafficking of mammalian lysosomal proteins: An extended view. *Int J Mol Sci*. 2017;18(1). doi:10.3390/ijms18010047
251. Gómez-Virgilio L, Silva-Lucero MDC, Flores-Morelos DS, et al. Autophagy: A Key Regulator of Homeostasis and Disease: An Overview of Molecular Mechanisms and Modulators. *Cells*. 2022;11(15). doi:10.3390/cells11152262
252. Levine B, Kroemer G. Autophagy in the Pathogenesis of Disease. *Cell*. 2008;132(1). doi:10.1016/j.cell.2007.12.018
253. Anding AL, Baehrecke EH. Cleaning House: Selective Autophagy of Organelles. *Dev Cell*. 2017;41(1). doi:10.1016/j.devcel.2017.02.016
254. Lieberman AP, Puertollano R, Raben N, Slaugenhaupt S, Walkley SU, Ballabio A. Autophagy in lysosomal storage disorders. *Autophagy*. 2012;8(5). doi:10.4161/auto.19469
255. Hori I, Otomo T, Nakashima M, et al. Defects in autophagosome-lysosome fusion underlie Vici syndrome, a neurodevelopmental disorder with multisystem involvement. *Sci Rep*. 2017;7(1). doi:10.1038/s41598-017-02840-8
256. Abuammar H, Bhattacharjee A, Simon-Vecsei Z, et al. Ion channels and pumps in autophagy: A reciprocal relationship. *Cells*. 2021;10(12). doi:10.3390/cells10123537

257. Wakabayashi K, Gustafson AM, Sidransky E, Goldin E. Mucolipidosis type IV: An update. *Mol Genet Metab*. 2011;104(3). doi:10.1016/j.ymgme.2011.06.006

10. SUPPLEMENTARY DATA

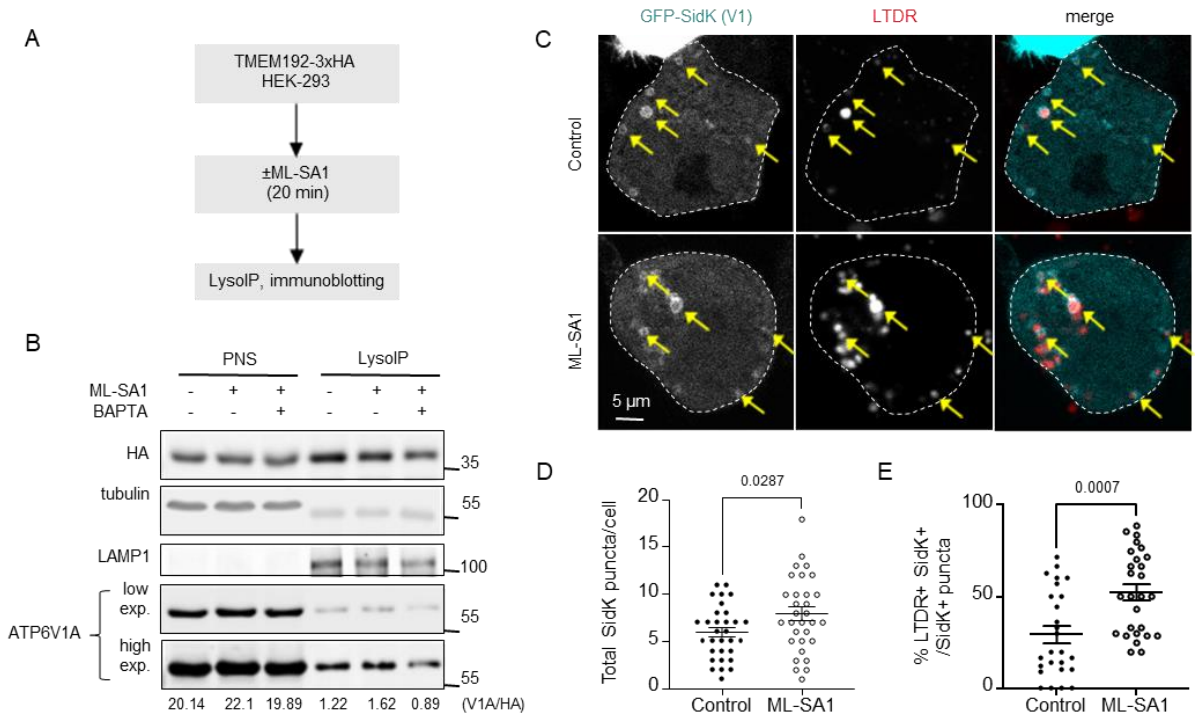

Figure S1: TRPML1 mostly enhances the activity of pre-assembled V-ATPase holocomplexes to drive acidification.

(A) Model shows lysosomal immunopurification (Lyso-IP) strategy which was followed.

(B) TRPML1 activation only slightly increases the enrichment of the v-ATPase subunit ATP6V1A to lysosomes during a short period of ML-SA1 treatment (20 minutes). LAMP1: lysosome marker, tubulin: cytosol marker.

(C) Expression of GFP-SicK (low level), v1 fluorescent reporter, along with LTDR in HEK-293 cells incubated with ML-SA1 solution (25 µM, 20 minutes). Arrows point to SidK-positive structures.

(D) The number of localized v1 is slightly increased during ML-SA1 treatment (20 minutes). N≥26 for both samples. Statistics: Mann-Whitney test was applied.

(E) SidK-positive structures that are positive for LTDR, greatly increase during ML-SA1 treatment. Highlighty acidification resulted in LTDR sequestration inside existing v1-containing structures. N=31 for both samples. Statistics: unpaired t test was applied.

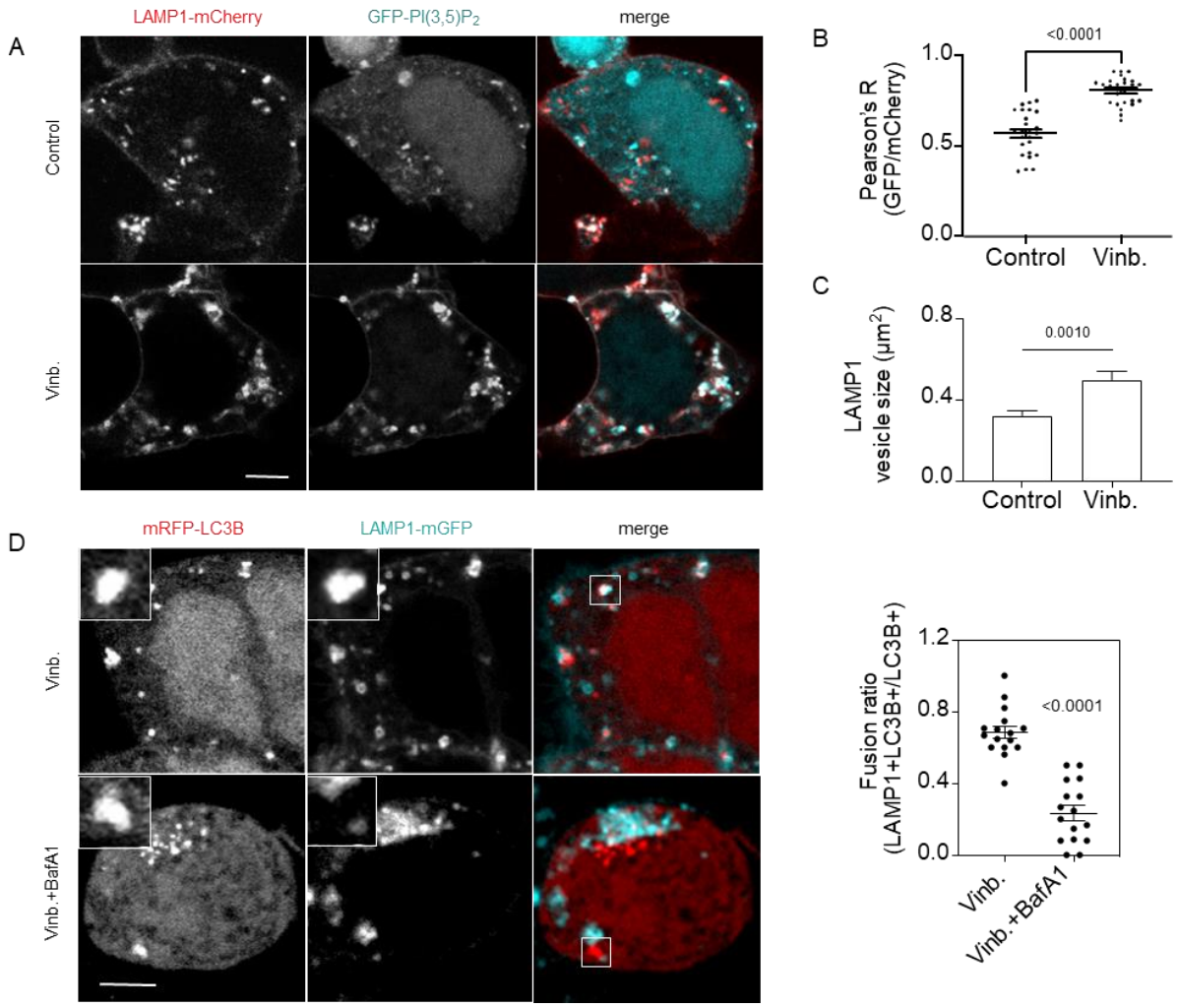

Figure S2: lysosomal PI(3,5)P_2 localization and local AP-LY fusion are increased in microtubule inhibitor vinblastine.

(A) HEK-293 cells were exposed to vinblastine treatment (20 μM, 2.5h). Bar: 5 μm.

(B) Quantification of colocalization using Pearson's coefficient between LAMP1-mCherry and GFP-PI(3,5)P_2 puncta from each cell. N=26 for both samples. Statistics: unpaired t test was applied.

(C) The size of the LAMP1-positive vesicle was greatly enlarged after 2.5 hours of vinblastine treatment due to homotypic fusion of lysosomes. N≥200 for both samples. Statistics: Mann-Whitney test was applied.

(D) HEK-293 cells were exposed to vinblastine only or together with bafilomycin A1 (100 nM). Inset demonstrating colocalized structures indicating AP-LY fusion in vinblastine-treated cells, which is disrupted after BafA1 treatment in vinblastine-pre-treated cells. Bar: 5 μm. Right: fusion ratio was counted. N=16 for both samples. Statistics: unpaired t test was applied.

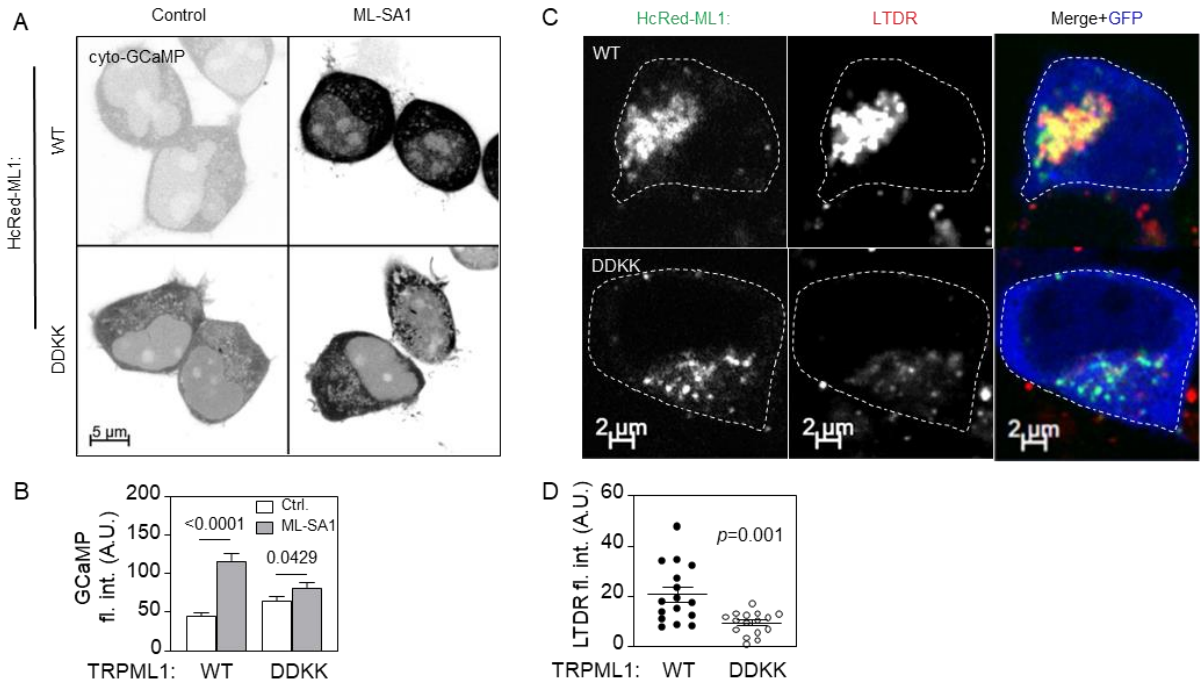

Figure S3: Additional features of GCaMP6m-TRPML1 fluorescent signal and acidification.

(A) cyto-GCaMP construct was co-expressed with TRPML1wt or TRPML1DDKK in HEK-293 cells to assess cytosolic Ca^{2+} changes due to lysosomal Ca^{2+} release after ML1-SA1 treatment (20 minutes).

(B) Cellular GCaMP fluorescence (background subtracted) was measured. N≥42 for all used samples. Statistics: unpaired t-test was applied within groups (wt and DDKK separately).

(C) HEK-293 cells expressing TRPML1wt or TRPML1DDKK were stained with LTDR to assess lysosomal acidification. Stronger LTDR staining was seen in wt as opposed to DDKK, as well as clustered in wild type vs. scattered in mutant. GFP (blue) labels a transfected cell.

(D) Fluorescent intensity from the whole cell was measured from (C). N=16 for both samples.Statistics: unpaired t test was applied.

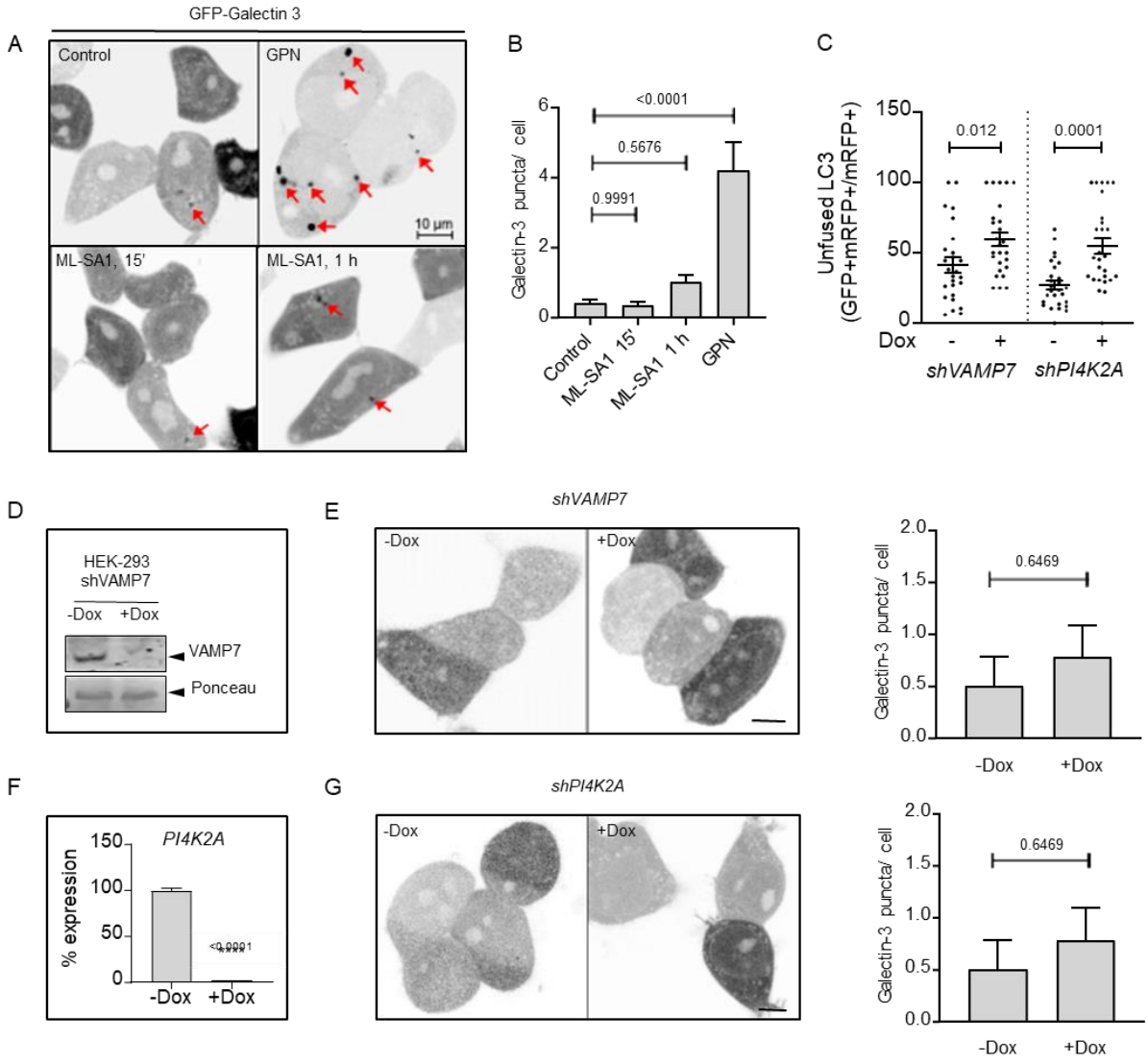

Figure S4: Lysosomal damage response during ML-SA1 treatment and fusion-deficient circumstances.

(A) HEK-293 cells expressing GFP-Gal 3 were treated with GPN (200 µM, 1 h), ML-SA1 (25 µM, 15 minutes and 1 hour). Red arrows indicate Gal-3-positive dots (damaged lysosomes). Bar: 10 µm.

(B) The number of Gal-3-positive puncta per cell. N≥60 for all samples. Statistics: one-way ANOVA test was applied with multiple comparisons against Control.

(C) Quantification of fusion ratio of yellow to total red (autophagosomes/autolysosomes) puncta in shRNA-expressing cells (shVAMP7 and shPI4K2A) pre-transfected with GFP-RFP-LC3 (tflc3). N=25 for all samples. Statistics: Mann-Whitney test was applied. See also Figures 4A and 4D.

(D) shVAMP7-expressing HEK-293 cells were exposed to doxycycline (2 µg/ml, 48-72 h) to attenuate the expression of shVAMP7, which was confirmed by western blotting.

(E) shVAMP7-expressing HEK-293 cells were transfected with GFP-Gal-3 construct. Right panel: the number of Gal-3-positive puncta per cell. N≥29 for both samples. Bar: 10 µm.

(F) shPI4K2A-expressing HEK-293 cells were exposed to doxycycline (2 µg/ml, 48-72 h) to attenuate the expression of shPI4K2A, which was confirmed by qRT-PCR.

(G) shPI4K2A-expressing HEK-293 cells were transfected with GFP-Gal-3 construct. Right panel: the number of Gal-3-positive puncta per cell. N≥30 for both samples. Bar: 10 μm. All statistics: Mann-Whitney test was applied.

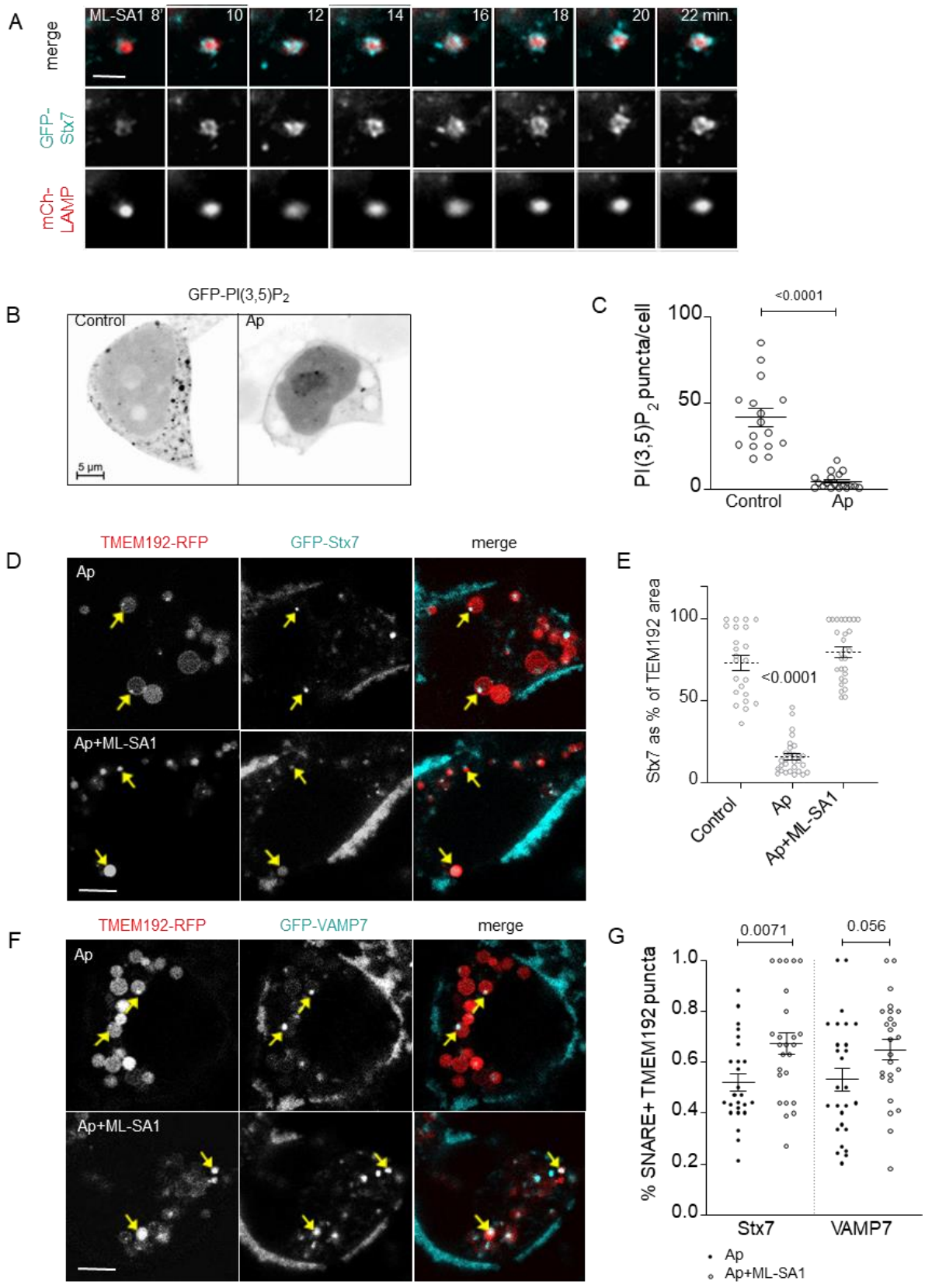

Figure S5: TRPML1 activation rescue aberrant SNARE distribution in apilimod-exposed lysosomes

(A) U2OS cells were co-transfected with GFP-Stx7 and mCherry-LAMP1 and then live imaged during ML-SA1 treatment, same way like Figure 5E. Bar: 2 µm.

(B) Profile of fluorescent LAMP1-positive structure at 8 minutes and 22 minutes of ML-SA1 treatment, demonstrating association of Stx7 (cyan line).

(C) HEK-293 cells were transiently transfected with GFP-PI(3,5)P_2 fluorescent reporter and exposed to Ap (1 μm, 1 h) to block PIKfyve fusion. PI(3,5)P_2-positive puncta significantly reduced after Ap treatment.

(D) The number of PI(3,5)P_2-positive puncta per cell. N=16; statistics: unpaired t-test was applied.

(E) Aberrant Stx7 and VAMP7 localization are observed in two forms: small foci on the lysosomal membrane (TMEM192-RFP signal) as well as sequestration inside lysosomes (TMEM192-RFP signal). This abnormal localization of both Stx7 and VAMP7 is restored by TRPML1 activation in PIKfyve-inhibited cells. Arrows indicate localization of GFP-SNARE on lysosomes marked with TMEM192-mRFP. Bars: 5 μm.

(F) Percentage of Stx7 occupying TMEM192 area in HEK-293 cells untreated (Control), treated with Ap alone, or co-treated with Ap+ML-SA1. N≥29 for all samples. Statistics: Mann-Whitney test was applied.

(G) Percentage of SNARE (Stx7 and VAMP7) occupying TMEM192 area increased after ML-SA1 treatment (15 minutes). N=25 for all samples. Statistics: unpaired t test was used between genotypes.

11. MY CONTRIBUTION IN THIS STUDY

- Cell culture, maintenance of human cell lines (HEK293, U2OS, and HeLa), plasmid DNA transfection
- Drug treatments (ML-SA1, apilimod, bafilomycin A1, concanamycin A, and BAPTA)
- Incubation of cells with lysotracker, Lysosensor, or FITC-Dx for pH measurements
- Bacterial transformation and plasmid DNA isolation
- Live imaging of GFP-Stx7 or GFP-VAMP7 with TMEM192-mRFP using olympus miscroscope
- Live imaging of four channels (SECFP-STX17TM, GCaMP6m-TRPML1 and mKate2-ML1N*2, and LTDR) using confocal microscope
- Lysosomal immunoprecipitation (Lyso-IP) using magnetic beads, followed by westernblotting
- Microscopic imaging
- Westernblotting
- Data collection, analysis, and visualization
- Cloning of inducible expression sysmtems of shRNAs (shVAMP7 and shPI4K2A)
- Involvment in writting and reviewing the research study
- qPCR